70-20,895

EREL, Bilgin, 1942-
PHYSICO-CHEMICAL MODEL ANALYSIS FOR
COMPRESSIBILITY OF PURE CLAY.

Carnegie-Mellon University, Ph.D., 1970
Engineering, civil

University Microfilms, A XEROX Company, Ann Arbor, Michigan

THIS DISSERTATION HAS BEEN MICROFILMED EXACTLY AS RECEIVED

PHYSICO-CHEMICAL MODEL ANALYSIS FOR COMPRESSIBILITY OF PURE CLAY

by

Bilgin Erel
B. S., Middle East Technical University, 1965
M. S., Carnegie-Mellon University, 1967

Submitted in Partial Fulfillment of the
Requirements for the Degree
Doctor of Philosophy

Department of Civil Engineering
Carnegie-Mellon University

April 1970

Carnegie-Mellon University

CARNEGIE INSTITUTE OF TECHNOLOGY

THESIS

SUBMITTED IN PARTIAL FULFILLMENT OF THE REQUIREMENTS

FOR THE DEGREE OF DOCTOR OF PHILOSOPHY

TITLE "PHYSICO-CHEMICAL MODEL ANALYSIS FOR COMPRESSIBILITY OF PURE CLAY"

PRESENTED BY Bilgin Erel

ACCEPTED BY THE DEPARTMENT OF Civil Engineering

Gerald A. Thiers — MAJOR PROFESSOR — May 1, 1970 — DATE

P. B. Stetson — DEPARTMENT HEAD — May 4, 1970 — DATE

APPROVED BY THE COMMITTEE ON GRADUATE DEGREES

[signature] — CHAIRMAN — 5/5/70 — DATE

TABLE OF CONTENTS

	Page
List of Figures	IV
List of Tables	VI
Acknowledgments	VII
Abstract	VIII
1 - INTRODUCTION	1
2 - SCOPE AND OBJECTIVE	4
3 - PHYSICAL AND CHEMICAL PROPERTIES OF CLAYS	6
3-1 Nature of Clay	6
3-2 Mineralogic Structure of Clay	7
3-3 Surface Charge of Clay Particles	12
3-4 Electric Double Layer Structure	14
3-5 Water In Clays	18
3-6 Interparticle Forces	20
4 - VOLUME CHANGE AND STRUCTURAL CHARACTERISTICS OF CLAY	23
4-1 Volume Change Characteristics of Clay	24
4-2 Clay Particle Structure	31
4-3 Present State of Knowledge	33
5 - A MODEL FOR A CLAY PARTICLE SYSTEM	35
5-1 Model System Geometry	35
5-2 Electric Double Layer Theory	37
5-3 Boundary Conditions	39
5-4 Pressure Distribution	43
5-5 Summary of Chapter	44
6 - PROCEDURE FOR CALCULATION OF VOLUME CHANGE CHARACTERISTICS OF MODEL	46
6-1 Finite Element Solution of Poisson-Boltzmann Equation	46
- Mathematical Problem	
- Finite Element and Nodal Values	
- Minimization of Functional	

Page

6-2 Solving the System of Non-linear Equations 52
- Newton's Method

6-3 Numerical Form of Boundary Conditions 55

6-4 Accuracy of Solution 56
- Space Charge
- Surface Charge
- Space Surface Charge Equivalency

7 - RESULTS OF COMPUTATIONS 59

7-1 Bulk Water Ion Concentration-Repulsive Pressure Relationship 59

7-2 Potential Distribution 62

7-3 Pressure Distribution 64

7-4 Model Particle Structure Force-Deformation Relationship 67

8 - ONE-DIMENSIONAL CONSOLIDATION TESTS 74

8-1 One-dimensional Consolidation Test and Apparatus 74

8-2 Soil Studied and Sample Preparation 74

8-3 Test Procedure 76

8-4 Calculation of Test Results 78

8-5 Test Results 79

9 - COMPARISON OF MODEL AND EXPERIMENTAL RESULTS 84

9-1 One-dimensional Consolidation 84

9-2 Two-dimensional Volume Change Behavior of Model Structure 88

10 - LIMITATIONS AND RECOMMENDATIONS 93

11 - SUMMARY AND CONCLUSIONS 95

REFERENCES 98

NOTATION 101

APPENDIX A: Computer Program and Description 102

APPENDIX B: Numerical Integration Over a Triangular Domain 118

APPENDIX C: Potential Distributions 120

APPENDIX D: Surface Charge Calculations For Clay Particles 142

LIST OF FIGURES

Number		Page
3-1	Structure of Tetrahedral Sheet	8
3-2	Structure of Octahedral Sheet	9
3-3	Structure of Clay Minerals	11
3-4	Diffuse Electric Double Layer Model According to Gouy (1910, 1917)	15
3-5	The Effect of Changes in System Properties on Diffuse Double Layer (After Lambe, 1958)	17
4-1	Typical Consolidation Curve for a Clay	24
4-2	Compression Void Ratio Relationships	27
4-3a	Hypothesized Flocculated Structure in Clays (From Hough 1969)	32
4-3b	Hypothesized Dispersed Structure in Clays (From Hough 1969)	33
5-1	Idealized Clay Particle System	36
5-2	Particle Orientations	37
5-3	Model Element and Boundary Conditions	48
6-1	Division of Region into Elements	61
6-2	Boundary Conditions for an Element and Regions of Surface and Space Charge	57
7-1	Potential Variation Between Infinite Plates	60
7-2	Void-Ratio Repulsive Pressure Relationships for Infinite Parallel Plates	63
7-3	Typical Subdivision of an Element	65
7-4	Typical Potential Distribution in an Element	65
7-5a	Model Element	66
7-5b	Typical Boundary Pressure Distribution	66
7-6	Model Particle Structure Element Boundary and External Pressures	70
7-7	Pressure Relationships for Several Plate Separation Distances	71
7-8	Vertical Pressure Void Ratio Relationship	72
7-9	Horizontal Pressure Void Ratio Relationship	73

		Page
8-1	Consolidometer	75
8-2	Time-Percent Consolidation Curve	77
8-3	Typical Void Ratio Pressure Relationship	77
8-4	Consolidation Pressure-Void Ratio Relationship	81
8-5	Consolidation Pressure-Void Ratio Relationship	82
8-6	Consolidation Pressure-Void Ratio Relationship	83
9-1	Comparison of Experimental and Model Results	86
9-2	Net-Force Distance Relationship Between Particles	87
9-3	Void Ratio Mean Pressure Relationship (Anisotropic Consolidation)	87
9-4	Model Structure Volume Change Behavior (Drained Shear)	92
B-1	Gaussian Integration Over A Triangle	
C-1 ∿ C-20	Potential Distribution and Pressure on Boundaries	

LIST OF TABLES

Number		Page
3-1	Properties of Clay Particles	13
7-1	Boundary Conditions for Several Values of Bulk Solution Ion Concentration	61
7-2	Void Ratio P_V, P_H, and P_V/P_H Values for Several Plate Separation Distances	69
9-1	Void Ratio P_V, P_H, and P_V/P_H Values Defining One-dimensional Volume Change Behavior	85
9-2	Void Ratio P_V, P_H, and P_V/P_H Values Defining Two-dimensional Volume Change Behavior	90

ACKNOWLEDGMENTS

I am indebted to my thesis advisor, Dr. G. R. Thiers, for his guidance and encouragement which made this project possible. I also wish to express my thanks to Dr. W. T. Grandquist at Mellon Institute for his assistance in obtaining the clay used in this study.

My appreciation is extended to Mrs. B. Green for typing the manuscript.

Special thanks are extended to my wife, Janet, and my parents for their patience and encouragement during the period of my studies at Carnegie-Mellon University.

ABSTRACT

The purpose of this thesis is to study the volume change characteristics of saturated clay. The study was concerned with the analysis of the mechanical behavior of an idealized clay particle system. The mechanical behavior, the relationship between forces and deformations of the system, is postulated to be governed by repulsive and attractive forces among the particles. The repulsive forces in the clay-water system are primarily caused by the interaction of the diffuse double layers on the surfaces of the particles. Although other types of interactions occur at closer ranges, interparticle spacings in natural soils and man-made soil deposits which have engineering importance are relatively large (Lee, 1968). Repulsive forces can therefore be adequately expressed in terms of double layer theory. The attractive forces between clay particles have been attributed to van der Waals's forces; these forces only become important when particle spacing is very small.

The objective of the analysis is to determine the repulsive forces among the particles, under various distortions of the model unit, in order to describe the volume change-force relationship for the model unit structure. Comparing the resulting volume change-force relationships to those obtained from experimental results confirms the value of the analysis.

The forces in the double layer can be found from a force-field potential, and the distribution of potential is given by the fundamental equation of the double layer, the Poisson-Boltzman equation. The nature of this equation is such that, with the exception of a few specialized cases, closed form solutions cannot be obtained. Numerical

methods must be resorted to. The results of the computations are pressure distributions on the planes of symmetry of the model unit, on the basis of which, repulsive forces may be determined.

For an experimental verification of the analytical results, one-dimensional consolidation tests were conducted on Sodium-Montmorillonite. Montmorillonite was selected because of its high specific surface characteristics which magnify the interparticle force effects.

Considering the method as a general technique for studying volume change characteristics of clayey soils; its limitations and applications to soils problems are discussed.

1 - INTRODUCTION

The engineering problems associated with clay soils are usually studied by using the bulk properties such as shear strength, compressibility, and permeability as functions of stress conditions and time. These problems include the bearing capacity and settlement of footings, the long and short term stability of cut slopes, stress distribution in deposits and many others. The realistic solution of these problems are often difficult on two counts: 1) lack of an appropriate method of analysis and 2) the problem of selecting the appropriate soil parameters to plug into the theoretical analysis. For example, the theory of elasticity is used for the solution of many stress distribution and soil deformation problems, even though it is known that soil is not an isotropic, linearly-elastic material. Moreover, selection of the appropriate value of elastic modulus for these calculations is difficult. Generally selection is based upon semi-empirical correlations between the results of laboratory tests and field measurements. For the correct solution of these problems it is necessary to formulate both a complete stress-strain law and a shear strength equation for soils. Similarly time dependent problems such as consolidation are solved through using conceptual models that seem to represent the observed behavior.

In the past several decades although the mechanical properties of soils have been widely studied, the findings do not allow the formulation of a complete unifying picture of the mechanical behavior of soils. This lack of an organized framework which would help to

understand the interrelationship between several mechanical properties or to explain why the properties are as they are, results in the use of high safety factors for engineering purposes, to take care of the possibilities of unpredicted behavior. Due to the urgency of practical solutions to problems the major effort has been devoted to the experimental study of the bulk behavior of clay soils, rather than to research on the fundamental causes of observed behavior. It is well-known that the bulk behavior of clay soils is mainly governed by the forces acting between the clay particles. These in turn depend on physico-chemical and mineralogical properties of clay-water system. It is hoped that an approach which specifically accounts for inter-particle forces, mineralogy, and physical-chemistry in studying the mechanical properties of clay soils may introduce a more basic and unified understanding of the material.

The study of the engineering behavior of clay soils in terms of fundamental causes may involve considerations of the type of clay mineral cation exchange capacity, type and amount of exchangeable ions in pore fluid, temperature, particle shape, particle size distribution and relative orientation of particles. The detailed study of the properties listed above is being carried out in specialized disciplines of science, such as clay mineralogy and clay colloidal chemistry.

The ultimate objective of a soils engineer is to use knowledge of the basic nature of soils to predict the bulk behavior; this avoids the use of mathematical models which seem to represent the observed behavior under certain conditions, but leave some doubt concerning

their generality.

During the last ten to fifteen years many papers have been published pointing out the importance of chemical and mineralogical factors for the prediction of engineering properties. Most of these papers have been of a qualitative nature; that is, even though numerical values are often given showing how much the shear strength, compressibility or permeability is influenced by chemical and physical changes, definite relationships for engineering use have not been established.

The principal reason that the classical theories of deformable bodies fail to explain the behavior of soil masses satisfactorily is due to the fact that they are based on the postulate of an inert continuum; that is, that behavior of soil can be understood and generalized from the measurement of force length, and time alone. Since in reality electrical and chemical phenomena actively participate in determining the properties of the material, classical theories of deformable bodies may no longer be satisfactorily used. Development of new techniques is required to establish a proper basis for the understanding of the behavior of soils.

2 - OBJECTIVE AND SCOPE

To reach a better understanding of the engineering behavior of clay soils (volume change characteristics, stress-strain relationships, shear strength, etc.), it is necessary to be able to explain the underlying mechanisms of each behavior. It is well-known that the behavior of clay soils is predominantly governed by interparticle forces which are greatly influenced by the physico-chemical properties of the constituent particles and their environment.

Studies of physico-chemical properties of clay-water systems are being carried out in various disciplines. Many findings of quantitative colloidal chemistry and mineralogy are pertinent to the engineering study of clay-water systems.

The purpose of this investigation is to study the volume change characteristics of saturated clay. The study will be based on the analysis of the forces acting between the particles of an idealized clay particle system. For analytical simplicity in determining the interacting forces between the particles, the particles are assumed to be held in equilibrium in an internal two-dimensional force network.

Upon application of external forces to a given system of particles, the particle framework will undergo deformation. The specific task is to find how the internal stresses alter to resist deformation.

The method will consist of assuming a geometrical arrangement for the particles and finding the stress components of the system by

means of a force field potential. The distribution of this potential in space is given by the fundamental equation of the double layer, the Poisson-Boltzmann equation. The relative positions of the particle are changed and new stress components are calculated establishing the volume change-force relationship for the given particle system.

Attempts will be made to verify some of the findings of the analytical study experimentally. Quantitative comparisons will be made between predicted behavior and general form of experimental results.

3 - PHYSICAL AND CHEMICAL PROPERTIES OF CLAYS

It is logical to assume that the type of mineral occurring in a soil will influence the engineering properties of the soil. The methods of mechanics satisfactorily describe the behavior of soils made of large particles. Many of the problem soils in engineering are clay soils, however, and for the description of their behavior the methods of mechanics are less successful. The changes in behavior are due to the increasing effect of the forces between the molecules of adjacent particle surfaces as the size of particles decreases.

Particles with diameter smaller than 0.001 mm but larger than molecular size (10^{-6}mm) are classified as colloids, or are said to be in the colloidal state. Clay particles fall within this range. Colloidal properties such as plasticity and adsorption of molecules arise from a large surface area being associated with a small volume. Not all minerals exhibit plasticity when in a finely ground state; those that do so are referred to as "clay minerals", among these are several groups of different chemical composition.

In this chapter nature and mineralogic structure, surface charge and double layer structure of clay particles, water in clays and interparticle forces will be discussed in some detail as they determine the behavior of clay soils.

3-1 Nature of Clay Minerals

The optical methods used in early investigations in identifying the larger minerals were not powerful enough to resolve particles of

the size of clay. Several thoughts were presented. Clay size material was thought to consist of amorphous aluminum and iron silicates with the properties of plasticity, water adsorption and ion-exchange. Ideas were presented that all clays are one particular mineral. The name "kaolin" was applied to clays and used synonymously with "clay". Different properties of clays were ascribed to different amounts of impurities within the kaolin.

Some early investigations have suggested that clay consists of very small particles of a limited number of crystalline minerals. The development of x-ray diffraction techniques in the early 1920's demonstrated this to be the correct concept, and it has come to be called the mineral concept (Grim 1953). More recently other research techniques, such as optical and electron microscopy, electron diffraction, differential thermal analysis and infrared absorption, have added evidence to the validity of the clay mineral concept.

3-2 Mineralogic Structure

The principle building elements of the clay minerals are two-dimensional arrays of silicon-oxygen tetrahedra and two-dimensional arrays of aluminum or magnesium-oxygen-hydroxyl octahedra. In most clay minerals such sheets of tetrahedra and octahedra are superimposed in different fashions.

In the silicon-oxygen sheet, the silicon atoms are coordinated with four oxygen atoms. The oxygen atoms are located on the four corners of a rectangular tetrahedron with the silicon atom at the center (Fig. 3-1a). In the sheet three of the four oxygen atoms of each tetrahedron are shared by three neighboring tetrahedra, (Fig. 3-1b).

forming a hexagonally symmetric sheet. This silicon-oxygen sheet is called the tetrahedral sheet or the silica sheet.

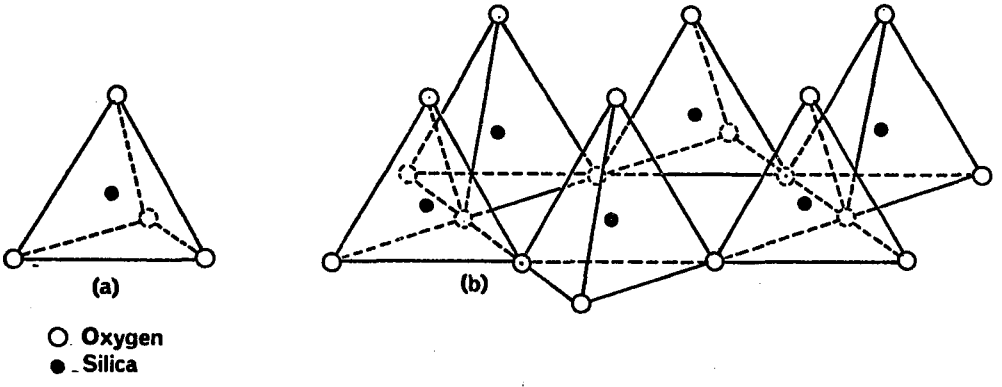

Fig. 3-1 Structure of Tetrahedral Sheet

In the aluminum or magnesium oxygen-hydroxyl sheets, the aluminum or magnesium atoms are coordinated with six oxygen atoms or hydroxyl groups. The oxygen atoms and hydroxyl groups are centered in the six corners of a rectangular octahedron (Fig. 3-2a).

The sharing of oxygen atoms by neighboring octahedrons results in a sheet such as that shown in perspective in Fig. 3-2b. This sheet is called various names including the octahedral sheet, gibbsite (when center atom is aluminum) and brucite (when center atom is magnesium).

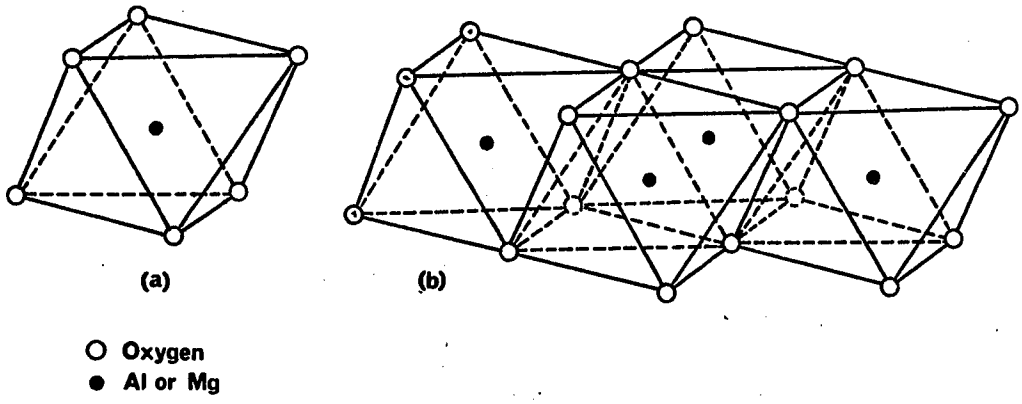

Fig. 3-2 Structure of Octahedral Sheets

The symmetry and almost identical dimensions in the tetrahedral and octahedral sheets allow the sharing of oxygen atoms between these sheets. According to the arrangement of the sheets, clays may be classified in two or three general groups. In Fig. 3-3 structures of these groups are schematically illustrated. They are kaolinite, Montmorilonite and illite. Kaolinite: Because of the unsatisfied valance forces in the upper oxygen atoms of the tetrahedra sheet and the spacing between them, it is possible for an octahedra sheet and a tetrahedra sheet to fit together to produce an electrically neutral layer, which forms a single sheet of the clay mineral Kaolin (Fig. 3-3a). Successive sheets of the crystal lattice may be stacked one on top of the other to form particles of kaolin with the forces holding the

layers together being of the hydrogen bond type between oxygen and hydroxl ions. Different stacking arrangements give rise to the different clay minerals as shown in Fig. 3-3. Although tetrahedra and octahedra sheets are capable of extending indefinitely in the direction of the planes, it is found that kaolin particles generally have a hexagonal shape and occur as plates whose lateral dimensions typically range in size from 0.5 to 1.0 micron and whose thicknesses are about 0.05 micron. Since the unit cell thickness is 7.1 - 7.2 A a particle may be 70 unit cells thick. Variation in sizes may be connected to the imperfections in the crystalline structure and the cleavage between the double sheets.

Montmorillonite: If the tetrahedra and octahedra sheets are arranged as shown in Fig. 3-3b the three-layer primary element of montmorillonite is formed. Different arrangements of primary elements result in polymorphic mineral variations of montmorillonite. In this case the bonds between the elementary sheets are those between oxygen ions, which are weaker compared with those between kaolinite layers. Consequently, water molecules can enter between montmorillonite sheets and cause considerable swelling. Because of the poor bonding between adjacent oxygen layers, montmorillonite sheets typically break into extremely small particles about 0.05 micron wide and having a ratio of width to thickness of up to 400:1.

Illite: Illites consist of the same structural elements as montmorillonites with the exception that potassium ions occupy positions between the adjacent oxygen base planes. The potassium ions bond the two sheets together more firmly than is the case in

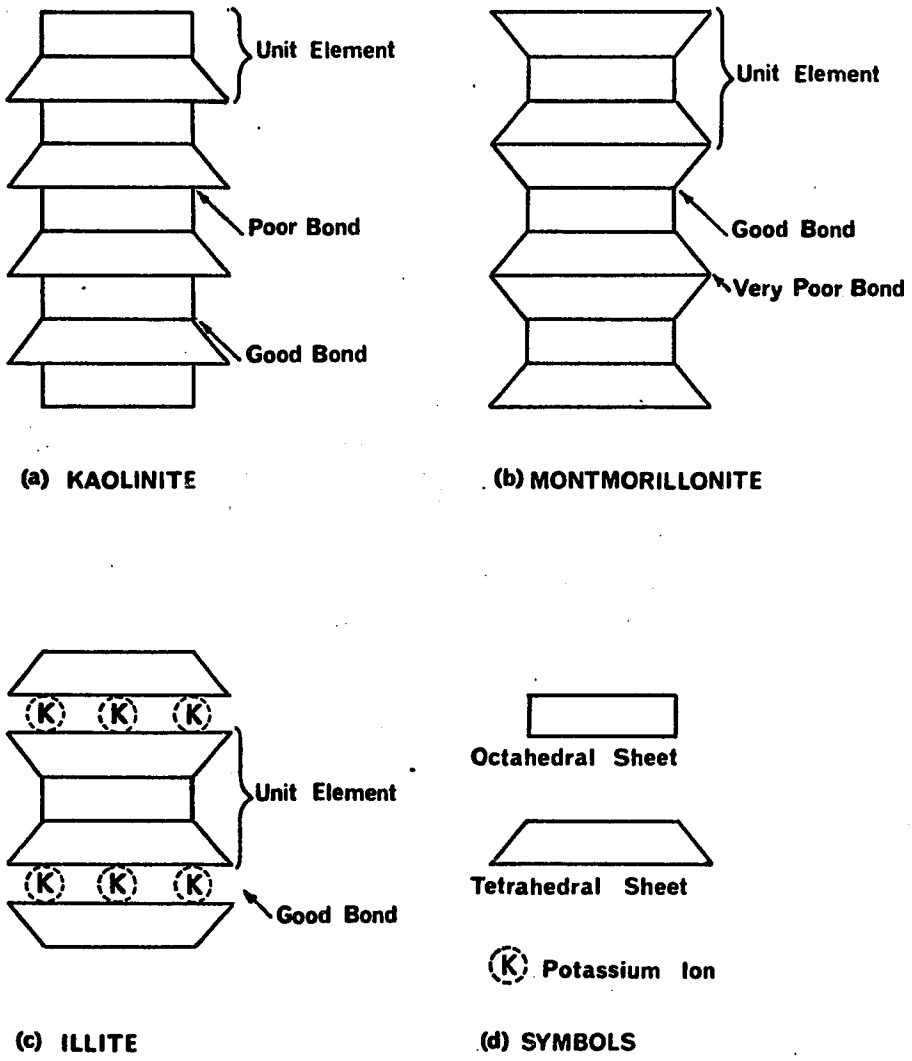

Figure 3-3 Structure of Clay Minerals

montmorillonite, with the result that the lattice is much less susceptible to cleavage and swelling. Typically illite particles have widths of about 0.5 micron, and width to thickness ratios are in the order of 50:1.

3-3 Surface Charge of Clay Particles

The clay minerals do not represent perfect crystals in the strict sense of the word. A perfect crystal is electrically neutral. However, substitution of one ion for another in the clay crystal lattice and imperfections at the surface especially at the edges lead to negative electrical charges on clay particles.

In the tetrahedral sheet, tetravalent silicon is sometimes partially replaced by trivalent aluminum. In the octahedral sheet there may be replacements of trivalent aluminum by divalent magnesium, without completely filling the third vacant octahedral position. Aluminum atoms may also be replaced by iron, lithium and other atoms. Since these atoms are small they can take the place of the silicon and aluminum atoms. This replacement is often referred to as isomorphous substitution.

A second source of electric charge on clay particles is due to unsatisfied charges at the edges of the particles. The amount of this charge per unit weight of clay of a given thickness increases with a decrease in particle size, because the portion of the edge area to total area is increased. Change due to broken bonds would also arise if pieces were broken out of the flat surfaces.

This excess of negative charge on the clay particle is compensated by the adsorption on the surface of cations which are too large to be accommodated in the interior of the lattice. In the presence of water, compensating conditions may easily be exchanged by other cations when available in solution; hence they are called "exchangeable cations". The total amount of these cations may be determined analytically. This amount expressed in milli-equivalents per 100 grams of dry clay is called the cation exchange capacity (CEC) or base exchange capacity (BEC) of the clay.

Since the exchangeable cations compensate the unbalanced charge of the clay particle, CEC may be used as a measure of surface charge density. The typical values of cation exchange capacity for several clays are summarized in Table 3-1. (See Appendix D for the calculation of surface charges.)

GROUP	PARTICLE SHAPE	PARTICLE SIZE	C.E.C. Meg/100 gm	SPECIFIC SURFACE $M^2/3M$
Kaolinite	6-sided flakes	0.1 - 4μ x 0.05 - 2μ	3 - 15	20 - 70
Montmorillonite	flakes (equi-dimensional)	> 10A x up to 10μ	80 - 150	700 ∿ 840
Illite	flakes	0.003 - 0.1μ x up to 10μ	10 - 40	65 ∿ 180

Table 3-1 Properties of Clay Particles

3-4 Electric Double Layer Structure

In the preceding paragraphs it has been shown that the clay crystal lattice carries a net negative charge as a result of isomorphous substitution or imperfections on particle surfaces. The net negative lattice charge is balanced by cations which are located on unit layer surfaces. In the presence of water, the compensating cations, due to their thermal energies, have a tendency to diffuse away from the layer surface since their concentration will be smaller in the bulk solution. On the other hand, they are attracted electrostatically to the charged lattice. The balance of electrical attraction and thermal diffusion leads to diffuse layers of cations with the concentration highest at the surface and gradually decreasing with distance from the surface. Such a distribution of cations is described as an "atmospheric" distribution. This is often called the diffuse double layer, one layer being the negatively charged surface, and the other layer being the diffuse layer of cations balancing the negative charge. More precisely formulated, the diffuse layer does not merely consist of an excess of ions of opposite sign, since simultaneously there is a deficiency of ions of the same sign in the neighborhood of the surface, these ions being electrically repelled by the particle surface charge. In Figs. 3-4a and 3-4b the distribution of negative and positive ions in the neighborhood of negative surface is schematically represented.

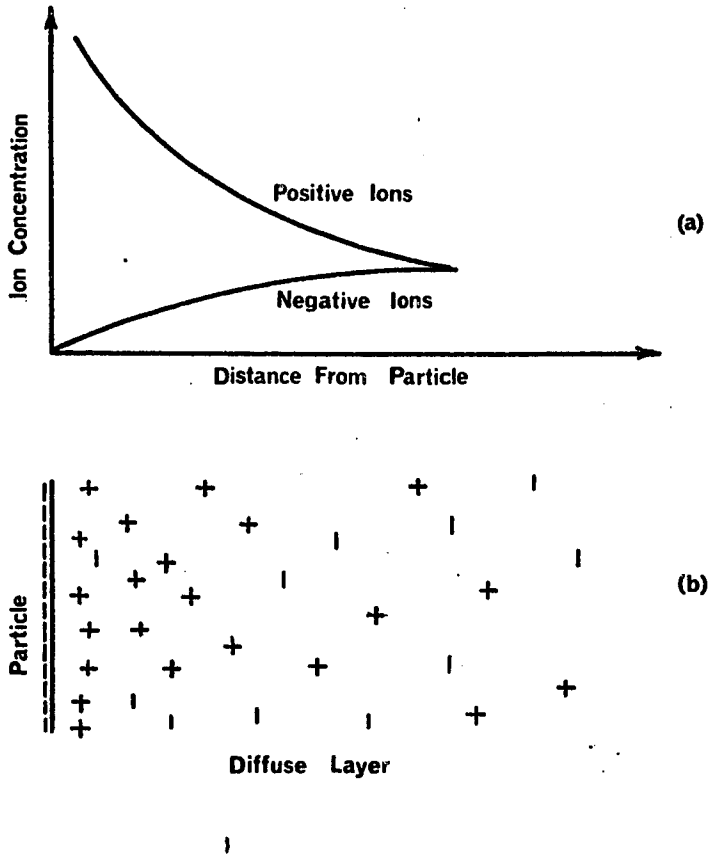

Fig. 3-4 Diffuse Electric Double Layer Model According to Gouy (1910, 1917)

The diffuse character of the counter-ion atmosphere was first recognized by Gouy (1910, 1917), and by Chapman (1913) and a theoretical treatment of counter-ion distribution was presented.

The main assumptions in the derivation of the theoretical distribution of ions in a diffuse layer are 1) that one layer is considered to be a simple charged plate--with a uniform surface charge density distribution--for which the electric field is described by the Poisson equation and 2) the distribution of ions in this field is described by the Boltzmann equation.

With these assumptions, the following differential equation was derived governing the distribution of electrical potential in a double

layer, in three dimensions;

$$\nabla^2\psi = \frac{8\pi n\nu e}{\epsilon} \text{ Sinh } (\nu e\psi/kT) \qquad (1)$$

in which

$$\nabla^2 = (\frac{\partial}{\partial x^2} + \frac{\partial}{\partial y^2} + \frac{\partial}{\partial z^2})$$

ψ = electrical potential

n = ion concentration

e = elementary charge

ν = valance of ions

ϵ = dielectric constant of the medium

T = absolute temperature

k = Boltzmann constant

Due to the non-linearity of the above differential equation, explicit solutions can be obtained only for specialized conditions. Solutions for more general conditions may be obtained through numerical solution techniques.

Of interest in interpreting soil behavior is the ion distribution around a particle. The effect of several system properties on the diffuse double layer is qualitatively represented in Fig. 3-5.

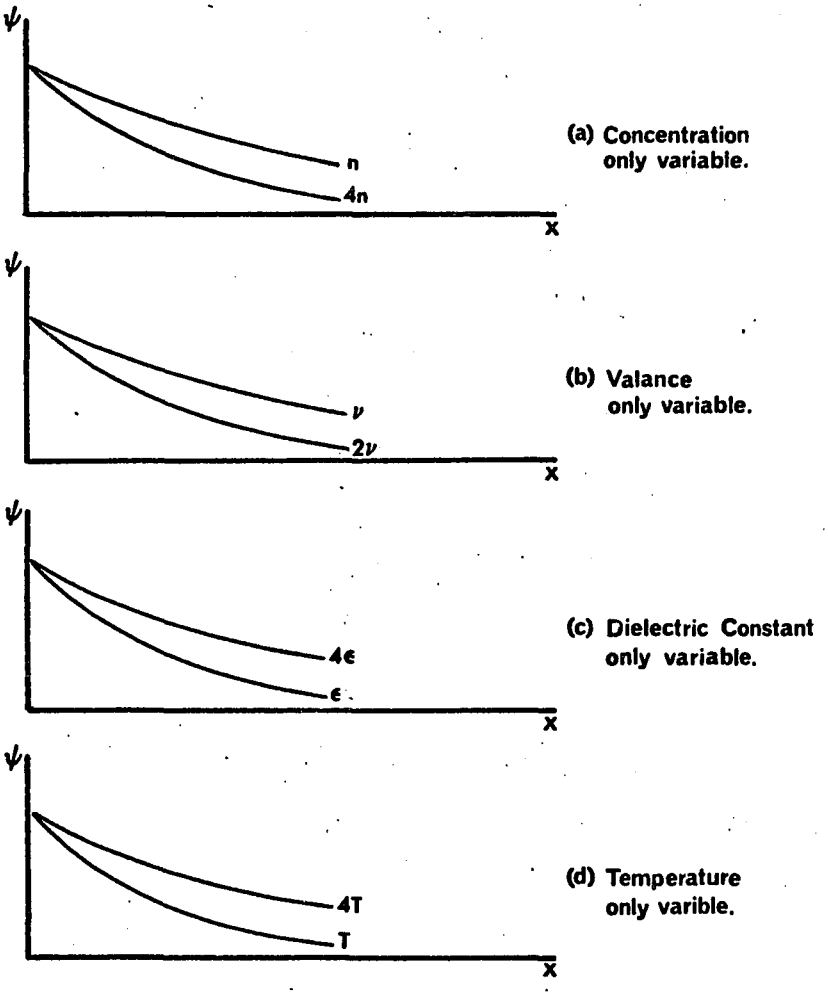

Fig. 3-5 The Effect of Changes in System Properties on Diffuse Double Layer (After Lambe (1958))

A further simplifying assumption in this theory is that ions are assumed to be point charges with negligible dimensions. In diluted solutions where the extension of the diffuse layer is considerable, neglecting the finite dimension of ions is in some degree permissible, but in more concentrated electrolyte solutions, the theory yields unreasonable high concentrations of counter-ions on the surface in view of the finite dimensions of ions. An improvement

was made by Stern (1924) to take the finite dimensions of the ions into consideration.

At the edges of the plates, the tetrahedral silica sheets and the octahedral alumina sheets are disrupted, and primary bonds are broken. Thus the atomic structure of the edge surfaces is entirely different from that of the flat surfaces and there is a good possibility that a different electrical double layer will exist on the edge surfaces.

Several observations support the concept of a positive edge charge. Thiessen (1942) mixed a kaolinite sol and a negative gold sol and prepared an electron micrograph of the mixture. It appears that the small negative sol particles were exclusively absorbed at the edge surface of the large kaolinite plates. This preferred edge attachment of the gold particles is a result of mutual attraction of the negative gold particles and the positive kaolinite edges.

Also supporting the concept of the positive edge charge is the fact that clays show a certain anion adsorption capacity under certain other conditions as well, although this capacity is rather small (van Olphen, 1950).

Olphen (1950), (1951) introduced the concept of positive double layer on the edge surfaces of particles in the interpretation of the stability of montmorillonite suspensions. Later Schofield and Samson (1954) adopted the same hypothesis in the interpretation of flocculation and anion adsorption in kaolinite sols. The fact that the idea that positive charges exist on particle edges can be used to explain the phenomena observed by van Olphen and Schofield and Samson leads indirect support to the idea itself.

3-5 Water in Clays

The water which can be driven off by heating to about 100° to 150°C is referred to as low-temperature water and is the water considered in soil mechanics. The nature of the low-temperature water and the factors that control its characteristics are of great importance since they largely determine the plastic, bonding compaction and other properties of clay materials.

The water lost at low temperatures may be classified into two categories. (1) Pore water: it fills the pore spaces and is free to flow through the pores. (2) Adsorbed water: it has different properties than the pore water. It is generally more dense and more viscous.

Many early workers, including Terzaghi (1928), explained the initially adsorbed water on the basis of the dipole character of the water molecule; the latter possesses positive and negative charges, the centers of which do not coincide. Since the surface of the clay particle is negatively charged, the positive end of the water dipole is strongly attracted to the negative surface, and a layer of strongly bound water is formed on the clay surface. The negative ends of all the water dipoles represent another negative surface and this surface attracts more oriented water molecules. As the thermal effects become more prominent as distance from the surface increases, orientation of the water molecules decreases.

Grim (1953) and many other investigators object to this explanation because the surface charge of clay particles and the charge distribution around a water molecule are not as simple as the explanation

indicates. Macey (1942) pointed out that the clay-mineral surface is not a uniformly charged plane and that the water molecules strictly do not act as little rods with positive and negative ends. Several investigators theorize that the water is bound to the clay surface in crystalline form. Winterkorn (1943) and Macey (1942) suggest that the adsorbed water film has the structure of ice.

While the clay mineralogists do not agree about the details of the configuration of the adsorbed water, they do agree that there is a definite configuration. This is the important fact to soil mechanics.

3-6 Interparticle Forces

Repulsive Forces: There are mainly two sources of repulsive forces which act between clay particles:

1. Repulsion may result from interpenetration of double layers of adjacent particles. This force acting between adjacent particles may be calculated based on the ion distribution in the interacting double layers of particles. The intensity of potential and ion-distribution is described by the Gouy-Chapman double layer theory. At the planes where electrical field forces are zero, ion concentration exceeds that of the bulk solution and a swelling pressure analogous to an osmotic pressure is exerted between clay particles. The precedure for calculating these forces will be discussed in detail in Section 5-4. Intensity of these forces depend on orientation and distance between particles, concentration and valance of ions, surface charge density of clay particles, dielectric constant of the fluid between the particles,

and temperature.

2. The second source of repulsive force acting between clay particles is due to the adsorption of water molecules on the surfaces of adjacent particles. This force may be visualized as being due to water attracted to the space between the particles forcing them apart. The repulsion arising from adsorbed water cannot yet be quantitatively specified. But it apparently has little effect to the total repulsive pressure, since the experimentally determined swelling pressures--which are due to repulsive pressure between the particles--can be theoretically accounted for just by the repulsion resulting from diffuse ion-layer interpenetration (Bolt, 1956).

Attractive forces: The attractive forces between clay particles have been attributed largely to Van der Waals' forces (Verwey and Overbeck, 1948)(Lambe, 1953). As a result of the movements of electrons in their orbits around atoms any molecule possesses an associated electrical field which is capable of interacting with the field of nearby molecules to give rise to an attractive force between the molecules. This force between the atoms is inversely proportional to the seventh power of distance, which means a rather rapid decay with increasing distance.

On the basis of this theory the attractive force between particles may be calculated approximately by the summation of the attractive forces for all atomic pairs formed by two atoms belonging to different particles.

If the medium between the plates is not a vacuum, the Van der Waal's forces will also depend on the dielectric constant of the separating medium. However, if water is the medium, it is generally considered that no variation in the attractive force will arise from minor changes in the constitution of the water, such as alterations in its electrolytic concentration, provided that only low concentrations are involved.

4 - VOLUME CHANGE AND STRUCTURAL CHARACTERISTICS OF CLAY

The preceding chapter dealt with the physico-chemical properties of clay particles such as mineralogical structure inter-particle forces and properties of absorbed water. In this chapter the volume change characteristics of clay water systems will be examined, with an attempt to relate the consolidation behavior to the structure of assemblies of particles and to their physico-chemical properties.

When a soil mass is subjected to an external loading it will deform. In granular soils this deformation is termed compression. In clay soils due to the time dependency of the compression response, the term consolidation is used to distinguish this type of compression. In fully saturated clays application of an external loading will generate pore-pressures in the system; with the dissipation of pore pressure, the applied stresses are fully sustained by the particle structure matrix; however, the particles are still surrounded by absorbed water. The process of reaching this ultimate state of zero pore pressure is called consolidation or primary consolidation. However, this state is not the full extent of the compressibility of the clay under load since a further compression takes place with time under the same loading. This further compression is termed secondary consolidation.

In this text the term consolidation will be used to indicate the relationship between void ratio and ultimate pressure (i.e., the inter-granular pressure at which the pore pressure is zero in the primary consolidation stage).

4-1 Volume Change Characteristics of Clay

The experimental results obtained from standard one-dimensional consolidation tests in the laboratory may be evaluated in terms of the decrease in void ratio resulting from an increase in pressure. The general form used for graphical representation is the e-log P relationship shown in Fig. (4-1).

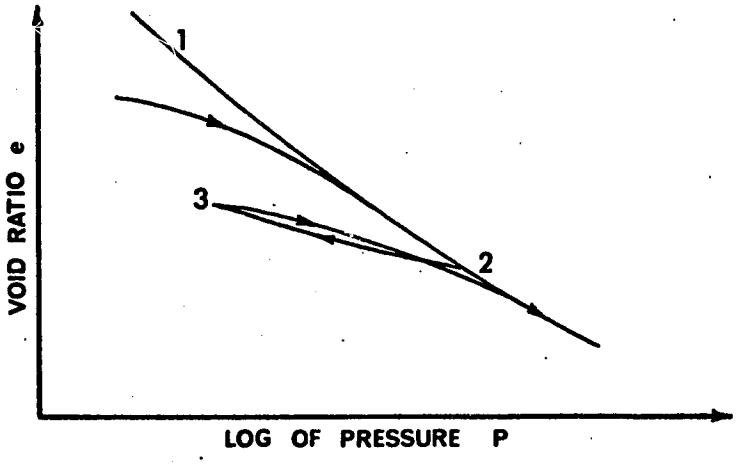

Fig. (4-1) Typical Consolidation Curve for a Clay

In soil mechanics the initial compression curve (curve 1-2 in Fig. 4-1) is referred to as the "virgin" compression curve and curve 2-3 as the rebound curve.

In most clay soils, the particles are arranged in a random fashion according to the mode and conditions of deposition of the material and the subsequent distortions of the soil due to different imposed stresses. The position of the virgin consolidation curve is related to the structure

of the soil (Casagrande, 1932; Mitchell, 1956) being lower as the soil particles are more nearly parallel.

When a randomly oriented clay is subjected to a compressive stress system deformations will occur, due in part to the approach of parallel clay particles under stress and in part to reorientation and elastic compression of the particles. From a purely mechanical point of view, upon removal of the externally applied stresses no mechanism other than possible bending of clay particles or elastic interactions at points of contact exists for the return of the oriented particles to their original positions. This argument gives a purely mechanical explanation for the difference between the initial compression and the rebound curves. This approach has been objected to by Salas and Serratosa (1953) and others, on the grounds that it does not explain the large changes in the positions of the curves due to changes in pore water electrolyte concentration, pore fluid, etc.

The effect of physico-chemical variables on the consolidation characteristics of clay has received considerable attention.

Bolt (1956) for example, utilizing clays of particle size less than 0.2 micron to magnify the effects of the physico-chemical variables, carried out a very careful study of the compressibility of clays. From Gouy-Chapmann double-layer theory a relationship was obtained between particle separation distance and the concentration of cations in the central plane between the particles. Swelling pressure was determined according to van Hoff's equation based on the difference between the central plane and bulk solution cation concentration. By assuming infinitely large parallel plates void ratio was expressed in terms of

distance between the particles, specific surface and density of particles. Using the above expressions a void ratio-swelling pressure relationship was established. The findings of Bolt are illustrated on Fig. (4-2). Apart from the restrictions mentioned above in the expression given by Bolt no account is made for the Van der Waals forces. Even if the validity of the theories involved are accepted, the soil samples prepared in the laboratory will depart from the theoretical model in one or two important respects. 1) The plates of mineral will not all be flat on the surface since electron photographs (Bolt 1956) indicate that minerals are terraced, so that the thickness of a particle will vary from place to place, rendering the relation of void ratio to specific surface only approximately true. 2) Unless the settling particles are deliberately oriented, say by an electric field (Marshall 1949), or by application of large shearing deformations when the sample is prepared from a paste of soil, there will be some random orientation of the particles in the soil. As pointed out by Bolt a parallel arrangement of particles represents a minimum energy condition and, therefore, is a preferred configuration. Hence a major proportion of the particles in a soil may be oriented with the plane of plates normal to the direction of stressing by repeatedly loading and unloading the sample.

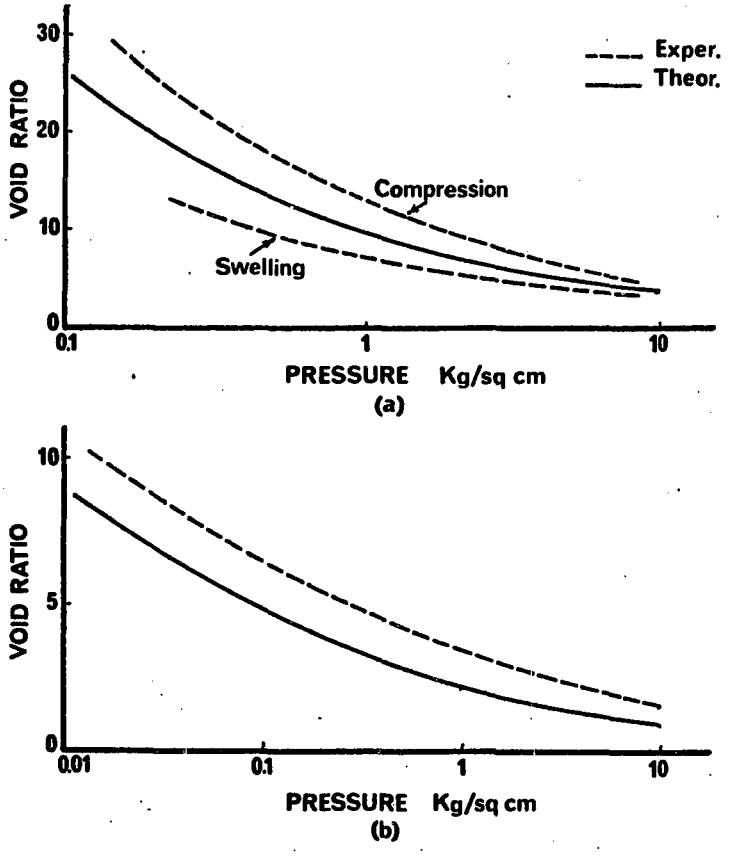

Fig. 4-2 Compression Void Ratio Relationships
(a) Sodium Montmorillonite
(b) Sodium Illite After Bolt (1956)

Bolt's results are given in Fig. (4-2a) and (4-2b) for sodium montmorillonite and sodium illite, respectively.

The comparison of the theoretical curves with the experimental results is seen to be fairly good, except that although the theory predicts only one curve for loading and unloading, separate e log P relationships exist for these two phenomena. This discrepancy was recognized by Bolt who commented, "It still has to be explained why the decompression curve is not identical with the theoretical curve."

It was also reported that the recompression curve follows almost exactly the same pattern as the decompression.

Further tests of this type have been performed by Bolt and Miller (1955), Warkentin, Bolt and Miller (1957), and Yong and Warkentin (1959). Samuels (1950) performed a series of one-dimensional consolidation tests on homoionic bentonite and kaolinite and obtained both e log P curves and permeability data. Samuels was unable to perform chemical analysis and so could not determine the salt concentration in the pore water. Salas and Serratosa (1953) performed one-dimensional tests on homoionic bentonite and kaolin, using water and other fluids in the pores. Wai d elich (1957) performed a comprehensive series of consolidation tests on bentonite and kaolinite using seven different pore fluids.

Many of the above studies have suffered from certain defects: (1) the mineralogy of the soils was either inadequately defined or too complex to yield meaningful results; (2) chemical analyses were not performed to substantiate the assumptions regarding the purity, pore water salt concentration, etc.; (3) chemical preparation procedures were so harsh that the properties of the clays were altered (e.g., by long electrodialysis or acid treatment; (4) the effect of soil structure was not recognized.

Olson and Mitromoyas (1962) have conducted several one-dimensional consolidation tests on <2μ fraction of homoionic Ca and Mg illite with different pore water electrolyte concentrations. Samples were prepared by sedimenting from a dilute suspension and by preparing paste at different molding water contents. It was assumed that different

initial molding water contents would affect the geometrical arrangement of the soil particles, introducing the effect of soil structure into the e log P relationships.

Experimentally obtained e log P relationships were compared with the theoretical e log P relationships obtained by Bolt (1956) based on Gouy-Chapmann double layer theory. The correlation between the theoretical relationships and experimental results was poor. Several factors assumed to contribute to the difference. (1) The terraced nature of the illite particles. (2) Possible non-parallel arrangement of particles. (During sample preparation no specific measure was taken to insure initial parallel arrangement of particles. It was assumed that high consolidation pressures reaching up to 64,000 psf would induce parallel arrangement of particles.) (3) The assumption of negligible void volume between the edges of the particles.

From this study it was concluded that the double layer phenomena seems to exert a smaller influence in explaining compressibility characteristics of clay than the classical approach where the compression characteristics are explained by elastic bending (reversible), slippage (partially reversible) and rupture (irreversible) of particles.

In flocculated soils, where edge to face orientations predominate the particle arrangements, compressibility analyses are less readily performed. Such a soil may be considered to act as an indeterminate three-dimensional structure whose members are of random lengths, randomly arranged and in which the joint reactions are unknown. The application of stresses to such an arrangement will cause joint rotations

and joint displacements since at some point one clay platelet will slide over another's surface under the action of microstresses, and bending of the plates will occur. It is possible that the rotation of joints might take place elastically, and therefore be reversible; on the basis of some experiments on soil gels it seems more reasonable to consider such joints as rigid or plastic. Van Olphen (1951) showed that at normal values of pH, attraction forces result from the different charges on the faces (negative) and the edges (positive). Measuring the yield stress of clay gels, Van Olphen (1956) concluded that the strength of a single edge to face bond is in the order of 10^4 dyne. Rausel and Colom (1958), on a theoretical basis, found the magnitude of electrostatic attraction between the face of a montmorillonite and the unit charge on a contact edge to be in the order of 7×10^{-5} dyne. Although some data (based on electrostatic forces) is available on the moment-rotation relationship of edge to face orientation of particles, determining the forces resisting the movement of the edge of a particle over the face of another is beyond the scope of this analysis. This is due to the frictional characteristic of absorbed water, or possibly the friction forces between the minerals. As these bond strengths are overcome by local stresses the particles undergo largely irreversible displacements. Conceivably, the bending of clay plates would result in elastic deformations which would disappear on the removal of load. Although it is not known to what extent any of these mechanisms predominate over the others, it seems reasonable to assume that the double-layer repulsive forces active in a dispersed clay between parallel plates are less predominant in a flocculated soil.

This brief discussion consequently indicates that, with the exception of very special cases involving ideal packing of uniform particles, detailed evaluation of contact forces and strengths within a skeleton of soil particles and the quantitative evaluation of physico-chemical forces are very complex tasks at the present time.

Systematic study of mechanical behavior of flocculated clay received very little attention due to the several complexities involved in such a system. Geuze (1966) and Geuze and Rebull (1968) studied the mechanical behavior of flocculated clay based on an idealized model of clay particles; a symmetrical parallelogram formed by four typical clay particles was taken as a representative unit of a flocculated clay and the deformation properties of this model unit were studied based on Gouy-Chapmann double layer theory. Although the general pattern of behavior of the model unit was found to be compatible with the mechanical behavior of clay, no specific comparison was made between the predicted and observed behavior, such as comparison of e log P relationships, etc.

4-2 Clay Particle Structure

The arrangement of soil particles influences the response behavior of the soil, i.e., response of the soil to an external set of constraints. The arrangement of soil particles is generally defined as the structure of the soil. Clay formations may result from chemical and physical weathering and the particle structure depends on the process of formation. One of the main processes by which clay formations are created is sedimentation. Another process is the weathering of rock and gravel to form residual soils. No quantitative measure has yet

been devised to describe structure precisely, though Mitchell (1956), using light scattering techniques, established experimental procedures to differentiate between different soil structures.

Qualitatively, clay soil structures are generally classified as flocculated and dispersed. Idealized pictures of these structures are shown in Fig. 4-3a and b.

Studies with electron microscope, (Marshall 1964), light scattering techniques (McEwen and Mould 1950), and indirect studies such as swelling properties (Emerson 1962, 1963), sensitivity studies on marine clays (Rosengvist 1959), and study of cohesion in clays (Michaels 1959), contributed to the better understanding of clay particle structures.

The structure of natural soils is the net product of the interaction between the forces of sedimentation, surface forces between the soil particles, and subsequent geologic forces.

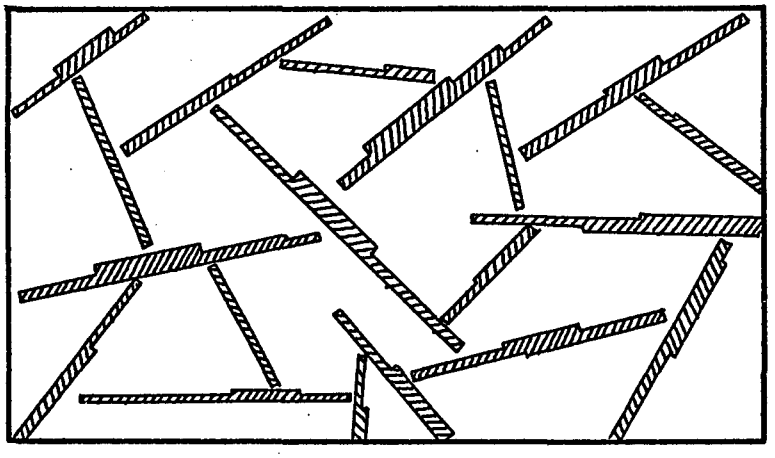

Fig. 4-3a Hypothesized Flocculate Structure in Clays (From Hough, 1969)

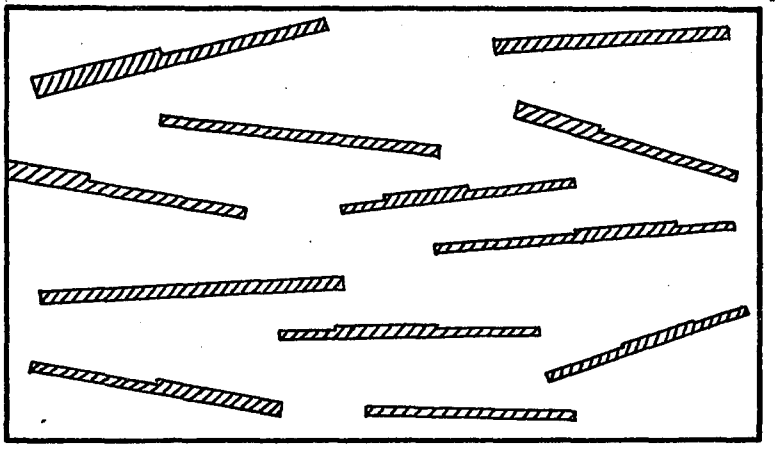

Fig. 4-3b Hypothesized Dispersed Structure in Clays (From Hough, 1969)

There are mainly three modes by which one particle can approach another face to face, edge to face, and edge to edge. Certain types of interparticle forces or environmental conditions may favor a given particle association. Consequently, the three types of association will not necessarily occur similtaneously or to the same extent. Predominate repulsive forces between the particles will result in face to face association between the particles, forming a dispersed structure. External forces may affect the particle structure; for example, a shearing action promotes parallel orientation. Edge to face association will result in a flocculated clay structure. Such an association occurs under the condition when electrostatic forces between oppositely changed edge and face of the particle and Van der Waal attractive forces are greater than repulsive forces.

4-3 Present State of Knowledge

The phenomena of compression and rebound of soil specimens are explained on the basis of two different mechanisms. The mechanical

concept involving the hypothesis of a shape and arrangement of clay particles susceptible to elastic deformations gives a qualitative explanation for the deformation characteristics of flocculated clays. But for a dispersed structure it fails to explain the compressibility phenomenon. On the other hand, compressibility of dispersed structures can be accounted for quantitatively by the consideration of the physico-chemical interaction forces between the clay particles.

Experience has shown that the relation between load and void ratio of a clay is highly dependent on the previous history of the loadings. When the existing stresses in the clay are less than any previously applied stress level, clay behaves more elastically and is fairly compressible. But when the highest stress level is exceeded irreversible deformations take place and compressibility of the clay decreases. Such stress history dependent behavior of clay is not explained by the previous investigations.

Although two different mechanisms of resistance against deformation are fairly well defined, for most of the cases it is very difficult to decide a priori which portion of compressibility of a clay soil is due to the mechanical properties of its constituents and which portion to the interaction between the soil particles.

5 - A MODEL FOR A CLAY PARTICLE SYSTEM

Clay particles are prescribed by the clay mineral concept to be crystalline fragments of a limited group of fairly well-defined minerals known as the clay minerals. They are all hydrous-alumino silicates and have layer-lattice structures such that they form extended flat sheets. Isomorphous substitutions in the clay lattice result in excess negative charge, and this charge is balanced by exchangeable ions. The ions diffuse and redistribute about the clay particles in the presence of water. Repulsion is generated by the diffuse ion layers resisting interpenetration. The extension of the diffuse layer is inversely dependent on the ion concentration and valence, for as these increase, charge balance is achieved closer to the particle surface. The double layer forces are thus the critical factor in determining the mechanical behavior of clays.

5-1 Model System Geometry

Natural clays consist of a diversity of shapes and sizes of particles, and in general, these may occur in a variety of positions and orientations in clay deposits. Different types of structure may result from both internal conditions and external constraints. As loads are imposed on a clay body, the geometry of the particle structure will change to a new state of equilibrium. The problem must be simplified in order to analyze the interparticle forces for different states of equilibrium. In this analysis, montmorillonite clay particles are idealized as two-dimensional sheets, 10 $\mathring{A}$ thick, 250 $\mathring{A}$ wide and infinitely long in the third direction. The surface charge is assumed to be uniformly

distributed over each particle. The postulated particle system consists of a two-dimensional symmetrical array of identical particles arranged as shown in Fig. 5-1. Considering a unit thickness of the material, the particles are arranged in a simple two-dimensional network such that the particles are located at the intersections of the grid. The grid spacings $\bar{x}$ and $\bar{y}$ may then be varied and the repulsive forces acting between the particles can be calculated for each set of values of $\bar{x}$ and $\bar{y}$.

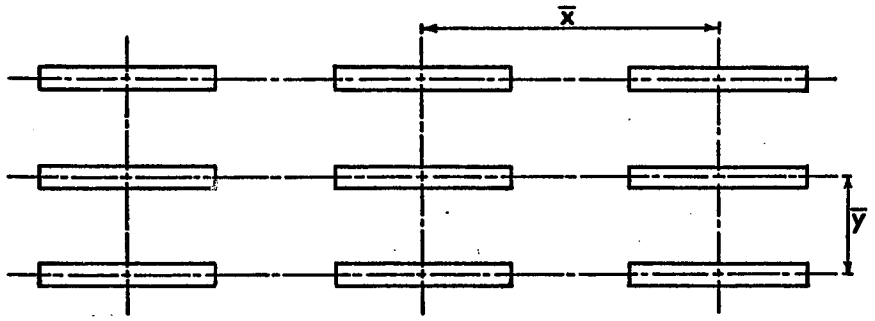

Fig. 5-1 Idealized Clay Particle System

In idealizing the clay particle system, repulsive forces are considered to be the factor which defines the geometrical arrangement of the particles. It can be shown that, when repulsion is the predominate force acting between clay particles, parallel orientation is the stable equilibrium configuration. Consider the particle B shown in Fig. 5a and b. (In the Fig. 5-2, particles A and C are assumed to be held in position externally and particle B is free to move.)

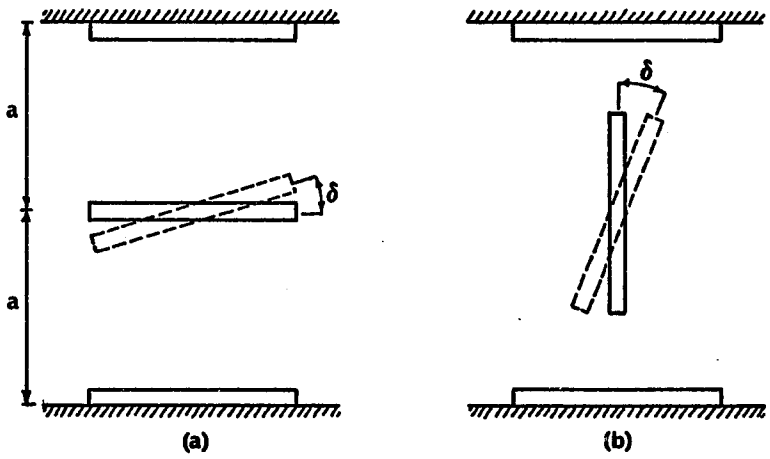

Fig. 5-2 Particle Orientations

In the case shown in Fig. 5-2a , when the particle B is rotated through an angle δ---remembering that the repulsive pressure between the particles are inversely proportional to the distance---the repulsive pressure towards the edge of the particle will be greater than the mean pressure, causing an unbalanced moment acting against the rotation. This moment will try to restore the system's original configuration. If a particle is rotated into the vertical position as shown in Fig. 5-2b it will be in unstable equilibrium. A small disturbance will cause the system's configuration to depart from the vertical position and the particle will rotate into the parallel arrangement. Thus the parallel orientation is the stable equilibrium position.

5-2 Electric Double Layer Theory

Evaluation of repulsive pressures between particles requires determination of the distribution of ions about the particles; this

distribution is governed by the electric double layer theory. This theory is developed below:

Consider a plane surface bearing a uniform negative charge density, in contact with a solution phase containing positive and negative ions. The positive ions of the double layer are subjected to two different tendencies. Electrostatic forces attract them to the charged surface, where as diffusion tends to bring them away from the surface toward the equilibrium solution, where their concentration is smaller. Simultaneously negative ions are repelled by the surface and the back-diffusion from the equilibrium solution toward the surface counteracts the electric repulsion. The electrical potential at the surface is taken to be ϕ_o and decreases away from the surface in a manner to be determined. At any point the electrical potential determines the potential energy $\nu e\phi$ of the ion in the electrical field, where ν is the valence of the ion and e is the charge on the electron. The probability of finding an ion at some particular point will then be proportional to the Boltzmann factor $e^{-\nu e\phi/kT}$, the situation being somewhat analogous to that of a gas in a gravitational field where the potential is mgh and the variation in concentration with altitude is then given by

$$n = n_o e^{-mgh/kT} \qquad (5\text{-}1)$$

where n_o is the concentration at zero altitude.

For the case of an electrode solution consisting of two kinds of ions of equal and opposite charge, $-\nu$ and $+\nu$

$$n^- = n_o e^{\nu e\phi/kT} \qquad n^+ = n_o e^{-\nu e\phi/kT} \tag{5-2}$$

The net charge density at any point is given by

$$\rho = \nu e(n^+ - n^-) = -2n_o \nu e \, \mathrm{Sinh}\,(\nu e\phi/kT) \tag{5-3}$$

where n_o now is the ion concentration in the bulk solution away from the effect of the electrical field.

Introducing Poisson's equation which relates the divergence of the gradient of the electrical potential at a given point to the charge density at that point.

$$\nabla^2\phi = -\frac{4\pi\rho}{\epsilon} \tag{5-4}$$

Where ∇^2 is Laplace operator $(\frac{\partial^2}{\partial u^2} + \frac{\partial^2}{\partial v^2} + \frac{\partial^2}{\partial w^2})$ and ϵ is the dielectric constant of the medium, and substituting the Eq. (5-3) in Eq. (5-4) the fundamental differential equation is obtained.

$$\nabla^2\phi = \frac{8\pi n \nu e}{\epsilon} \, \mathrm{Sinh}\,(\frac{\nu e\phi}{kT}) \tag{5-5}$$

By introducing the following substitution:

$$\psi = \frac{\nu e\phi}{kT} \quad \kappa^2 = \frac{8\pi n e^2 \nu^2}{\epsilon kT} \quad x = \kappa v \quad y = \kappa v \tag{5-6}$$

The fundamental differential Eq. (5-5) for a two-dimensional case is brought into the simple form

$$\frac{\partial^2\psi}{\partial x^2} + \frac{\partial^2\psi}{\partial y^2} = \mathrm{Sinh}\ \psi \tag{5-7}$$

5-3 Boundary Conditions

Advantage may be taken of the symmetry of the system by subdividing it so that only the smallest element composing the system need be analyzed. Appropriate subdivisions are shown in Fig. 5-3a and the

typical element in Fig. 5-3b . The fundamental differential equation is solved over this element by using a finite element numerical technique. The details of the numerical technique used for the solution are discussed in detail in the following chapter.

The gradient of the potential function normal to the lines of symmetry between particles must be zero in order to fulfill the laws of symmetry. These constitute the boundary conditions for the boundaries of the element which are not on the particle surface. See Fig. 5-3b . The boundary condition along the surface of the particle is defined by the postulate of uniform negative charge on the clay particle. The charge on the surface of the particle is proportional to the negative value of the normal potential gradient, i.e.,

$$\sigma = - \frac{\varepsilon \bar{u}}{4\pi L} \left(\frac{\partial \phi}{\partial v}\right)_s \qquad (5\text{-}8)$$

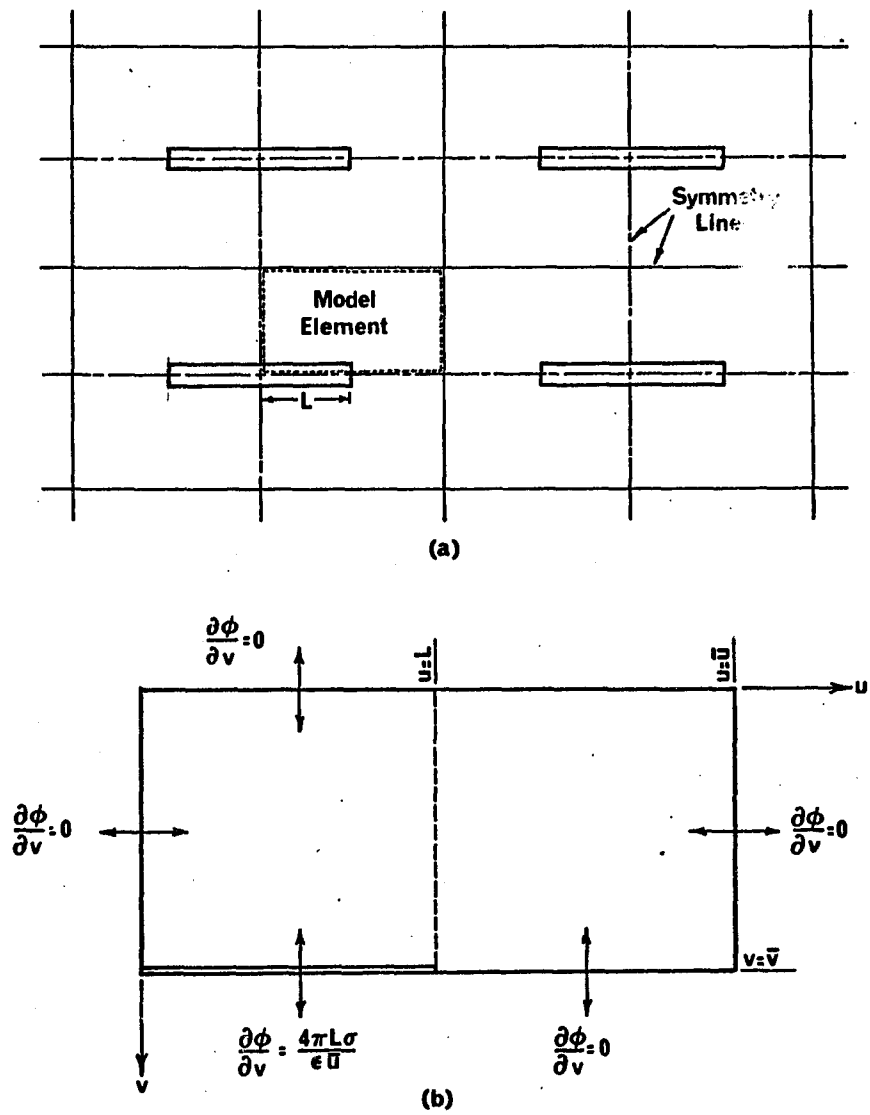

Fig. 5-3 Model Element and Boundary Conditions

where

σ = surface charge density.

$(\frac{\partial\phi}{\partial v})_s$ = potential gradient at the surface of the particle.

This relationship may be derived from the surface charge-space charge equivalency. Equating the integral of space charge density over the domain shown in Fig. 5-3b to the surface charge, σL,

$$\sigma L = - \int_{v=0}^{v=\bar{v}} \left| \int_{u=0}^{u=L} \rho du + \int_{u=L}^{u=\bar{u}} \rho du \right| dv \qquad (5\text{-}9)$$

where σL is total surface charge.

Substituting ρ from Eq. (5-4) into Eq. (5-9)

$$\sigma L = - \frac{\varepsilon}{4\pi} \int_{v=0}^{v=\bar{v}} \left| \int_{u=0}^{u=L} \left(\frac{\partial^2\phi}{\partial u^2} + \frac{\partial^2\phi}{\partial v^2}\right) du + \int_{u=L}^{u=\bar{u}} \left(\frac{\partial^2\phi}{\partial u^2} + \frac{\partial^2\phi}{\partial v^2}\right) du \right| dv \qquad (5\text{-}10)$$

$$\sigma L = - \frac{\varepsilon}{4\pi} \int_{v=0}^{v=\bar{v}} \left| \int_{u=0}^{u=L} \frac{\partial^2\phi}{\partial u^2} du + \int_{u=0}^{u=L} \frac{\partial^2\phi}{\partial v^2} du + \int_{u=L}^{u=\bar{u}} \frac{\partial^2\phi}{\partial u^2} du + \int_{u=L}^{u=\bar{u}} \frac{\partial^2\phi}{\partial v^2} du \right| dv \qquad (5\text{-}11)$$

Integrating with respect to u and using the boundary condition shown in Fig. 5-3b

$$\sigma L = - \frac{\varepsilon}{4\pi} \int_{v=0}^{v=\bar{v}} \left| \frac{\partial\phi}{\partial u}\Big|_{u=L} + \frac{\partial^2\phi}{\partial v^2} L - \frac{\partial\phi}{\partial u}\Big|_{u=L} + \frac{\partial^2\phi}{\partial v^2} \bar{u} - \frac{\partial^2\phi}{\partial v^2} L \right| dv. \qquad (5\text{-}12)$$

Simplifying

$$\sigma L = - \frac{\varepsilon}{4\pi} \int_{v=0}^{v=\bar{v}} \frac{\partial^2\phi}{\partial v^2} \bar{u} \, dv$$

Integrating with respect to v and introducing the boundary conditions

$$\sigma = - \frac{\varepsilon \bar{u}}{4\pi L} \left(\frac{\partial\phi}{\partial v} \right)_s . \qquad (5\text{-}13)$$

Equation (5-13) may be expressed in terms of a non-dimensional potential and coordinate system as follows:

$$\sigma = \frac{\tilde{u}}{L} \left| \frac{\varepsilon n k T}{2\pi} \right|^{1/2} \left(\frac{\partial \psi}{\partial y}\right)_s \qquad (5\text{-}14)$$

The boundary condition along the surface of the particles is defined by the postulate of a uniform negative charge, since on the surface the negative value of the potential gradient is proportional to the charge.

5-4 Pressure Distribution

The pressure distribution within the element is found from the equilibrium condition that at every point of the solution phase the gradient of the liquid pressure balances the force on the space charge. In two-dimensional space, the equilibrium condition becomes

$$\frac{\partial P}{\partial u} = - \rho \frac{\partial \psi}{\partial u}$$

and (5-15)

$$\frac{\partial P}{\partial v} = - \rho \frac{\partial \psi}{\partial v}$$

from which it is evident that the electromechanical force-field pressures in the fluid may have different values in the different directions.

This equation arises from the fact that the charge distribution cannot possibly be maintained in static equilibrium under the action of electrical forces alone. The equilibrium must be established with mechanical forces of some other type, and the only ones available in the element are through the liquid pressure.

These pressures within the solution phase are balanced by the electrical forces and do not contribute to the forces acting between the particles.

When two clay particles approach so closely that their diffuse layers interact the ion concentration at the central planes (lines a-a

and b-b in Fig. 5-3a) will exceed that of bulk solution. The potential gradients normal to these central planes are zero; therefore, no electric forces are acting normal to these planes. This implies that in a clay system, in equilibrium with an electrolyte solution situated outside the range of influence of the clay particles' electrical fields, the hydrostatic pressure in the central plane acts as a net pressure pushing the particles apart. The "swelling pressure", therefore, equals the difference between the osmotic pressure in the central phases and the osmotic pressure in the bulk solution. Thus the swelling pressure of the system is caused by the tendency of the liquid phase to re-enter the system.

The swelling pressure between two particles can be derived directly from the ionic concentration on the control planes: Following the derivation by Langmuir (1938). The excess ion concentration at a point on a central plane is given by

$$(e^{\psi_o} - 1) + (e^{-\psi_o} - 1) = 2n(\text{Cosh}\ \psi_o - 1) \qquad (5\text{-}16)$$

where ψ_o is non-dimensional potential at a point on a central plane.

Using van Hoff's osmotic pressure equation, the pressure acting along the central planes

$$P = 2n\ kT(\text{Cosh}\ \psi_o - 1) \qquad (5\text{-}17)$$

5-5 Summary of Chapter

Differential equation governing the variation of potential in non-dimensional form is:

$$\frac{\partial^2\psi}{\partial x^2} + \frac{\partial^2\psi}{\partial y^2} = \text{Sinh}\ \psi$$

The boundary conditions for the problem are the normal gradients as shown in Fig. 5-3b.

A numerical solution to the problem defined by the above equation and boundary conditions is developed in the next chapter.

6 - PROCEDURE FOR CALCULATING VOLUME-CHANGE CHARACTERISTICS OF MODEL

6-1 Finite Element Solution of Poisson-Boltzmann Equation

Advances in the finite element methods of solution of elasticity problems and recognition that this procedure, originally introduced as a method of direct structural analysis, can in fact be interpreted in terms of variational procedures (as the minimization of a functional) leads to its extension to other boundary value field problems.

If the unknown function can be uniquely specified throughout the field by a discrete number of its values associated with specified nodal points of the region (which divide it into polygonal elements), and if, in addition, the value of the function at a particular node influences the function only in the adjacent polygon elements, then the minimization of the functional throughout the whole region (with respect to these nodal values treated as parameters) results in a series of simultaneous equations, the solution of which gives an approximate solution to the original problem.

Unlike the well-known finite difference method which directly approximates the differential equation, the finite element method is an approximation applied to the variational formulation terms. The freedom of choice of the shape and size of elements, and the ease of treating irregular boundaries make the finite element method more versatile.

Mathematical Problem

The non-dimensionalized Poisson-Boltzmann equation has the following form:

$$\frac{\partial^2\psi}{\partial x^2} + \frac{\partial^2\psi}{\partial y^2} - \text{Sinh}\ \psi = 0 \qquad (6\text{-}1)$$

and with the boundary conditions (usually given in terms of known values of ψ or its normal gradient) the problem is specified in a unique manner. However, an alternative formulation is possible with the aid of the calculus of variations. The well-known Euler Theorem, Berg (1962), states that if the integral

$$I(\psi) = \int\int f(x, y, \psi, \frac{\partial\psi}{\partial x}\ \frac{\partial\psi}{\partial y})\ dx\ dy$$

is to be minimized, then the necessary and sufficient condition for this minimum to be reached is that the unknown function $\psi(x,y)$ should satisfy the following differential equation

$$\frac{\partial}{\partial x}\left|\frac{\partial f}{\partial(\partial\psi/\partial x)}\right| + \frac{\partial}{\partial y}\left|\frac{\partial f}{\partial(\partial\psi/\partial y)}\right| - \frac{\partial f}{\partial\psi} = 0$$

within the same region, provided $\psi(n,y)$ satisfies the same boundary conditions in both cases.

It can be verified (Berg,1962) that in the case of Eq. (6-1), the equivalent formulation to that of the Poisson-Boltzmann equation is the requirement that the integral given below and taken over the whole region, should be minimized;

$$\chi = \int\int_R \left| \frac{1}{2}\left(\frac{\partial\psi}{\partial x}\right)^2 + \frac{1}{2}\left(\frac{\partial\psi}{\partial y}\right)^2 + \text{Cosh}\ \psi \right| dxdy \qquad (6\text{-}2)$$

subject to the same boundary conditions.

Finite Element and Nodal Values

The region in which the problem is to be solved is divided into small, triangular elements as shown in Fig. 6-1 . Considering a typical triangle defined by the nodes, i, j, and k, the function may

be approximated over the triangle by a linear function defined uniquely by the nodal values of the function ψ_i, ψ_j and ψ_k.

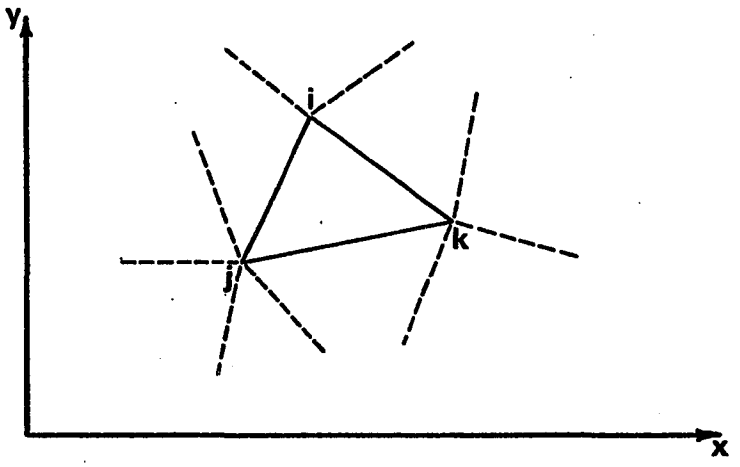

Fig. 6-1 Division of Region into Trangular Elements

Thus within the element

$$\psi = [(a_i + b_i x + c_i y)\ \psi_i + (a_j + b_j x + c_j y)\ \psi_j$$

$$(a_k + b_k x + c_k y)\ \psi_k]/2\Delta$$

in which

$$2\Delta = \det \begin{vmatrix} 1 & x_i & y_i \\ 1 & x_j & y_j \\ 1 & x_k & y_k \end{vmatrix} = 2x \text{ area of triangle ijk}$$

and

$$a_i = x_k y_i - x_j y_k$$

$$b_i = y_k - y_i$$

$$c_i = x_j - x_k$$

the other coefficients may be obtained by cyclic permutation of subscripts in the order of i, j, and k.

Using matrix notation Eq. (6-3) may be rewritten as follows:

$$\psi = \left| \frac{a_i+b_i x+c_i y}{2\Delta} \quad \frac{a_j+b_j x+c_j y}{2\Delta} \quad \frac{a_k+b_k x+c_k y}{2\Delta} \right| \begin{matrix} \psi_i \\ \psi_j \\ \psi_k \end{matrix}$$

or simply

$$\psi = [N_i, N_j, N_k] \{\psi\}^e \qquad (6\text{-}4)$$

in which the vector $\{\psi\}^e$ defines the nodal function values for the element.

When the function ψ is defined by Eq. (6-3) for all the elements of the region no discontinuities in its value will occur. Along the lines joining the nodal points the function varies linearly and therefore must be uniquely defined by the two nodal values irrespective of which element is considered. This continuity is one of the prerequisites of the minimization procedure as, if it is not satisfied, the expression inside the integral of Eq. (6-2) becomes infinite. However, the values of the slopes determined from two adjacent elements may not be the same along the boundary of an element. If the values of the slopes do not tend to infinity, the contribution of the discontinuity in the slope to the integrated values of the function is zero.

Minimization of the Functional

When minimizing the functional χ (given by Eq.(6-2)) with respect to the nodal value of the function ψ in the domain, it is only necessary to derive the relevant equations for a typical element. The influence of other elements will follow identical patterns, and to obtain the general equations it is simply necessary to add the contributions of all elements.

Thus if χ^e represents the contribution to the functional from an element i, j, k, its contribution is limited to the differentials with respect to parameters ψ_i, ψ_j and ψ_k only. Writing in matrix notation, these are

$$\frac{\partial \chi}{\partial \psi}^e = \begin{matrix} \frac{\partial \chi^e}{\partial \psi_i} \\ \frac{\partial \chi^e}{\partial \psi_j} \\ \frac{\partial \chi^e}{\partial \psi_k} \end{matrix}$$

To obtain each of the terms explicitly it is necessary to differentiate Eq. (6-2) with respect to each of the nodal values of ψ, thus

$$\frac{\partial \chi^e}{\partial \psi_i} = \int\int_A \left| \frac{\partial \psi}{\partial x} \frac{\partial}{\partial \psi_i}\left(\frac{\partial \psi}{\partial x}\right) + \frac{\partial \psi}{\partial y} \frac{\partial}{\partial \psi_i}\left(\frac{\partial \psi}{\partial y}\right) + \frac{\partial}{\partial \psi_i}(\text{Cosh}\ \psi) \right| dxdy$$

with the integration taken over the area of the element. Substituting Eq. (6-4) we have

$$\frac{\partial \chi^e}{\partial \psi_i} = \int\int_A \left| \frac{\partial N_i}{\partial x} \frac{\partial N_j}{\partial x}, \frac{\partial N_k}{\partial x} \right| \{\psi^e\} \left| \frac{\partial N_i}{\partial x} \right| dx dy$$

$$+ \int\int_A \left| \frac{\partial N_i}{\partial y} \frac{\partial N_j}{\partial y}, \frac{\partial N_k}{\partial y} \right| \{\psi^e\} \left| \frac{\partial N_i}{\partial y} \right| dx dy$$

$$+ \int\int_A N_i \text{ Sin h } ([N_i, N_j, N_k] \{\psi^e\}) dx dy$$

or using the definitions of N_i, N_j, and N_k

$$\frac{\partial \chi^e}{\partial \psi_i} = \frac{1}{4\Delta} [(b_i b_i + c_i c_i), (b_i b_j + c_i c_j), (b_i b_k + c_i c_k)] \{\psi^e\}$$

$$+ \int\int N_i \text{ Sin h } \{[N_i, N_j, N_k] \{\psi^e\}\} dx dy$$

For the whole element we have thus by differentiating Eq. (6-2) with respect to the other two nodal values of the typical element ψ_i and ψ_k

$$\frac{\partial \chi}{\partial \psi}^e = [h] \{\psi^e\}^e + \{F\}^e \tag{6-6}$$

where

$$[h] = \frac{1}{4\Delta} \begin{vmatrix} b_{ii} & b_{ij} & b_{ik} \\ b_{ji} & b_{jj} & b_{jk} \\ b_{ki} & b_{kj} & b_{kk} \end{vmatrix} + \frac{1}{4\Delta} \begin{vmatrix} c_{ii} & c_{ij} & c_{ik} \\ c_{ji} & c_{jj} & c_{jk} \\ c_{ki} & c_{kj} & c_{kk} \end{vmatrix}$$

or

$$h_{rs} = (b_r b_s + c_r c_s)/4\Delta$$

and

$$\{F\}^e = \begin{matrix} \int\int_A N_i \text{ Sin h } \{[N_i, N_j, N_k] \{\psi^e\}\} dx dy \\ \int\int_A N_j \text{ Sin h } \{[N_i, N_j, N_k] \{\psi^e\}\} dx dy \\ \int\int_A N_k \text{ Sin h } \{[N_i, N_j, N_k] \{\psi^e\}\} dx dy \end{matrix}$$

The determination of vector $\{F^e\}$ requires the evaluation of above integrals over the area of the triangle. The numerical technique used for the integration is discussed in Appendix C.

The final equations involved in the minimization procedure require the assembly of all the contributions to the differentials of χ and equating of each appropriate sum. Typically:

$$\frac{\partial \chi}{\partial \psi_i} = \Sigma \frac{\partial \chi^e}{\partial \psi_i} = 0 \tag{6-7}$$

the summation being taken over all the elements.

By Eq. (6-6) this can be written as

$$\frac{\partial \chi}{\partial \psi_i} = \Sigma \Sigma h_{im} \psi_m + \Sigma F_i \tag{6-8}$$

the summation being taken over all the elements and nodes. Eq. (6-8) represents (n) non-linear simultaneous equations for n nodes. The solution of the above system of equations with given boundary conditions, results in an approximate solution for the Poisson-Boltzmann equation.

Solving the System of Non-linear Equations

The method of successive approximations (Newton's Method) where used for the solution of the simultaneous equations is based upon finding a sequence of numbers which converge to a limit and which are the desired roots. The method consists of developing a recursion formula for the new approximation in terms of a present approximation so that one may be calculated after the other is known.

Newton's Method

The Newton's method can best be explained by a simple example of two nonlinear simultaneous equations in two unknowns x and y.

$$f(x,y) = 0$$
$$g(x,y) = 0 \qquad (6\text{-}9)$$

Let x_o and y_o be the initial estimated values for the roots. Since these are only an approximation to the solution they do not necessarily satisfy the system of equations.

The method seeks to obtain corrections δx and δy so that the corrected values for the roots will be

$$x = x_o + \delta x$$
$$y = y_o + \delta y$$

In order to find δx and δy the equations $f(x,y) = 0$ and $g(x,y) = 0$ are each expanded in a Taylor series in two variables, about the point (x_o, y_o)

$$f(x_o + \delta x, y_o + \delta y) = f(x_o,y_o) + \frac{\partial f(x_o,y_o)}{\partial x}\delta x + \frac{\partial f(x_o,y_o)}{\partial y}\delta y + \frac{1}{2}\left[\frac{\partial^2 f(x_o,y_o)}{\partial x}\delta x^2 + 2\frac{\partial^2 f(x_o,y_o)}{\partial x \partial y}\delta x \delta y + \frac{\partial^2 f(x_o,y_o)}{\partial y^2}\delta y^2 + \ldots\right.$$

$$g(n_o + \delta x, y_o + \delta y) = g(x_o,y_o) + \frac{\partial g(x_o,y_o)}{\partial x}\delta x + \frac{\partial g(x_o,y_o)}{\partial y}\delta y + \frac{1}{2}\left[\frac{\partial^2 g(x_o,y_o)}{\partial x^2}\delta x^2 + 2\frac{\partial^2 g(x_o,y_o)}{\partial x \partial y}\delta x \delta y + \frac{\partial^2 g(x_o,y_o)}{\partial y^2}\delta y^2 + \ldots\right.$$

If the Taylor series expansions are truncated after terms of second degree in δx and δy, the resulting equations constitute a system of two

linear equations in two unknowns δx and δy. The changes in $f(x,y)$ and $g(x,y)$ are given by the total differentials.

$$\begin{aligned} \delta f &= \frac{\partial f}{\partial x}(x_o,y_o) + \frac{\partial f}{\partial y}(x_o,y_o)\delta y \\ \delta g &= \frac{\partial g}{\partial x}(x_o,y_o) + \frac{\partial g}{\partial y}(x_o,y_o)\delta y \end{aligned} \tag{6-10}$$

A solution for the system of equations can be obtained by determining δx, δy such that the total differentials δf and δg satisfy the constraints

$$\delta f = - f(x_o,y_o)$$

$$\delta g = - g(x_o,y_o)$$

A set of linear equations in δx and δy can be found by substituting these constraints into Eq. (6-10).

$$\begin{aligned} -f(x_o,y_o) &= \frac{\partial f}{\partial x}(x_o,y_o)\delta x + \frac{\partial f}{\partial y}(x_o,y_o)\delta y \\ -g(x_o,y_o) &= \frac{\partial g}{\partial x}(x_o,y_o)\delta x + \frac{\partial g}{\partial y}(x_o,y_o)\delta y \end{aligned} \tag{6-11}$$

and these linear equations can be solved for δx and δy.

If the functions f and g are evaluated at (x_o,y_o) and expressed in a linear Taylor expansion, it follows from Eq. (6-11) that the right sides of the resulting equation are zero, i.e.,

$$f(x_o+\delta x,\ y_o+\delta y) \doteq f(x_o,y_o) + \frac{\partial f}{\partial x}(x_o,y_o)\delta x + \frac{\partial f}{\partial y}(x_o,y_o)\delta y$$

$$g(x_o+\delta x, y_o+\delta y) \doteq g(x_o,y_o) + \frac{\partial g}{\partial x}(x_o,y_o)\delta x + \frac{\partial g}{\partial y}(x_o,y_o)\delta y$$

If the linear Taylor expansions are sufficiently accurate it is clear that $(x_o+\delta x,\ y_o+\delta y)$ are fairly good approximations of the solutions of Eq. (6-9). If

$$|\delta x| > \varepsilon \quad \text{or if} \quad |\delta y| > \varepsilon \qquad \text{where } \varepsilon \text{ is a small}$$

positive quantity, it is necessary to replace x_o by $x_o+\delta x$ and y_o by $y_o+\delta y$ and repeat the entire process. Usually a few iterations of

this process will produce accurate values of the roots of Eq. (6-9) provided that the original estimates (x_o, y_o) are sufficiently close to the true solutions.

6-3 Numerical Form of Boundary Conditions

The problem is not completely defined until the boundary conditions of the problem are specified. The boundary conditions for the model element are in the form of derivatives of the potential field. They may have either of two values 1) at planes of symmetry the gradient of the potential normal to the plane of symmetry is zero, and 2) at boundaries coinciding with the charged surfaces the gradient has the values.

$$\left(\frac{\partial \phi}{\partial n}\right)_s = \left[\frac{2\pi}{\epsilon n k T}\right]^{1/2} \frac{\sigma L}{u}$$

The boundary conditions exert their influence on the finite element procedure as follows. Although it is possible to introduce the slope on boundary conditions by placing direct constraints on the value of the function in the boundary elements it is more advantageous to modify the variational approach.

By variation principles explained fully in Berg (1962) it is possible to show that if a portion of the boundary is subjected to the condition

$$\frac{\partial \psi}{\partial n} = q = \text{constant}$$

then the functional given by Eq. (6-2) has to be modified to

$$\chi = \int\int \left[\frac{1}{2}\left(\frac{\partial \psi}{\partial x}\right)^2 + \frac{1}{2}\left(\frac{\partial \psi}{\partial y}\right)^2 + \text{Cosh } \psi\right] dxdy + \int_c q\psi ds$$

in which the last integral is taken along the boundary subject to the

above boundary conditions.

All that is necessary is to add the differentials of the last term (with respect to the nodal values of ψ) to Eq. (6-8).

6-4 Accuracy of Solution

Solution of the non-linear equations given by Eq. (6-8) gives a set of values which are an approximate solution of the Poisson-Boltzmann equation. The Poisson-Boltzmann differential equation originates from a mathematical description of a natural phenomenon. For a mathematical problem to correspond to physical reality, the mathematical formulation must have a solution, and the problem should not have mutually contradictory properties.

The condition that the total electrical charge contained in the element must be equal to the total surface charge on the particle is employed to assess the accuracy of the numerical solution.

Space Charge

The total volumetric charge may be found by integrating the volume charge density over the element. The volume charge density is given by

$$\rho = -2\,\nu e n \,\mathrm{Sinh}\,\left(\frac{ze}{kT}\,\phi\right)$$

where

ν = valency of ions

e = electric charge

n = ion concentration

kT = Boltzmann constant x absolute temperature

Surface Charge

The total surface charge is found by multiplying the surface charge density times the area over which it is spread. The surface charge density is given by:

$$\sigma = - \frac{\varepsilon \bar{u}}{4\pi L} \left(\frac{\partial \phi}{\partial n}\right)_s$$

where ε is the dielectric constant of the medium and $\left(\frac{\partial \phi}{\partial n}\right)_s$ is the normal gradient of the potential at the charged surface.

Figure 6-2 illustrates regions over which space and surface charges are calculated.

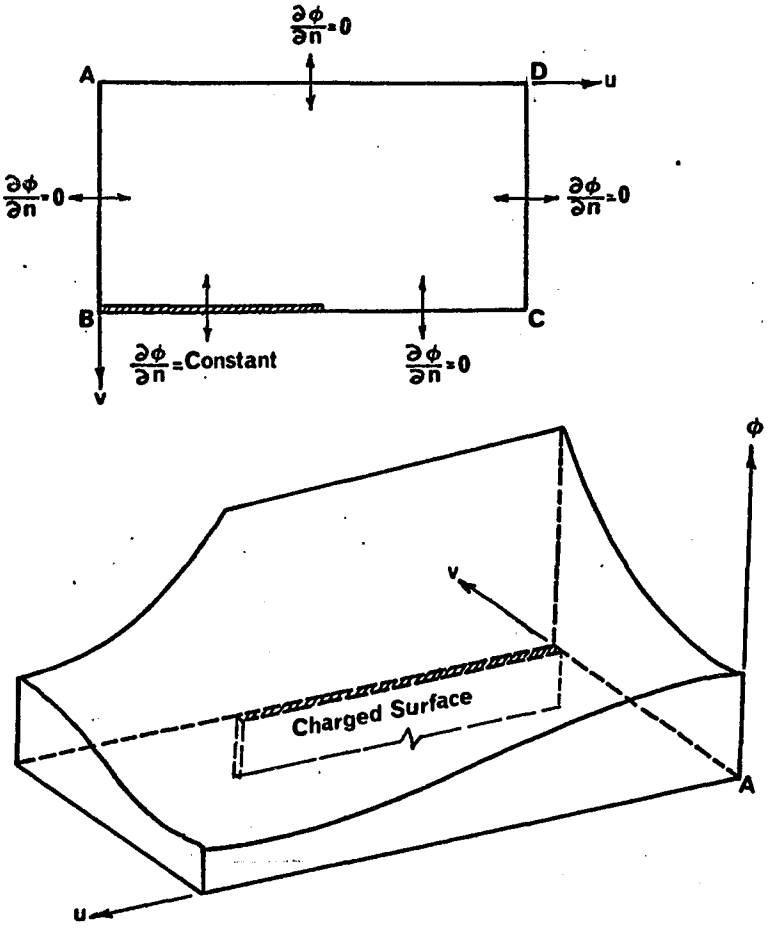

Fig. 6-2 Boundary Conditions for an Element and Regions of Surface and Space Charge

Surface-Space Charge Equivalency

The condition that the total charge in the element must be equal to the total charge on the charged surface can be used to check the accuracy of the solution. This equality may also be used as a convergence criterion for the successive approximation solution of the non-linear simultaneous equations.

The accuracy with which the nodal potentials and, consequently, the space charge can be determined depends upon the shape and the size of the finite elements used over the region. Empirically it was established that with use of smaller elements at the points of high potential gradient, better approximations for the space charge may be obtained.

7 - RESULTS OF COMPUTATIONS

Employing the numerical technique derived in the previous chapter, potential distribution within the element (Fig. 7-5a) can be determined and by using the boundary potentials the pressures acting between the clay particles can be calculated. With the given model particle geometry, void ratios of the model are determined and void ratio-pressure relationships are established.

Repulsive pressure is related to the bulk water ion concentration and the central plane potential as indicated in Eq. (5-17)

$$p = 2nkT\ (\text{Cosh}\ \psi_o - 1)$$

The central plane potential in return is dependent on the bulk water ion concentration introduced through the boundary conditions given by Eq. (5-14). As the bulk water ion concentration is decreased to zero (to idealize fresh water clay deposit structures) the repulsive pressures cannot readily be determined from Eq. (5-17). This is because ψ_o is inversely related to the bulk water ion concentration and, therefore, approaches infinity as n approaches zero. The variation of repulsive pressure with decreasing bulk water ion concentration requires careful discussion. In the following section this relationship is briefly analyzed.

7-1 Bulk Water Ion Concentration - Repulsive Pressure Relationship

The discussion of the relationship between bulk water ion concentration and repulsive pressure may be considerably simplified, without losing generality, by using the one-dimensional Poisson-Boltzmann

equation.

In the one-dimensional case the non-dimensional Poisson-Boltzmann's equation will take the form

$$\frac{d\psi}{dx} = \text{Sinh } \psi \qquad (7\text{-}1)$$

For this case the soil particles are idealized by parallel infinite plates with a uniform surface charge density. The variation of potential between two parallel plates is illustrated in Fig. 7-1 where ψ_s is the plate surface and ψ_o is the central plane potential.

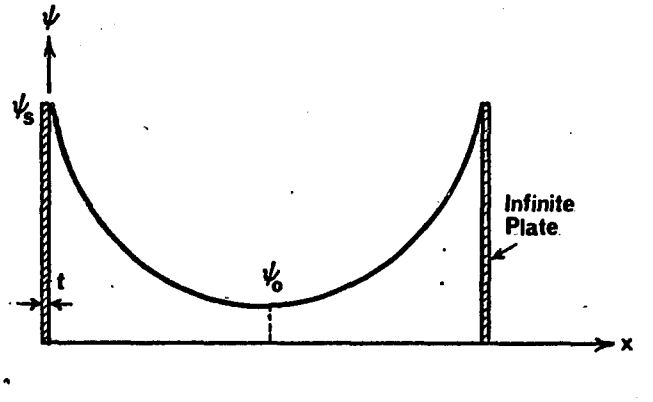

Fig. 7-1 Potential Variation Between Infinite Plates

The boundary conditions for solving Eq. (7-1) are

$$\frac{d\psi}{dx} = 0 \qquad @\ x = d \qquad (7\text{-}2a)$$

$$\frac{d\psi}{dx} = -\left[\frac{2\pi}{\epsilon nkT}\right]^{1/2} \sigma \qquad @\ x = 0 \qquad (7\text{-}2b)$$

(The second boundary condition is obtained from Eq. (5-14) by using the infinite plate condition, i.e., $\bar{u} = L$.)

Surface charge density σ is taken as 4×10^4 esu/cm, corresponding to the surface charge density of the Montmorillonite used for the experiments.

The following numerical values for the physical constants are obtained from van Olphen (1963).

ϵ = Dielectric constant = 80 for water

kT = Boltzmann constant x absolute temperature = 0.4×10^{-13} ergs at 20°C

n = Local ion concentration in number of ions/cm^3 = normality (N) x 10^{-3} x Avagadro's number (6.02×10^{23})

Using these constants Eq. (7-2a) will take the following form

$$\frac{d\psi}{dx} = 2.28 \left(\frac{1}{N}\right)^{1/2} \qquad (7\text{-}2c)$$

where N is the normality of the solution.

In Table 7-1, Eq. (7-2c) is evaluated for different normalities

Normality	$\frac{d\psi}{dx} = 2.28 \left(\frac{1}{N}\right)^{1/2}$
10^{-1}	7.3
10^{-2}	22.8
10^{-3}	72.5
10^{-4}	228.0

Table 7-1 Boundary Conditions for Several Values of Bulk Solution Ion Concentration

Using these boundary conditions, solutions to Eq. (7-1) can be computed for several plate separation distances by the finite element procedure and repulsive pressures can be calculated using Eq. (5-17)

$$p = 2nkT\ (\text{Cosh}\ \psi_o - 1).$$

For infinite parallel paltes the void ratio of the system may be expressed in terms of plate thickness, t, and particle separation distance, 2d, as follows

$$\text{Void Ratio} = \frac{2d}{t}$$

If plate thickness t is taken as 10 Å, Fig. (7-2) shows the repulsive pressure-void ratio relationships for different values of bulk water ion concentration (normality). The figure shows that the pressure-void ratio relationship approaches a limiting curve as the normality N decreases. For further calculations using the model particle structure described above, a normality of $N = 10^{-4}$ was considered to be low enough to simulate the behavior of a fresh water clay deposit.

7-2 Potential Distribution

The objective of computing the potentials is to use them to determine the repulsive pressures between the model clay particles. This is possible because repulsive pressures are functions of boundary potentials.

The results of the computation of potentials are the numerical values of the dimensionless potentials in the region defined by the element. The area of the element is transformed to dimensionless form by means of a constant which depends on the concentration of ions in the bulk solution (among other factors, see Eq. (5-5a). The non-dimensional area is subdivided into triangular elements and through the computer program, potentials are calculated at the verticies of

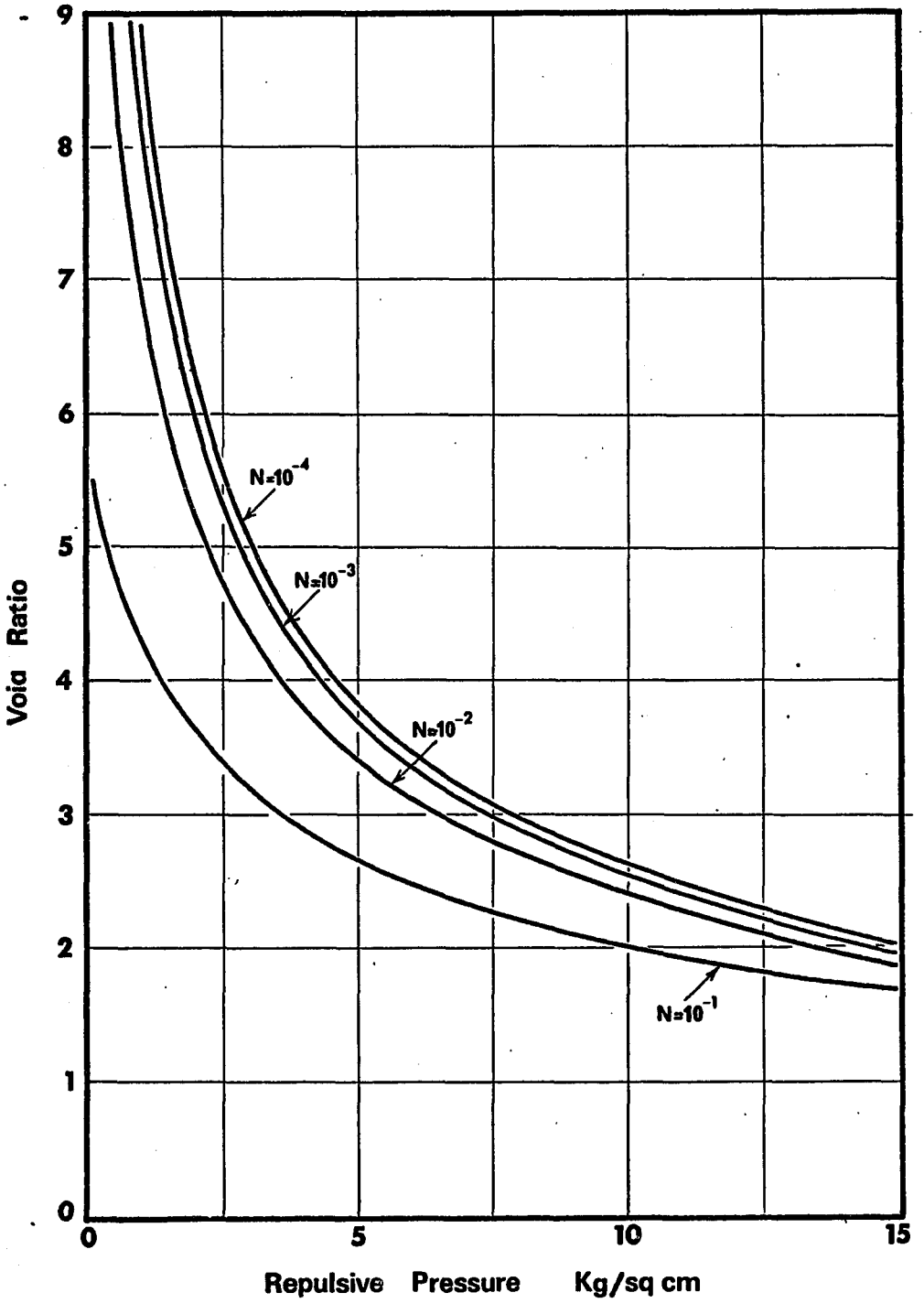

Fig. 7-2 Void Ratio-Repulsive Pressure Relationships For Infinite Parallel Plates

the triangular elements.

A typical subdivision of an element is shown in Fig. 7-3 . The potential distribution in an element is shown in Fig. 7-4 . The potential fields are calculated for different lateral and vertical plate separation distances, i.e., for various sets of values of dimensions a and b. (See Fig. 7-5a for the dimensions a and b.) In Appendix B potential distributions are given for 20 configurations of the element defined by the dimensions a and b.

7-3 Pressure Distribution

Repulsive pressures along the two boundaries of each element common with the symmetry lines between the particles (lines a-a and b-b in Fig. 7-5a) are calculated based on Eq.(5-17). Pressures on the other two boundaries (boundaries common with lines c-c and d-d) are internally balanced by the electrical forces within the element and do not contribute to the forces acting between the particles.

The ion concentration of the bulk solution expressed in normality is taken as $N = 10^{-4}$. With $kT = 0.4 \times 10^{-13}$ ergs, Eq. takes the numerical form

$$p = 4.8 \times 10^{-2} \ (\text{Cosh } \psi_o - 1) \qquad (7\text{-}3)$$

where repulsive pressure p is in Kg/cm^2. In Appendix B boundary repulsive pressures are given for the elements analyzed. In Fig. 7-5b a typical boundary pressure distribution is shown.

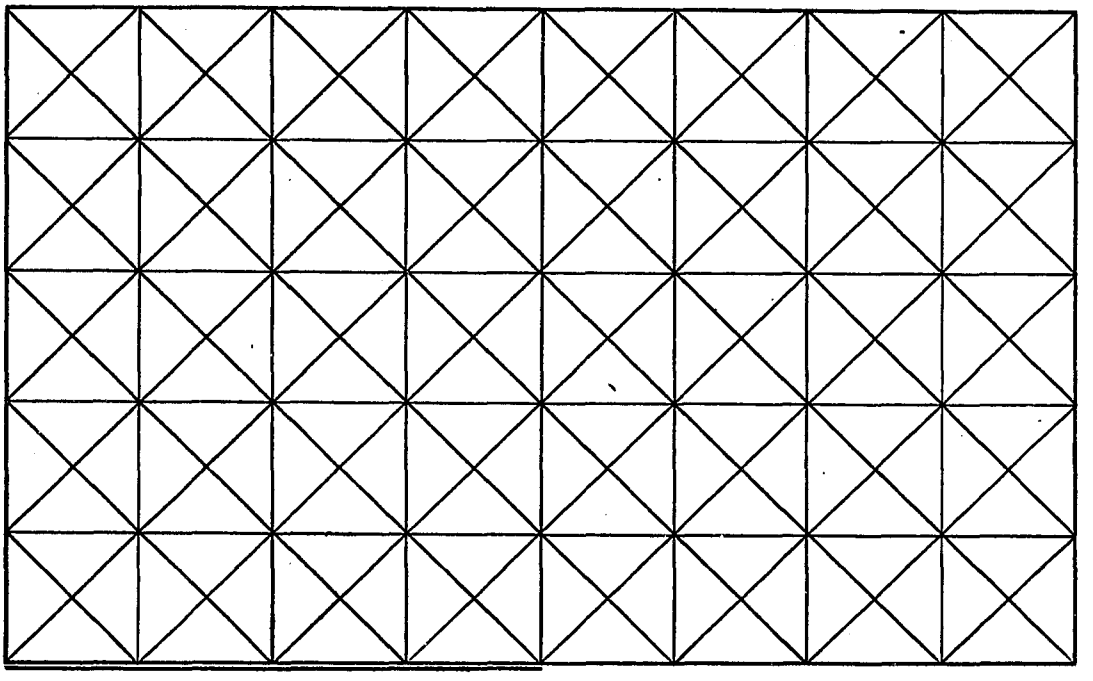

Fig. 7-3 Typical Subdivision of an Element

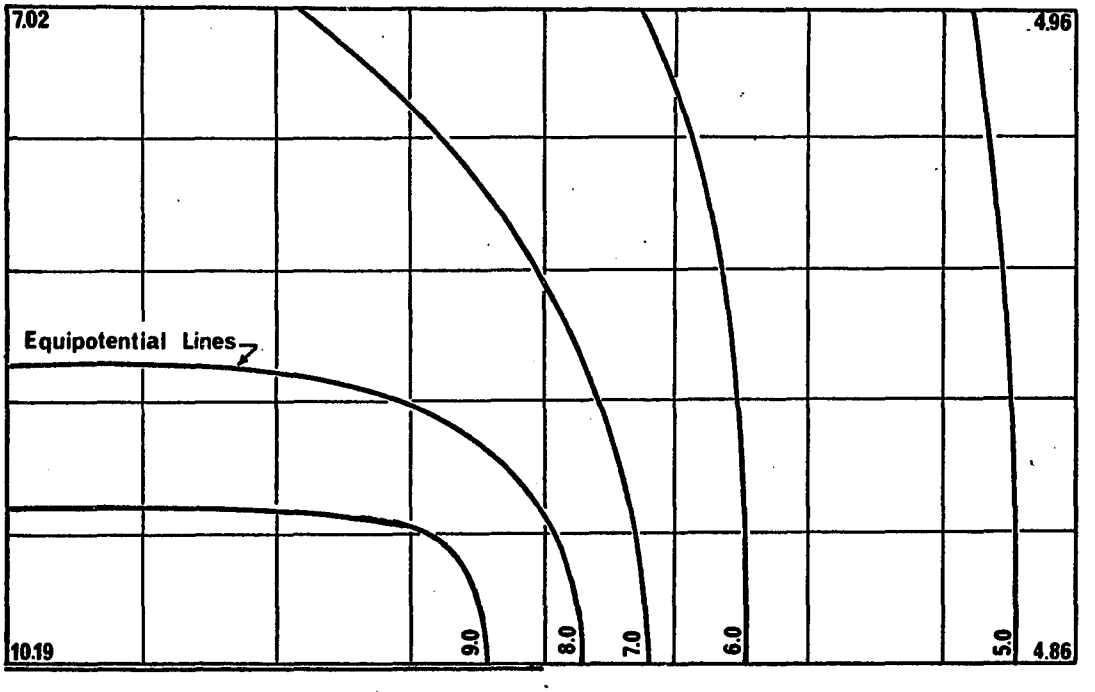

Fig. 7-4 Typical Potential Distribution in an Element

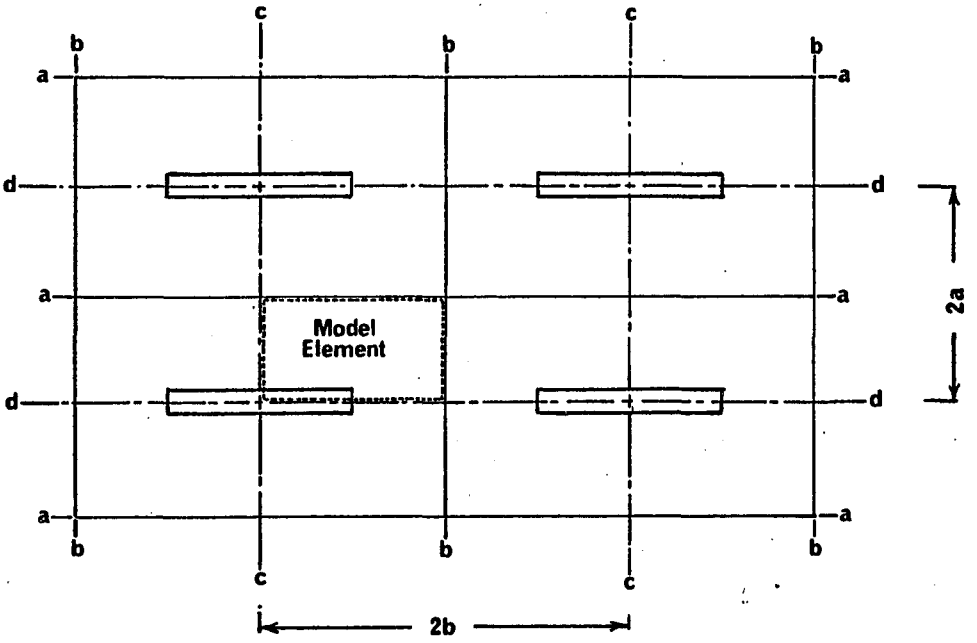

Figure 7-5a Model Element

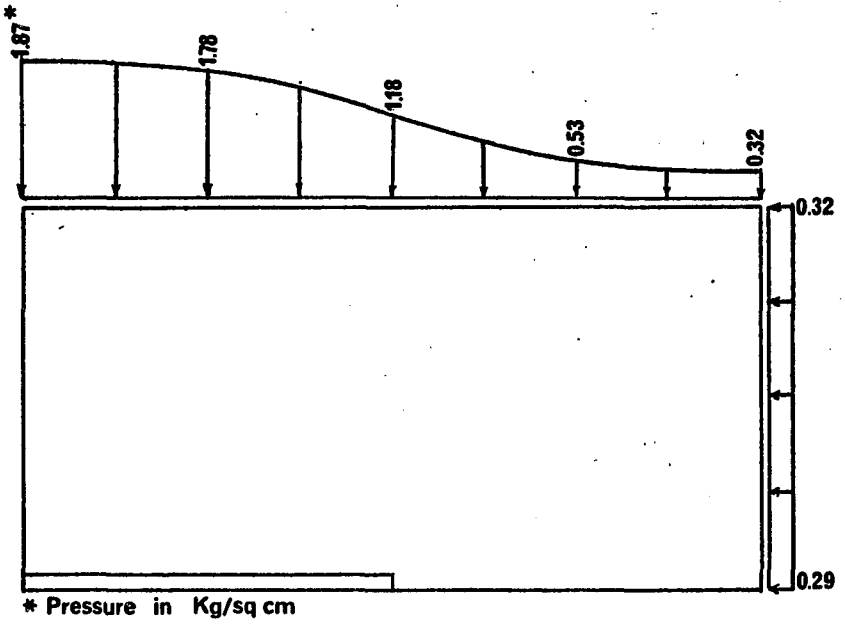

Figure 7-5b Typical Boundary Pressure Distribution

7-4 Model Particle Structure Force-Deformation Relationship

The repulsive pressures acting between the particles tend to expand the particle structure unless they are balanced by external for-es. In Fig. 7-6 a model particle structure is illustrated showing the internal and external forces. It is assumed that the internally unbalanced repulsive pressures are balanced by uniform external pressures applied along the boundaries of the structure.

From static equilibrium, externally applied pressures P_V and P_H are equal to the average of the interparticle repulsive pressures acting along the x and y directions, respectively (see Fig. 7-6); and since the void ratio of the structure may be calculated as the ratio of the area of water in an element to the area of solid, the pressure-void ratio is readily determined. In Table 7-2 void ratio, P_V, P_H and P_V/P_H values are given as functions of vertical and horizontal particle separation a and b.

In Fig. 7-7 P_V, P_H and void ratio relationships are given for constant particle separation distances.

With a given model particle geometry (defined by a set of dimensions a and b) vertically and horizontally applied external pressures, P_V and P_H, may uniquely be determined. Conversely for given boundary pressures there is a unique set of a and b dimensions defining the model particle geometry. The solid lines in Fig. 7-7 indicate the P_V, P_H relationships for constant particle separation 2a in the vertical (y) direction. Moving in the decreasing P_H direction horizontal separation of the particles increases and P_V decreases to a minimum for the given vertical separation. Moving in the opposite

direction along a solid line, P_V approaches a maximum value corresponding to a one-dimensional particle model. Numbers beside the points in the figure indicate the void ratio of the model structure for the given geometry.

P_V void ratio and P_H void ratio relationships are illustrated in Fig. 7-8 and in Fig. 7-9, respectively.

a (Å)	b (Å)	Void Ratio	P_V Kg/cm^2	P_H Kg/cm^2	P_V/P_H
120	15	13.7	0.49	1.06	0.46
	30	15.4	0.46	0.53	0.87
	45	17.2	0.43	0.33	1.30
	60	19.0	0.39	0.24	1.62
90	15	10.3	0.84	1.30	0.65
	30	11.6	0.77	0.64	1.20
	45	12.9	0.72	0.41	1.76
	60	14.2	0.67	0.27	2.48
60	15	6.9	1.76	1.85	0.95
	30	7.7	1.58	0.81	1.95
	45	8.6	1.44	0.47	3.06
	60	9.4	1.32	0.32	4.12
54	15	6.2	2.13	2.07	1.03
	30	7.0	1.91	0.84	2.28
	45	7.7	1.72	0.49	3.50
	60	8.5	1.58	0.32	4.95
48	15	5.5	2.65	2.34	1.13
	30	6.2	2.30	0.90	2.55
	45	6.9	2.10	0.51	4.12
	60	7.5	1.93	0.33	5.85

Table 7-2 Void Ratio P_V, P_H and P_V/P_H Value for Several Plate Separation Distances

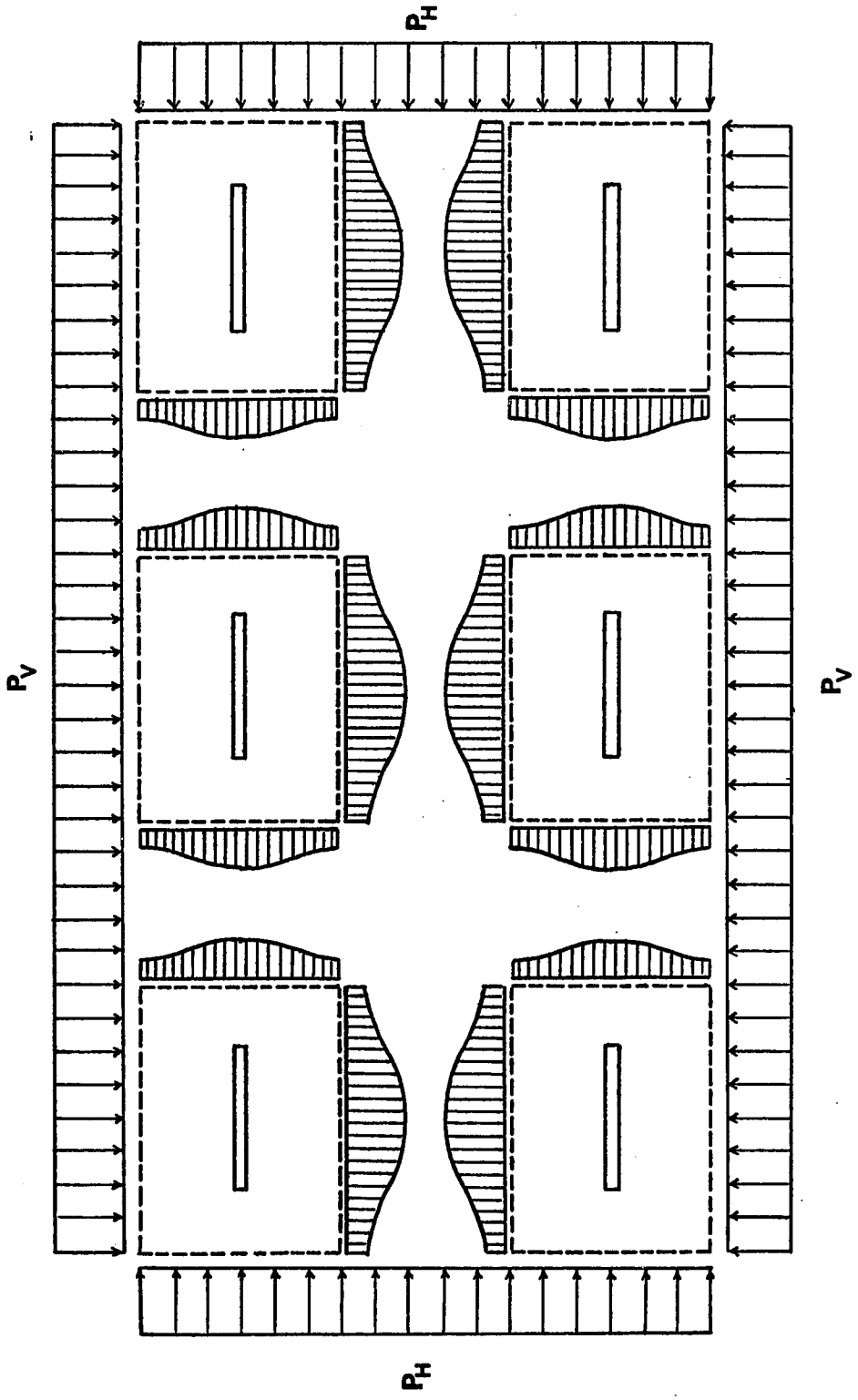

Figure 7-6 Model Particle Structure Element Boundary and External Pressures

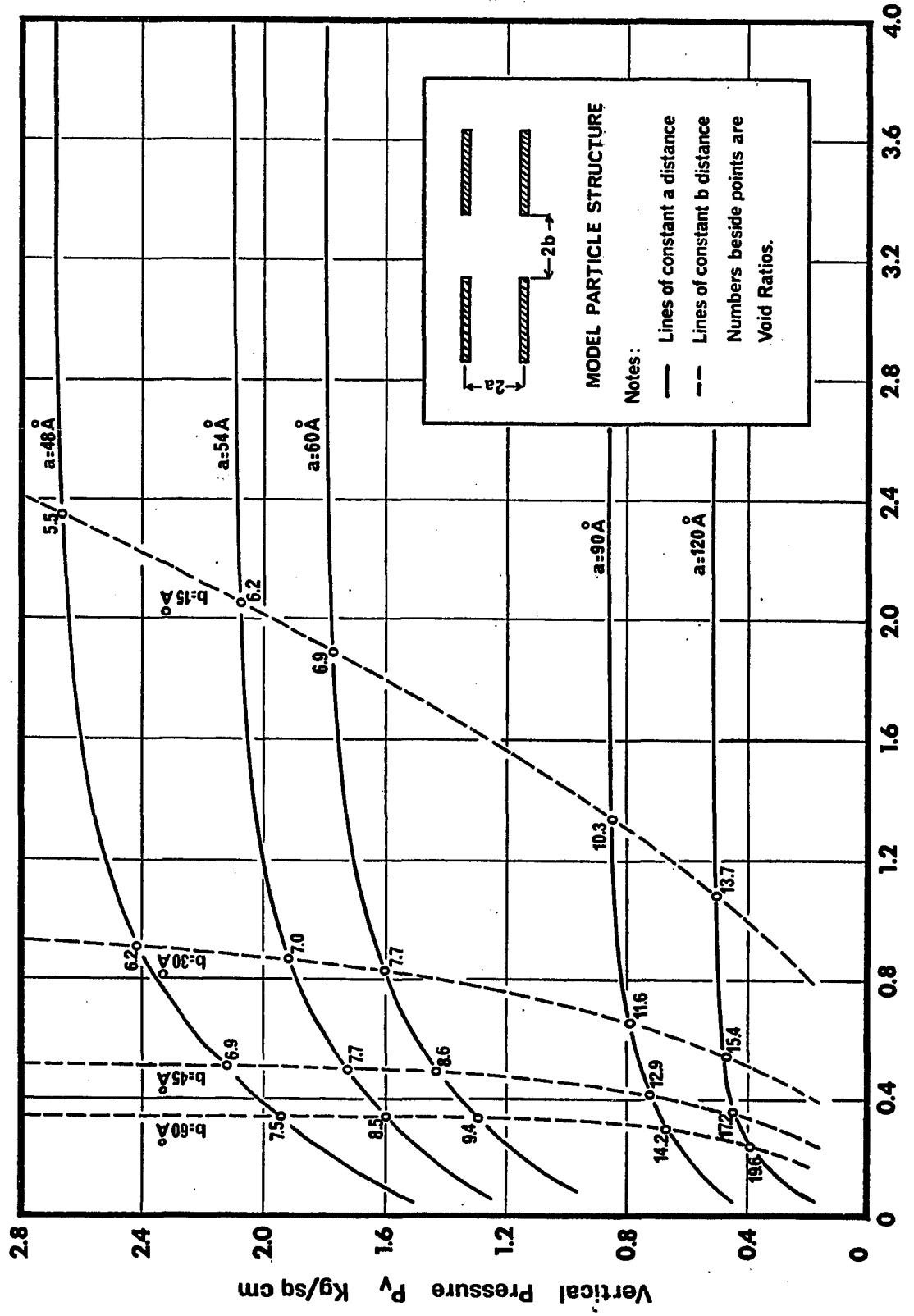

Figure 7-7 Pressure Relationships For Several Plate Separation Distances

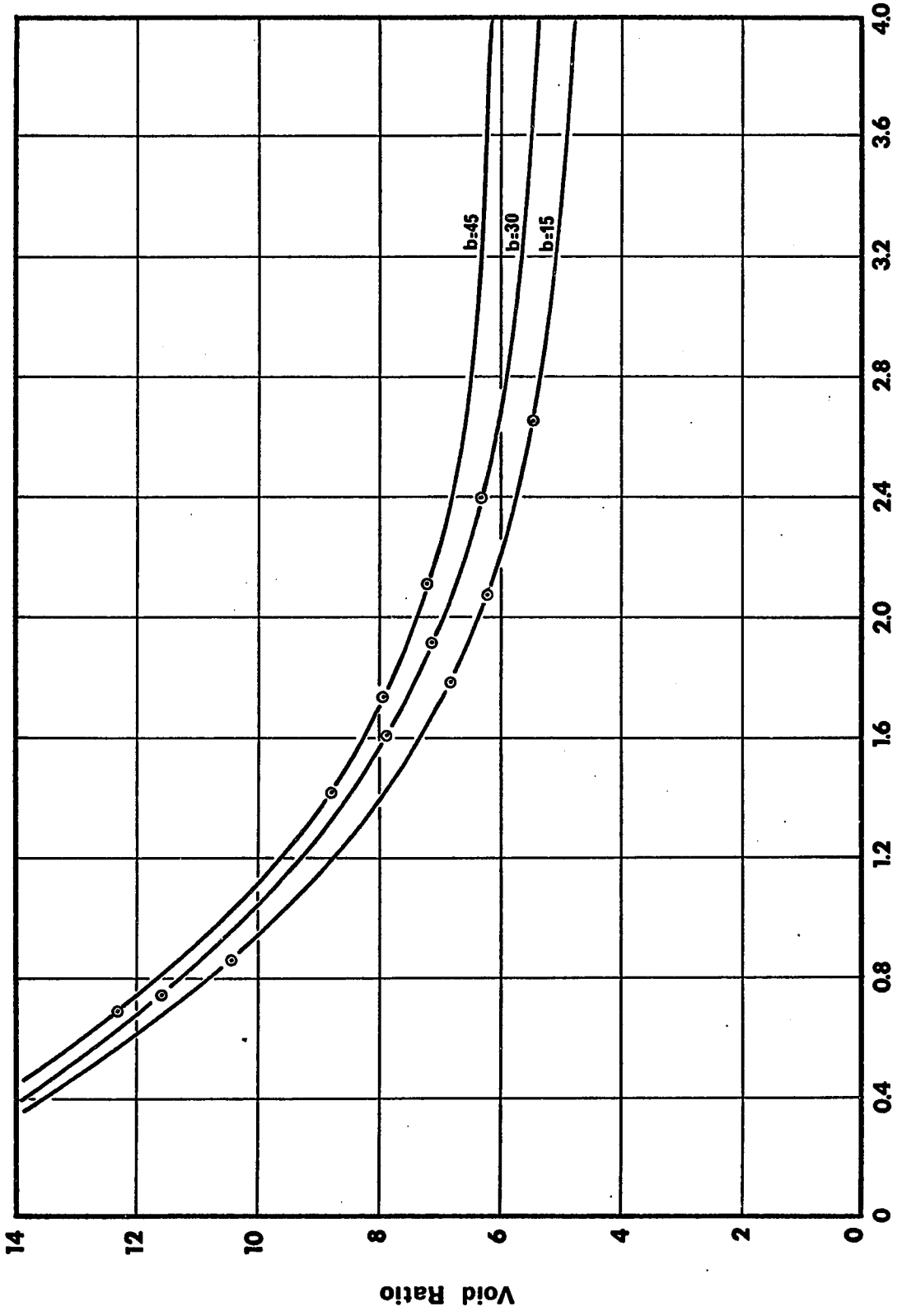

Figure 7-8 Vertical Pressure Void Ratio Relationship

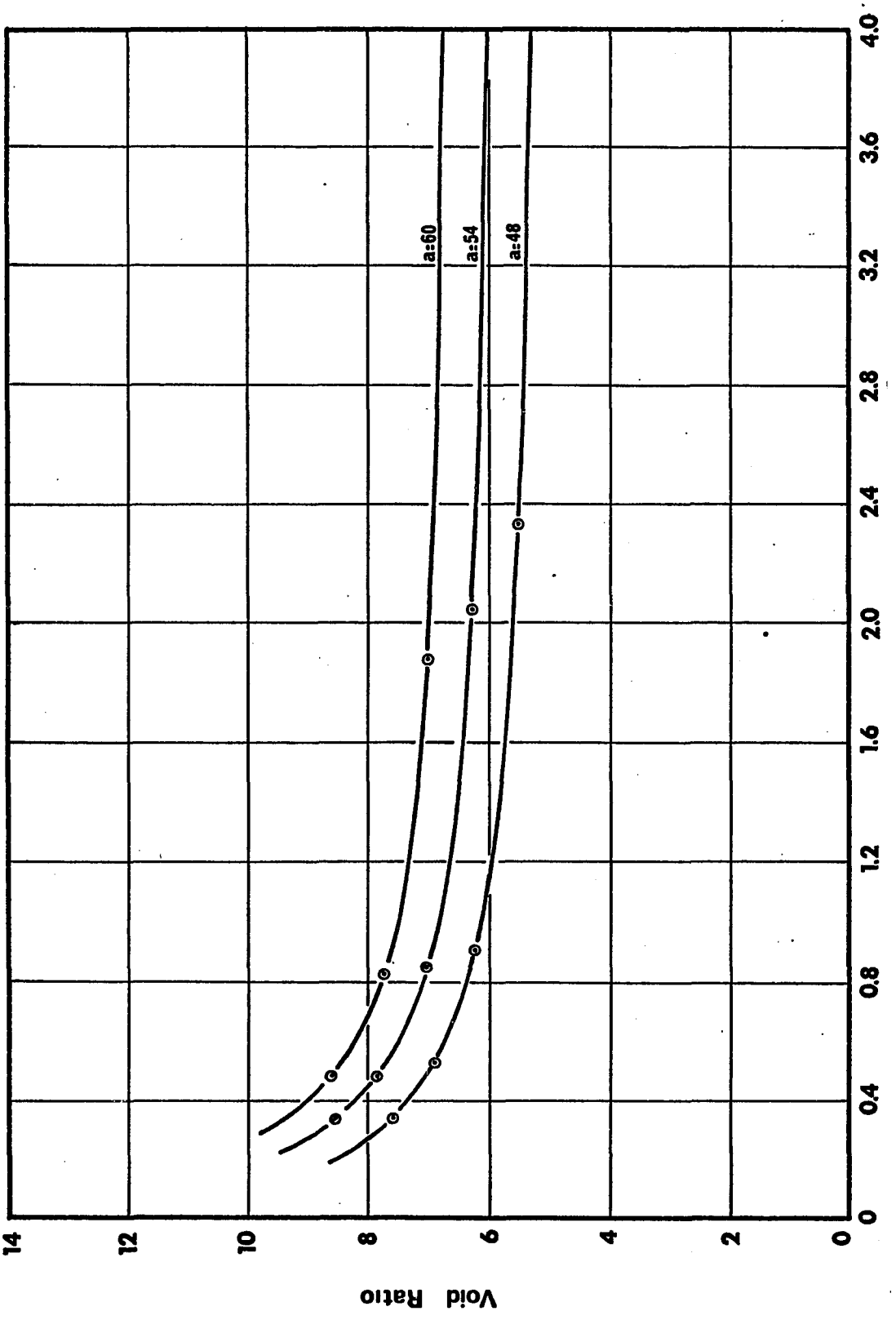

Figure 7-9 Horizontal Pressure Void Ratio Relationship

8 - ONE DIMENSIONAL CONSOLIDATION TESTS

An experimental study of volume change characteristics of clay can be carried out in a variety of ways. The major items to be considered are the type of test to be used, the soil to be stuided, the method of specimen preparation and the testing procedure.

8-1 One-dimensional Consolidation Test and Apparatus

The one-dimensional consolidation test is widely used in studying the consolidation characteristics of soils. The use of thin soil samples (approximately one-half inch thick) with two-way drainage allows faster consolidation. The fixed ring consolidometer used in this study is shown in Fig. 8-1. The consolidation rings are made of teflon-coated steel, reducing the friction on the sides of the ring and approximately maintain a one-dimensional state of stress in the sample tested. Pressures were applied in consolidation frames by a lever arm arrangement. The applied pressures ranged from 0.1 Kg/cm^2 to 10 Kg/cm^2. The soil samples were 2.5 inches in diameter and one-half inches thick.

8-2 Soil Studied and Sample Preparation

To obtain significant results from an experimental investigation it is necessary to control important variables. In this study the emphasis was on interparticle forces. For this reason Montmorillonite was selected for the experimentation. Montmorillonite with high specific surface characteristics magnifies the effects of interparticle forces.

The soil used in this study was supplied by Baroid Division, National Lead Company of Houston, Texas. The clay was ion exchanged, centrifuged, and spray dried. The exchange properties of the clay were as follows: C.E.C.: 96 meq/100 gr exchangeable ions; 97 percent of the total exchangeable cations were sodium. Therefore, the clay for all practical purposes was homoionic. The soil tested was mixed manually at water contents ranging between 300 to 1,000 per cent until a uniform mixture was obtained. A piston was then placed in the consolidometer ring and the soil was then placed in the ring with continuous spreading as the piston was slowly lowered.

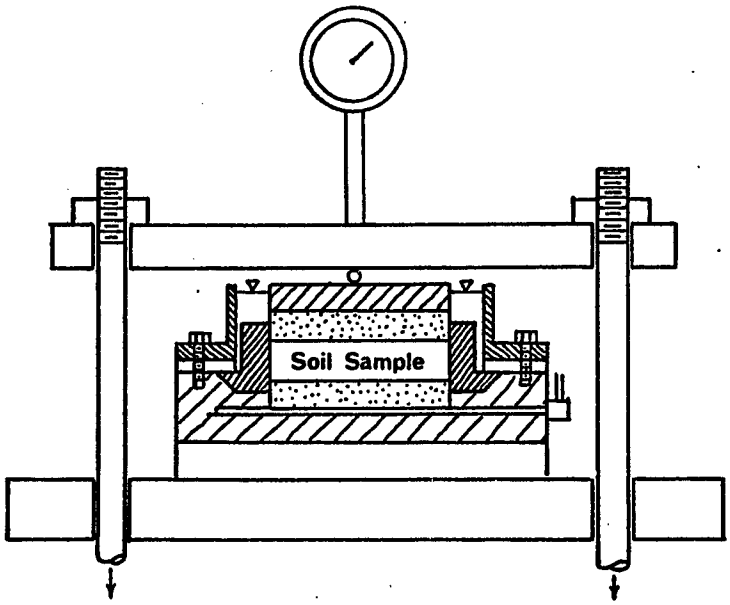

Figure 8-1 Consolidometer

The purpose of this continuous shearing of the soil was to attain a more parallel-oriented structure in the soil. Then the sample was left to

age under water with a small load about two days before the commencement of the consolidation test.

8-3 Test Procedure

A sample of soil which had been left to age with the consolidation samples was used to determine the initial water content of the sample. The initial thickness of the consolidation sample was recorded.

In performing the consolidation test, each load increment was allowed to remain on the sample until the consolidation in the preceding four hours was negligible or, until a straight line branch of deflection-time curve (representing the secondary consolidation) was well-defined. (See Fig. 8-2 for typical curve.) In all the tests, the first load increment was 0.1 Kg/cm^2. Different load increments were used for different samples---for the purpose of defining the pressure-void ratio relationship more accurately---but for all cases successive load increments were no greater than twice the value of the preceding load. All samples were consolidated to a maximum pressure of 10 Kg/cm^2. The samples were allowed to swell by reducing the applied loading with increments to a value of 0.1 Kg/cm^2, and they were then re-loaded by increments to the consolidation pressure which had existed before the commencement of swelling. (See Fig. 8-3 for typical curve.) For each sample tested, swelling and reloading branches were obtained starting from different consolidation pressures.

After each application of a load increment, subsequent thickness changes were recorded in order to establish a rate of compression. A new load increment was applied as soon as the sample attained the 95

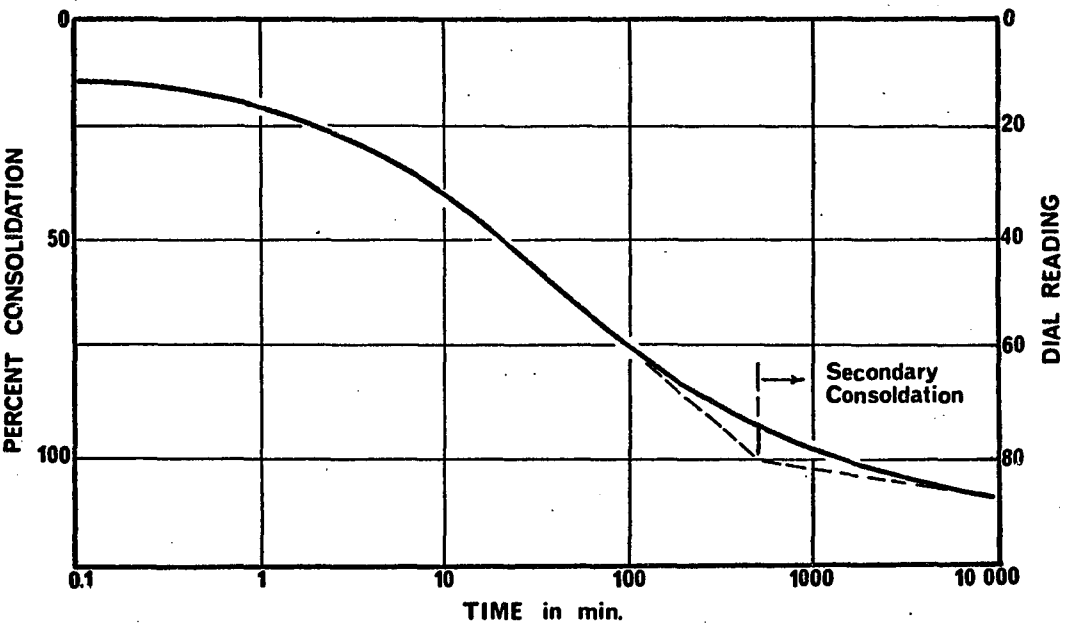

Figure 8-2 Time-Percent Consolidation Curve

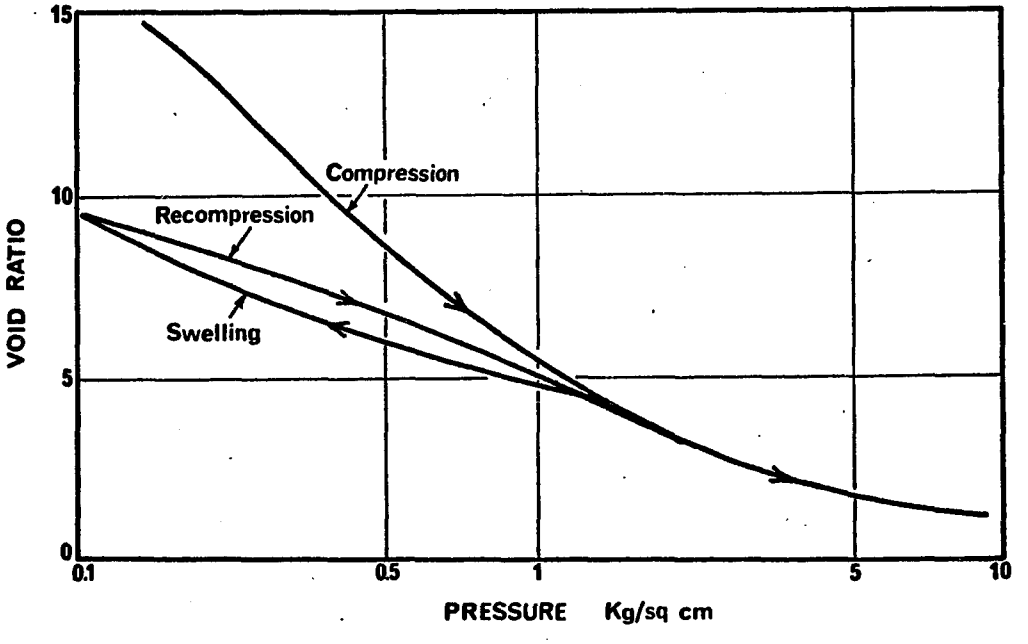

Figure 8-3 Typical Pressure-Void Ratio Curve

percent consolidation under the preceding loading.

During the consolidation test the temperature of the water in the consolidometer was recorded. Attention was given to keep the sample at room temperature (20°C).

After the completion of a consolidation test, the final water content of the sample was determined.

8-4 Calculation of Test Results

It is a general practice to report the results of a consolidation test in the form of compression diagrams. Although changes in specimen thickness for a given load increment are observed during the test, it is customary to convert this data to change in void ratio and to construct logarithm of pressure versus void ratio curves. The relation between change in thickness and change in void ratio of an element for a layer of soil which is laterally confined may be expressed as follows:

$$\Delta e = \frac{\Delta H}{H}(1 + e) \qquad (8\text{-}1)$$

in which

H = initial thickness

ΔH = change in thickness

e = initial void ratio

Δe = change in void ratio

At each point on a given pressure-void ratio curve the coordinates are, respectively, pressure due to the applied load and the void ratio of the specimen after equilibrium under the load has been reached. These curves do not indicate in any way the time required to reach

equilibrium under a given load increment. Time consolidation relationships, which indicate the rate of change of void ratio with respect to time, are generally obtained by plotting void ratio versus square root of time. (See Fig. 8-2 for typical curve.)

8-5 Test Results

Consolidation Pressure-Void Ratio Relationships:
Six consolidation tests were performed using three different molding water contents, data from these tests are represented graphically in Figs. 8-4, 8-5, and 8-6. The curves indicate the manner in which the volume change occurs as pressures are voried to define compression, swelling, and recompression behavior of the soil tested. Although semi-log plotting of consolidation data for most soils has the effect of converting the virgin compression curve to an essentially straight line within the range of the ordinary pressures, in these tests pressure-void ratio curves exhibit a distinct curvature. This behavior was also observed in the consolidation tests conducted on homoionic Montmorillonites by Bolt (1956) and Yong and Warkentin (1959). This difference has been attributed to the possibility that the consolidation behavior of montmorillonites is predominately governed by the osmotic pressures acting between the soil particles.

As shown in Fig. 8-6, the samples prepared at 310 percent water content exhibit a lower void ratio-pressure curve compared to the samples mixed at 700 and 1060 percent water contents. This indicates that the soil particles are not completely dispersed and that osmotic repulsive pressure is balanced by Van der Waal forces which prevent

the soil from swelling. As the mixing water contents are increased, the samples have larger void ratios at a given consolidation pressure, indicating a more dispersed soil particle structure.

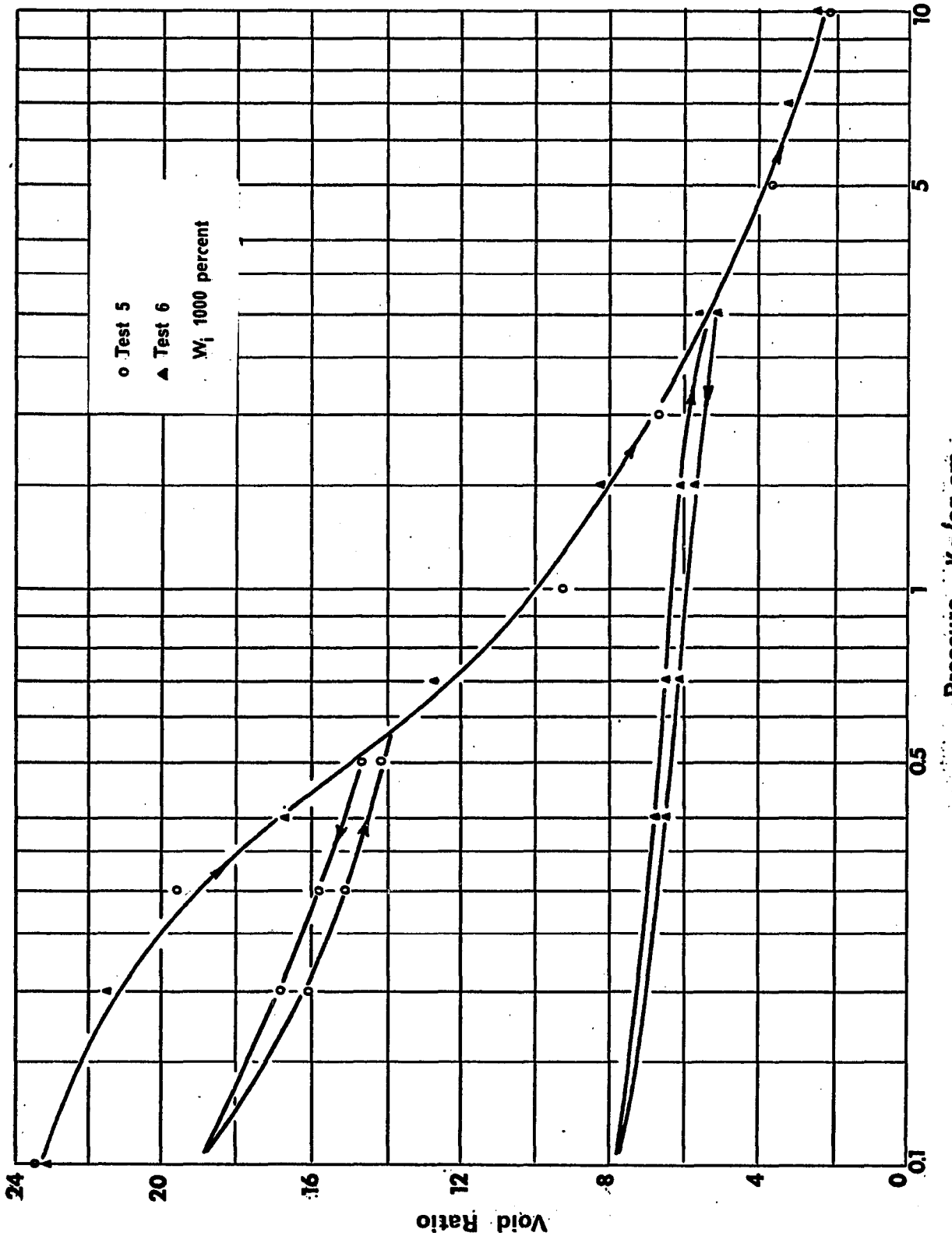

Figure 8-4 Consolidation Pressure-Void Ratio Relationship

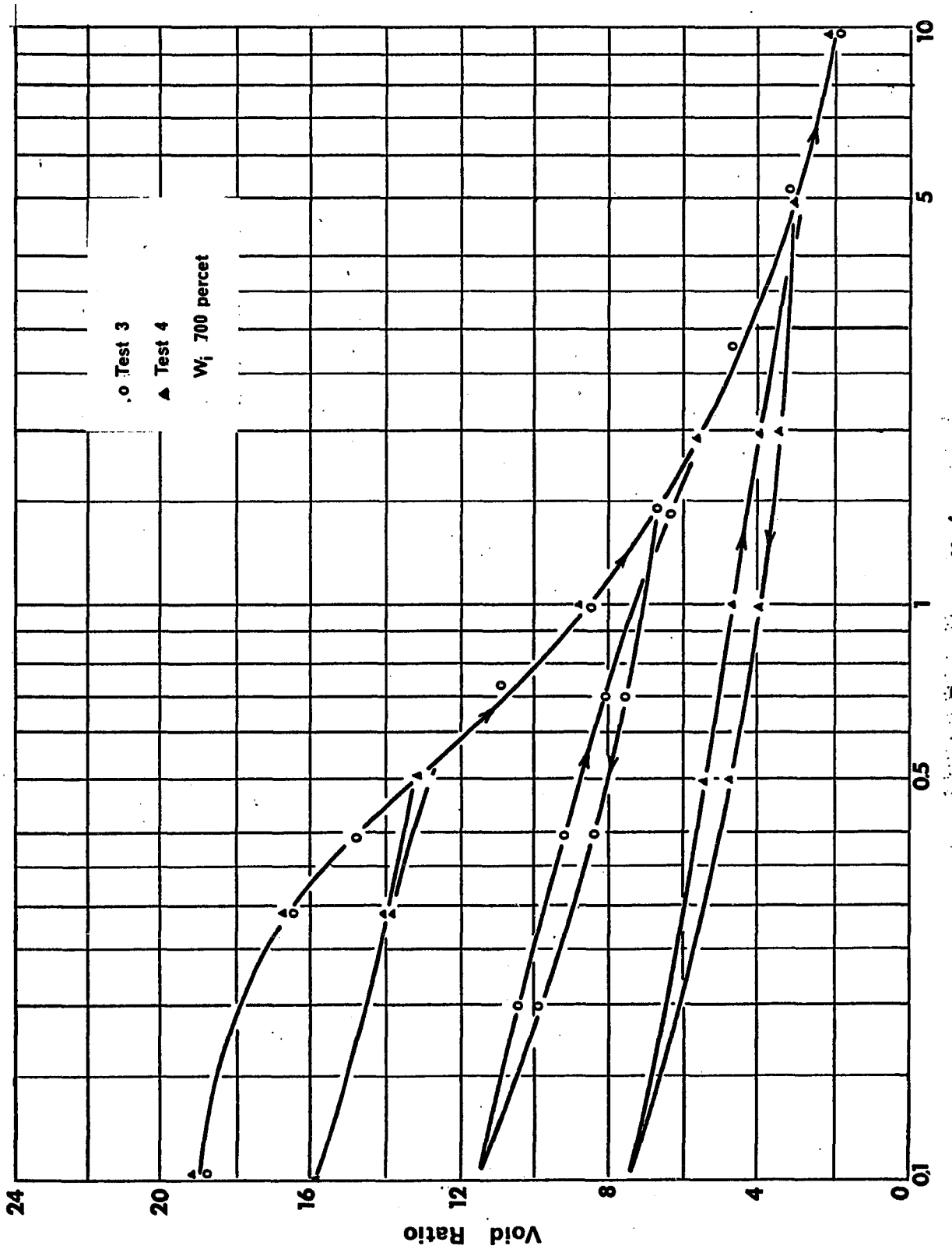

Figure 8-5 Consolidation Pressure-Void Ratio Relationship

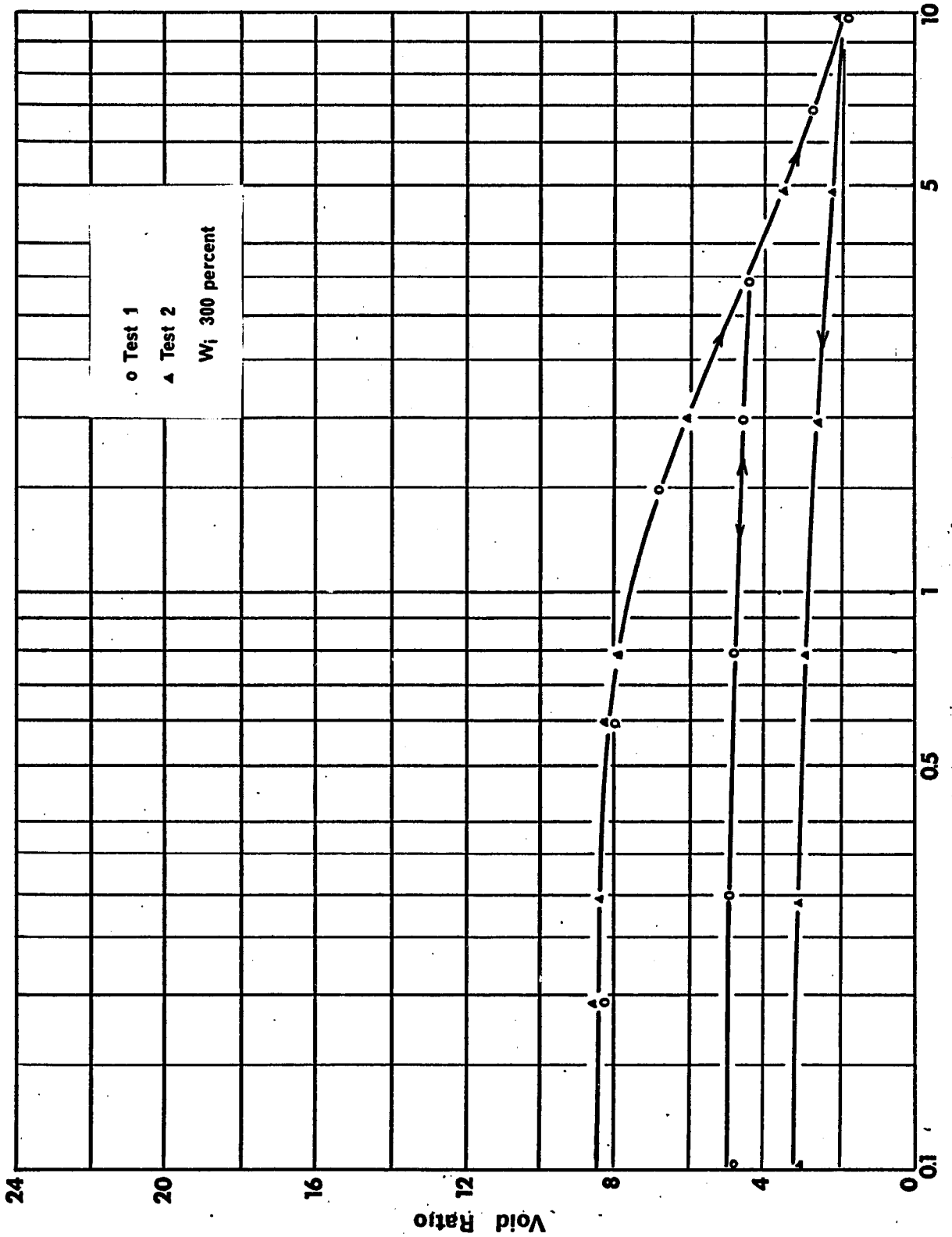

Figure 8-6 Consolidation Pressure-Void Ratio Relationship

9 - COMPARISON OF MODEL AND EXPERIMENTAL RESULTS

In Chapter 7 model particle structure was analyzed and boundary pressures were related to the void ratio of the structure (See Fig. 7-7). Based on these findings void ratio pressure relationships are obtained to define the volume change behavior of the model structure under various stress conditions. One and two dimensional stress conditions are studied.

For a one-dimensional model when the predicted void ratio-pressure relationship is compared with the experimental results, a good agreement is observed.

9-1 One-dimensional Consolidation

The one-dimensional consolidation test apparatus is illustrated in Fig. 8-1. It should be noted that this test produces compression in the vertical direction only, while the lateral dimensions remained unchanged. Before the commencement of the compression the soil sample is subjected to a small, approximately isotropic stress system. With the increase in vertical compression the sample is brought into an anisotropic state of stress.

The model may be used to simulate the volume change behavior of clay under one-dimensional state of stress as follows.

The model particle structure is initially assumed to be under a small isotropic stress condition with a given initial particle structure geometry as defined by dimensions a and b in Fig. 7-5a. The initial particle geometry is selected in such a way that the initial

void ratio will approximate the initial void ratio of the test sample. To define the volume change under a one-dimensional state of stress, the condition of no lateral deformation is used. This may be achieved by keeping the lateral spacing of the particles constant. As the vertical particle spacing is reduced the required void ratio-pressure relationship is defined. Vertical and horizontal pressures and void ratios may be determined from Table 7-2 for given sets of values of a and b. In Table 9-1 such values are given for constant lateral particle spacing b = 45Å and varying vertical particle spacing a.

a (Å)	b (Å)	Void Ratio	P_V kg/cm^2	P_H kg/cm^2	P_V/P_H
120	45	17.2	0.43	0.33	1.30
90	45	12.9	0.72	0.41	1.76
60	45	8.6	1.44	0.47	2.40
54	45	7.7	1.72	0.49	3.50
48	45	6.9	2.10	0.51	4.20

Table 9-1 Void Ratio P_V, P_H, P_V/P_H Values Defining One-Dimensional Volume Change Behavior

The vertical pressure P_V-void ratio relationship defined in Table 9-1 is illustrated in Fig. 9-1. Comparing the experimental curve with the model curve, it is found that the agreement is very good. The model structure used in this study gives a better approximation to the observed curve than does the infinite particle model.

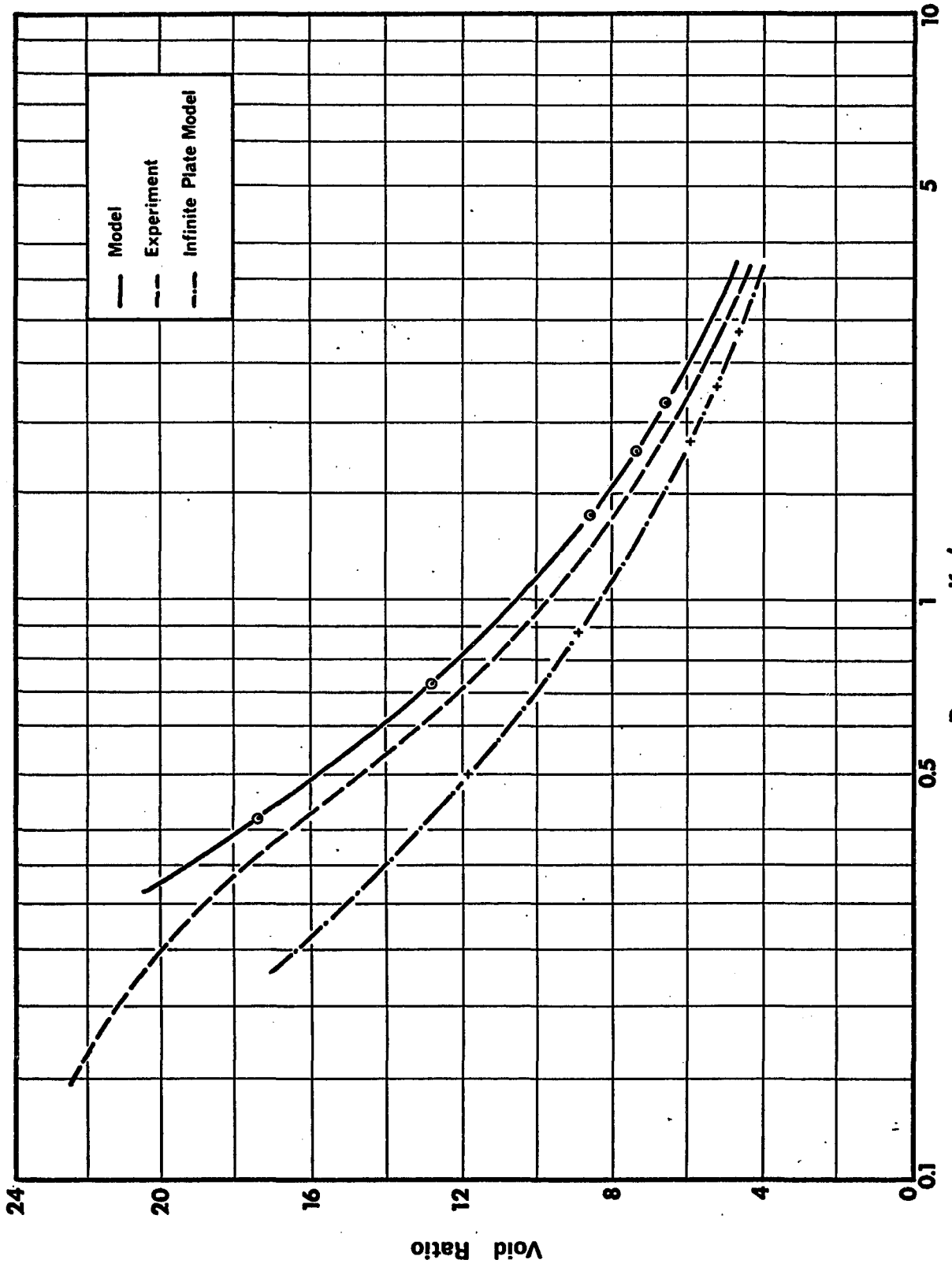

Figure 9-1 Comparison of Experimental and Model Results

The model void ratio-pressure curve predicts a single curve for both compression and swelling; however, the experimental swelling curve follows a lower void ratio pressure relationship (see Fig. 8-4). A possible explanation to this deviation is hypothesized as follows.

Taking the van Der Waal!s attractive forces into consideration (in addition to the repulsive forces) the net-force particle-distance relationship will take the form quantitatively illustrated in Fig. 9-2.

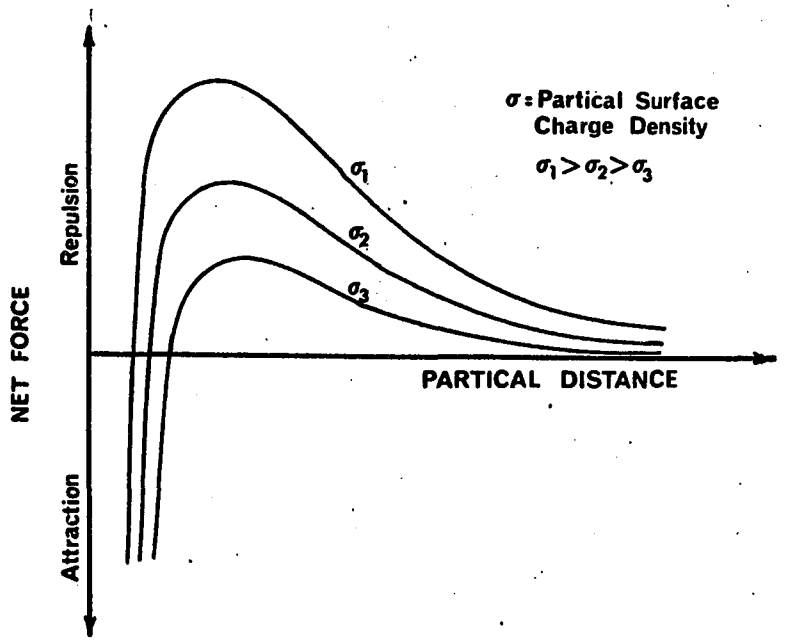

Fig. 9-2 Net-Force Distance Relationship Between Particles

The figure shows that at large distances there is a net repulsive pressure between the particles. As the distance is reduced repulsive pressure reaches a maximum and with a slight further decrease in distance a net attractive force acts between the particles. The maximum value of repulsive pressure decreases with decreasing particle surface

charge density because repulsive pressures between the particles are directly proportional to the surface charge density of the particles. With possible variations in surface charge density of particles and with the added effect of micro stress concentrations, at a given mean stress level some particles may be forced to go over the maximum repulsive stress barrier forming flocks. Upon removal of the compressive pressure these particles will remain together due to the large van Der Waal's attractive forces and will not contribute to the swelling of the structure, consequently causing a lower void ratio pressure curve for the overall sample. An estimate of the distribution of surface charge density values is needed before this effect can be accounted for quantitatively.

9-2 Two-dimensional Volume Change Behavior of Model Structure

Volume change of the model structure under more complex stress conditions than one-dimensional compression may be obtained from the pressure-void ratio relationships obtained in Chapter 7.

Two stress systems are analyzed; both of these systems are of practical interest in studying volume change behavior of clayey soils:

(a) Volume change under a constant ratio of vertical to horizontal stresses. (Anisotropic Consolidation)

(b) Volume change with a varying ratio of vertical to horizontal stresses. (Drained Shear Testing)

The volume change behavior of soils under triaxial stress systems is commonly expressed in terms of the void ratio-mean pressure relationship. In triaxial testing the sample is subjected to two independent

principal stresses---a vertical stress and a radial stress. The two-dimensional model is considered as an approximation to this system with P_V being the vertical stress and P_H being the horizontal or radial stress.

For the model structure, the mean pressure $\bar{P}$ will take the form

$$\bar{P} = \frac{P_H + P_V}{2}$$

In Fig. 9-3 model volume change behavior for constant P_V/P_H ratios is given. (Data for these curves are taken from Table 7-2.) The behavior for a higher P_V/P_H ratio follows a lower void ratio-mean pressure curve. This finding agrees well with the experimental data available on anisotropic consolidation of clayey soils. (Roscoe et al)

When considering higher and higher P_V/P_H ratios one point should be noted: for all soils there is a maximum P_V/P_H ratio that the soil can resist without a shear failure. The model clay structure considered in this study does not simulate a shear failure. Consequently, P_V/P_H ratios for the model particle structure may attain high values that cannot be observed in experiments. Nevertheless, the model behavior has the general form that can be observed in anisotropic consolidation tests.

Volume change with varying vertical to horizontal stress ratio is achieved during drained shear testing of soils. Most common drained shear testing used in the laboratories are conducted under constant radial stress with increasing vertical stress. The tests are conducted at slow enough strain rates to allow time for drainage without

building pore pressure in the sample.

With the model structure pressure void ratio relationships (see Fig. 7-7), the drained testing explained above can be simulated as follows.

The particle structure is initially subjected to a given all around (isotropic) pressure; therefore, a point is selected from Table 7-2 with $P_V/P_H \simeq 1$ defining the void ratio and all around pressure at the outset of the test. Keeping P_H constant at the given value, other points may be selected with increasing P_V. Such points will simulate the volume change behavior during shear testing before shear failure. Figure 9-4 illustrates the void ratio-pressure relationship and the corresponding stress path.

The predicted behavior agrees well with the general form of published experimental findings. (Lambe and Whitman 1969)

a	b	e	P_V	P_H	P_V/P_H	$\frac{P_V+P_H}{2}$	$\frac{P_V-P_H}{2}$
120	30	15.4	0.46	0.53	0.83	0.50	$\simeq 0$
60	45	8.6	1.44	0.47	3.06	0.95	0.42
54	45	7.7	1.72	0.49	3.50	1.10	0.62
48	45	6.9	2.10	0.51	4.12	1.30	0.80

Table 9-2 Void Ratio P_V, P_H, and P_V/P_H Values Defining Two-dimensional Volume Change Behavior

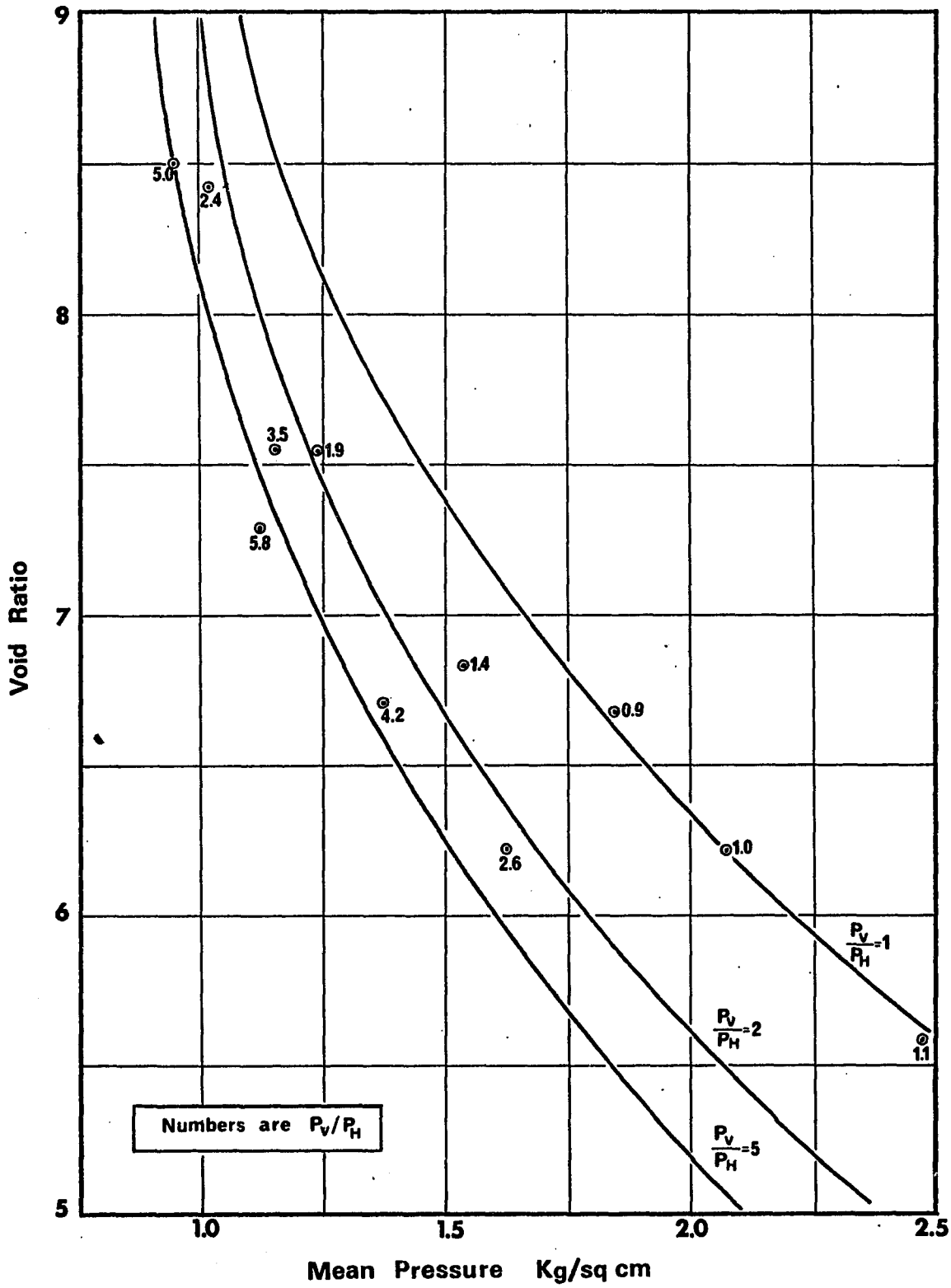

Figure 9-3 Void Ratio Mean Pressure Relationship (Anisotropic Consolidation)

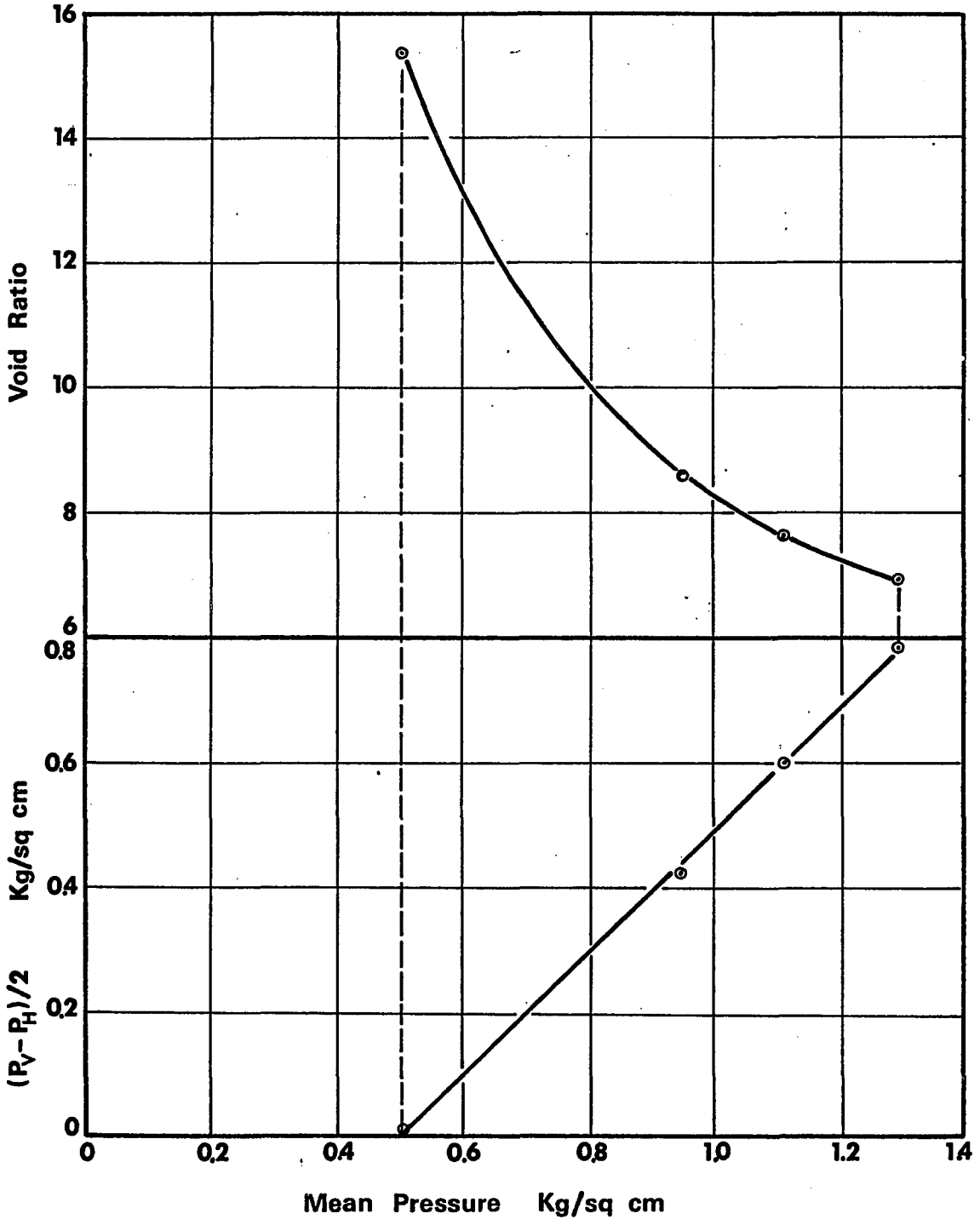

Figure 9-4 Model Structure Volume Change Behavior (Drained Shear)

10 - LIMITATIONS AND RECOMMENDATION

The limitations on the analyses presented in this study may be classified into two main groups:

1. Validity and applicability of double layer theory to clay particle systems.
2. Idealization of clay particle system and solution of double layer equation.

Validity and applicability of double layer theory to clay particle system: A detailed discussion of the validity of double layer theory is not within the scope of this study. The theory assumes that the ions are point charges and that the solution concentration is low. The theory was completely developed and formally applied to colloidal particles by Vervey and Overbeck in 1948. Considerable effort had gone into refining the theory for the interpretation of experimental results, and much attention has been given to its range of validity and causes for deviations. Corrections have been discussed by Haydon (1964). Bolt (1956) successfully applied the theory in studying the compressibility of clays. The concensus is that the thoery remains valid in its general form for typical clay colloidal systems.

Idealization of clay particle system and solution of double layer equation: The most obvious limitation is the two-dimensional definition of the model. A two-dimensional model was selected because clay particles are generally quite flat and the additional programming and labor involved in a three-dimensional formulation were not warranted.

As a check on the numerical procedure the solution for a one-dimensional situation was compared with the closed form solution (Vervey and Overbeck); the values were identical.

A working analytical model has been developed herein for predicting the volume change behavior of saturated clay for different loading conditions based on the physico-chemical properties of the soil water system. The applicability and the value of the model has been demonstrated by the comparison with experimental results.

Based on these results it is suggested that the model be extended in several aspects.

The primary reason for disagreement in the literature concerning the volume change behavior of clay soils is that the mechanisms which govern these properties are not well-known. This study has shown that the volume change behavior may be accounted for by the physico-chemical properties of a clay water system. The analysis can be a valuable tool for studying the mechanisms which govern the soil water system behavior. However, in this study only a simple model clay structure has been analyzed. It is suggested that the method of analysis presented herein be extended to other soil particle structure geometries. It is also suggested that by introducing particle to particle contacts a more generalized model can be developed covering a wider range of soil conditions.

The flexibility of the finite element method provides the investigator with a tool for solving the Poisson-Boltzmann differential equation for various boundary conditions and soil structure geometries.

11 - SUMMARY AND CONCLUSIONS

Summary

The analysis and description of clay volume change behavior is a topic of central interest in civil engineering. This thesis has presented an analytical model capable of predicting the volume change behavior of clayey soils. The model is formulated based on the interparticle repulsive forces, which may be determined from the electrical potential distribution between particles. Electrical potential distribution is defined by the Poisson-Boltzmann differential equation. A computer program is presented which can be used to solve the Poisson-Boltzmann equation using a finite element numerical technique. The volume change behavior of the model is evaluated to simulate the stress conditions observed in one-dimensional and two-dimensional isotropic and anisotropic loading.

One-dimensional consolidation tests were conducted on homoionic sodium montmorillonite and the results were compared with the behavior predicted from the model.

The two-dimensional volume change behavior of the model was evaluated and the findings were compared with experimental data obtained by previous investigators on soils tested under similar stress conditions.

Differences between compression and rebound void ratio-pressure relationships are examined and a hypothesized explanation is presented based on interparticle forces.

Conclusions

1) Comparing the model volume change behavior under one-dimensional stress conditions with that observed experimentally, it is concluded that the volume change behavior of dispersed clays under these

conditions can be accounted for by the model particle structure presented in this study. This observation suggests that the repulsive pressure acting between the particles is the factor determining the compressibility of expanding clays.

2) A hypothesized explanation is given for the observed difference between the initial compression and rebound void ratio-pressure curves. The reasoning is based on possible variation in interparticle force and local micro stress concentrations resulting in progressive parallel orientation of the dispersed structure with increasing preswelling pressures. The lower void ratio-pressure relationship was attributed to the failure of the collapsed particles to rebound upon removal of compressive stresses.

3) The volume change behavior of clay soils subjected to isotropic and anisotropic stress conditions has been widely studied. The experimental findings of the other investigators may be summarized as follows:

a. Samples tested under constant anisotropic stress ratio (increasing vertical and radial stress, while keeping the ratio of vertical to radial stress constant) follow a void ratio mean pressure relationship which is similar to that of isotropic consolidation but falls below it. This curve gets lower with increasing anisotropic stress ratio.

b. The samples tested subjected to increasing anisotropic stress ratio (constant radial stress, increasing vertical stress) follow the corresponding points defined by the constant anisotropic stress ratio testing.

These tests indicate a unique relationship between void ratio, mean stress and anisotropic stress ratio independent of the stress path used.

Comparing the form of the volume change behavior predicted for two-dimensional isotropic and anisotropic loading with that observed by other investigators it is concluded that the model is capable of accounting for the volume change behavior of dispersed clay subjected to two-dimensional stress systems as well as one-dimensional compression.

The study has presented a working model establishing relationships between physico-chemical properties of the clay water system and the volume change behavior which has engineering importance.

REFERENCES

1. Berg, P. N., "Calculus of Variations," Handbook of Engineering Mechanics, Chap. 16, ed. W. Flugge, McGraw-Hill (1962).

2. Bolt, G. H., "Physico-Chemical Analysis of the Compressibility of Pure Clay," Geotechnique, 6, 86-93 (1956).

3. Bolt, G. H. and R. D. Miller, "Compression Studies of Illite Suspensions," Soil Science Society of America Proceedings, 19, p. 285 (1955).

4. Casagrande, A., "The Structure of Clay and Its Importance in Foundation Engineering," (1932), J. Boston Society of Civil Engineers Contribution to Soil Mechanics 1925-40, 72-126.

5. Chapman, D. L., "A Contribution to the Theory of Electrocapillarity," Philosophy Magazine, 25, No. 6, 475-481 (1913).

6. Emerson, W. W., "The Structure of Soil Crumbs," J. Soil Science, 10, p. 235 (1959).

7. Geuze, E. C. W. A., "Rheological and Mechanical Models of Saturated Clay Particle Systems," (1964), Proceedings of Grenoble Symposium: Rheology and Soil Mechanics, Springer-Verlag, Berlin 1966.

8. Geuze, E. C. W. A. and P. M. Rebull, "Mechanical Force Fields in a Clay Particle System," Clays and Clay Minerals, 14th Conference, Pergamon Press, New York, 103-116 (1968).

9. Gouy, G., "Sur la Costitution de la Charge E'lectrique a'la Surface d'un E'lectrolyte," Ann. Phys. (Paris) Série 4, 9, 457-468 (1910).

10. Gouy, G., "Sur la Fonction E'lectrocapillaire," Ann. Phys. (Paris) Série 9,7, 129-184 (1917).

11. Haydon, D. A., "The Electrical Double Layer and Electrokinetic Phenomena," Recent Progress in Surface Science, 1, Danielli et al. eds., Academic Press, New York (1964).

12. Hough, B. K., Basic Soil Engineering, Chapter 1, Ronald Press Company, New York (1969).

13. Lambe, T. W., "The Structure of Inorganic Soils," Proc. American Society of Civil Engineers, 79, No. 315 (1953).

14. Lambe, T. W., "The Structure of Compacted Clay," J. Soil Mechanics and Foundation Engineering, American Society of Civil Engineers, 84 (1958).

15. Langmuir, I., "The Role of Attractive and Repulsive Forces in the Formation of Tactoids, Thixotripic Gels, Protein Crystals and Coacervates," J. Chem. Phys. 6, 873-896 (1938).

16. Low, P. F., "Physical-Chemical Properties of Soil-Ion Exchange Phenomena," Discussion, A. W. Taylor's paper, J. Soil Mechanics and Foundation Engineering, American Society of Civil Engineers, 88, 178-181 (1959).

17. Macey, H. H., "Clay-Water Relationships and the Internal Mechanism of Drying," Trans. Ceramics Society (England) 41, p. 73 (1942).

18. Marshall, C. E., The Colloidal Chemistry of the Silicate Minerals, Academic Press, New York (1949)

19. Marshall, C. E. The Physical Chemistry and Mineralogy of Soils, I Soil Minerals, J. Wiley & Sons, New York (1964).

20. McEwen, M. B. and D. L. Mould, "Gelation of Montmorillonite," Nature, 166, p. 437, London (1950).

21. Michaels, A. S., "Physico-Chemical Properties of Soils: Soil Water Systems," Discussion, J. Soil Mechanics & Foundation Engineering, American Society of Civil Engineers, SM2, p. 98, (1959)

22. Mitchell, J. K., "The Fabric of Natural Clays and its Relation to Engineering Properties," Proc. Highway Research Board, 35, 693-713 (1956).

23. Olphen, van, H., "Rheological Phenomena of Clay Soils in Connection with the Charge Distribution on the Micelles," Discussion, Faraday Society, 11 (The Size and Shape Factors in Colloidal Systems), 82-84 (1951).

24. Olphen, van, H., "Chemical Treatment of Drilling Fluids," Thesis, Delft(1950-b).

25. Olphen, van, H., "Forces Between Suspended Bentonite Particles," Fourth Conference on Clays and Clay Minerals, 204-224, Pergamon Press, New York (1956).

26. Olphen, van, H., An Introduction of Clay Colloid Chemistry, Interscience Publishers (1963).

27. Olphen, van, H., "Stabilization of Montmorillonite Soils by Chemical Treatments," Rec. Trav. Chem., 69, 1308-1312 (1950-a).

28. Ohlson, R. E. and F. Mitronovas, "Shear Strength and Consolidation Characteristics of Calcium and Magnesium Illite," Ninth Conference of Clays and Clay Minerals, 348-349, Pergamon Press, New York (1962).

29. Rosenqvist, I. M., "Physico-Chemical Properties of Soils: Soil-Water Systems," J. Soil Mechanics & Foundation Engineering, American Society of Civil Engineers, SM2, p. 31 (1959)

30. Raussell-Colom, J. A. "El hinchameinto de la montmorillonita-sodica y del complejo montmorillonita-krilium en electrolitos," Doctoral Thesis, University of Madrid (1958).

31. Salas, J. A. and J. M. Serratosa, "Compressibility of Clays," Proc. Third International Conference on Soil Mechanics and Foundation Engineering, 1, 192-198, Zurich (1953).

32. Samuels, S. G., "The Effect of Bolsa Exchange on the Engineering Properties of Clays," Building Research Station, Note C-176, p. 28, Dept. Science & Industrial Research, Garston, England (1950).

33. Schofield, R. K. and H. R. Samson, "Fiocculation of Kaolinite due to the Attraction of Oppositely Charged Crystal Forces," Discussions, Faraday Society, 18, 135-145 (1954).

34. Stern, O., Z. Elektrochem. (30), p. 508 (1924).

35. Terzaghi, K., "The Physical Properties of Clays," Massachusetts Institute of Technology Tech. Engr. News, 9:10, 11 (1928).

36. Thiessen, P. A., "Wechselseitige Adsorption von Kalloiden," Z. Elektrochem. 48, 675-681 (1942).

37. Verwey, E. J. W. and J. T. G. Overbeck, Theory of the Stability of Lyophobic Colloids, Elsevier, New York (1948).

38. Warkentin, B. P., G. H. Bolt and R. D. Miller, "Swelling Pressure of Montmorillonite," Soil Science, 21, 435-437 (1957).

39. Waidelich, W. C., "Physico-Chemical Factor Influencing the Consolidation of Soils," M.S. Thesis, Princeton University (1957).

40. Winterkorn, H., "The Conditions of Water in Porous Systems," Soil Science, p. 103,(1943).

NOTATION

a, b	Particle separation distances as defined in Fig. 7-5a.
e	Elementary charge or void ratio
i, j, k	Finite element nodal points
k	Boltzmann Constant
L	Half plate length
n	Ion concentration
T	Absolute temperature
P	Interparticle pressure
P_H	Horizontal pressure on model structure
P_V	Vertical pressure on model structure
u, v, w	Dimensional coordinate system
$\bar{u}$	Half element length
Δ	Area of finite elements
ε	Dielectric Constant
κ	Defined in Eq.(5-5a)
ν	Valence of ions
ρ	Charge density
σ	Surface charge density
ϕ	Electrical potential
ψ	Non-dimensional potential
χ	Defined in Eq. (6-2)

APPENDIX A

Computer Program and Description

APPENDIX A

Computer Program and Description

Description of Computer Program: The program presented in this Appendix is written to solve the Poisson-Boltzmann differential equation using the finite element technique, over a domain subjected to given boundary conditions. Two cases of boundary conditions are concidered: 1) specified values of the potential and 2) specified normal gradients of the potential. The program determines the potentials at the verticies of the finite elements, in addition the total space charge is calculated using the nodal potentials. Because of the non-linearity of the Poisson-Boltzmann equation, an initial guessed set of nodal potentials must be substituted into the algorithm. These guessed values can be determined by using the space-surface charge equivalency. With the known surface charge distribution over the domain, the magnitude of the uniform potential may readily be determined from Eg. (5-3)

$$\rho=-2n_o\nu e \sinh(\nu e\phi/kT)$$

The initial guesses determined with the above procedure were empirically found to be satisfactory; i.e., the algorithm converged.

The program is written in Fortram V to be run on the Univac 1108. The following data cards are required to run the program:

Card-1 COEF 1, CONC, NDSL,SCD

COEF 1= Coefficient defined as $e\nu/kT$

CONC = Ion concentration (Normality)

NDSL = Length of charged surface (non dimensioralized)

SCD = Surface charge density in e.s.u.

Card-2 NUMNP, NUMEL, NUMSBC

NUMNP = Number of nodes

NUMEL = Number of finite elements

NUMSBC = Number of slope boundary conditions

Card-3 X(I), Y(I)

X(I) = X coordinate of node I

Y(I) = Y coordinate of node I

Card-4 KOD1, KOD2, FN(I)

KOD1 = 1 if potential is fixed, 0 otherwise

KOD2 = 1 if potential is fixed, 0 otherwise

FN(I) = Initial guessed potential

Card-5 N, NP(1), NP(2), NP(3)

N = Element number

NP(1), NP(2), NP(3) = Nodes of the element, (entered in counter clockwise sequence)

```
1*   C      SOLUTION OF POISSON-BOLTZMAN EQUATION BY FINITE ELEMENT METHOD
2*          REAL N1,N2,N3,N4,NDSL
3*          DIMENSION X(250),Y(250),KODE(250),NP(3),FX(250),A(3),B(3),
4*         1C(3),SN(3),S(3,3),D(250,27),NY(3,250),FN(250),
5*         1F1(4,4),AREA(4),H(4),X1(4,4),Y1(4,4),
6*         1N1(4,4),N2(4,4),N3(4,4),N4(50,3),KOD1(250),KOD2(250),
7*         1AREA1(4),AREA2(4),AREA3(4),SM(3,3),
8*         1FM(4,4)F2(4,4),F3(4,4)
9*          READ(5,1500) COEF1,CONC,CNSL,SCD,
10*   1500 FORMAT()
11*         COEF2=32800000*SQRT(CONC)
12*         SURFLT=NDSL/COEF2
13*         SCHG=SCD*SURFLT
14*         WRITE(6,1501)
15*   1501 FORMAT(1H1,49HPHYSICAL CONSTANTS**********************************//)
16*         WRITE(6,1502) COEF1
17*   1502 FORMAT(1H ,27HCONSTANT-1.....,..... ,E7.3,3X10H1/STATVOLT/)
18*         WRITE(6,1503) COEF2
19*   1503 FORMAT(1H ,27HCONSTANT-2..... ,E7.3,3X,4H1/CM/)
20*         WRITE(6,1504) SURFLT
21*   1504 FORMAT(1H ,27HLENGTH OF CHARGED SURFACE,E7.3,3X,2HCM/)
22*         WRITE(6,1507) CONC
23*   1507 FORMAT(1H ,27HNORMALITY OF SOLUTION....,E7.3,3X,1HN/)
24*         WRITE(6,1506) SCHG
25*   1506 FORMAT(1H ,27HSURFACE CHARGE ..... ,E7.3,3X,6HE.S.U.///)
```

```
      WRITE(6,1505)
 1505 FORMAT(1H ,49HFINITE ELEMENT INFORMATION**********************//)
      READ(5,1000)NUMNP,NUMEL,NUMSBC
 1000 FORMAT()
      WRITE(6,2000)NUMNP,NUMEL,NUMSBC
 2000 FORMAT(1H ,24HNUMBER OF NODAL POINTS--,15,6X,18HNUMBER OF ELEMENTS
     1,2H--,15//,1X,24HSLOPE ON BOUNDARY COND--,15////)
      WRITE(6,2001)
 2001 FORMAT(1H ,6X,8HN.P. NO.,6X,1HX,14X,1HY/)
C
C     READ NODAL POINT INFORMATION
C
      DO 1 I=1,NUMNP
      READ(5,1001)X(I),Y(I)
 1001 FORMAT()
      X(I)=-X(I)*0.02
       Y(I)=Y(I)*0.05
    1 WRITE(6,2002)I,X(I),Y(I)
 2002 FORMAT(1H ,I10,2E15.6)
C
C     READ INITIAL VALUES
C
      WRITE(6,2103)
 2103 FORMAT(1H1,6X,8HN.P. NO.,3X,6HCODE 1,4X,6HCODE 2,4X
     1,13HINITIAL-GUESS/)
```

```
      DO 2 I=1,NUMNP
      READ(5,1102) KOD1(I),KOD2(I),FN(I)
 1102 FORMAT()
    2 WRITE(6,2104) I,KOD1(I),KOD2(I),FN(I)
 2104 FORMAT(1H ,3110,E15.6)
C
C     READ ELEMENT INFORMATION
C
      WRITE(6,2008)
 2008 FORMAT(1H1,2X,11HELEMENT NO.,2X,6HNODE I,3X,6HNODE J,3X,6HNODE K
     1//)
      CONT=-1.0
      DO 500 NB=1,20
      CHARGE=0.0
      DO 603 I=1,250
      FX(I)=0.0
      DO 603 J=1,27
  603 D(I,J)=0.0
      IF(NB-1)601,600,601
  600 DO 602 NN=1,NUMEL
      READ(5,1004)N,NP(1),NP(2),NP(3)
 1004 FORMAT()
      WRITE(6,2007)N,NP(1),NP(2),NP(3)
 2007 FORMAT(1H ,5X,I5,6X,I5,4X,I5,4X,I5/)
      DO 602 I=1,3
  602 NY(I,NN)=NP(I)
```

```
C
C     FORM ELEMENT MATRIX
C
  601 DO 300 NN=1,NUMEL
      DO 301 I=1,3
      DO 301 J=1,3
      SM(I,J)=0.0
  301 S(I,J)=0.
      IP=NY(1,NN)
      JP=NY(2,NN)
      KP=NY(3,NN)
      A(1)=(X(JP)*Y(KP)-X(KP)*Y(JP))
      A(2)=(X(KP)*Y(IP)-X(IP)*Y(KP))
      A(3)=(X(IP)*Y(JP)-X(JP)*Y(IP))
      B(2)=Y(KP)-Y(IP)
      B(3)=Y(IP)-Y(JP)
      B(1)=-(B(2)+B(3))
      C(2)=X(IP)-X(KP)
      C(3)=X(JP)-X(IP)
      C(1)=-(C(2)+C(3))
      DET=(X(JP)*Y(KP)-Y(JP)*X(KP))-(X(IP)*Y(KP)-Y(IP)*X(KP))+(X(IP)*Y(J
     1P)-Y(IP)*X(JP))
      DO 302 I=1,3
      DO 302 J=1,3
```

```
101*          S(I,J)=(B(I)*B(J)+C(I)*C(J))/(DET*2.)
102*        302 CONTINUE
103*    C
104*    C     NUMERICAL INTEGRATION
105*    C
106*          AA(1)=-0.8611363116
107*          AA(2)=-0.3399810436
108*          AA(3)=-AA(2)
109*          AA(4)=-AA(1)
110*          H(1)=0.3478548551
111*          H(2)=1.0-H(1)
112*          H(3)=H(2)
113*          H(4)=H(1)
114*    C
115*    C     COMPUTE GRID COORDINATES AND EVALUATE THE FUNCTIONS
116*    C
117*          DO 20 J=1,4
118*          XX=X(IP)+(X(JP)-X(IP))*(AA(J)+1.0)/2.0
119*          YY=Y(IP)+(Y(JP)-Y(IP))*(AA(J)+1.0)/2.0
120*          DO 20 I=1,4
121*          X1(I,J)=XX+(X(KP)-XX)*(AA(I)+1.0)/2.0
122*          Y1(I,J)=YY+(Y(KP)-YY)*(AA(I)=1.0)/2.0
123*          N1(I,J)=(A(1)+B(1)*X1(I,J)+C(1)*Y1(I,J))/DET
124*          N2(I,J)=(A(2)+B(2)*X1(I,J)+C(2)*Y1(I,J))/DET
125*          N3(I,J)=(A(3)+B(3)*X1(I,J)+C(3)*Y1(I,J))/DET
```

```
126*      20 CONTINUE
127*         DO 200 II=1,3
128*         IF(II-2) 21,22,23
129*      21 DO 24 I=1,4
130*         DO 24 J=1,4
131*         BETA=EXP(N1(I,J)*FN(IP)+N2(I,J)*FN(JP)+N3(I,J)*FN(KP))
132*         FM(I,J)=N1(I,J)*(BETA-1./BETA)/2.
133*         F1(I,J)=N1(I,J)*N1(I,J)*(BETA+1./BETA)/2.
134*         F2(I,J)=N1(I,J)*N2(I,J)*(BETA+1./BETA)/2.
135*      24 F3(I,J)=N1(I,J)*N3(I,J)*(BETA+1./BETA)/2.
136*         GO TO 27
137*      22 DO 25 I=1,4
138*         DO 25 J=1,4
139*         BETA=EXP(N1(I,J)*FN(IP)+N2(I,J)*FN(JP)+N3(I,J)*FN(KP))
140*         FM(I,J)=N2(I,J)*(BETA-1./BETA)/2.
141*         F1(I,J)=N2(I,J)*N1(I,J)*(BETA+1./BETA)/2.
142*         F2(I,J)=N2(I,J)*N2(I,J)*(BETA+1./BETA)/2.
143*      25 F3(I,J)=N2(I,J)*N3(I,J)*(BETA+1./BETA)/2.
144*         GO TO 27
145*      23 DO 26 I=1,4
146*         DO 26 J=1,4
147*         BETA=EXP(N1(I,J)*FN(IP)+N2(I,J)*FN(JP)+N3(I,J)*FN(KP))
148*         FM(I,J)=N3(I,J)*(BETA-1./BETA)/2.
149*         F1(I,J)=N3(I,J)*N1(I,J)*(BETA+1./BETA)/2.
150*         F2(I,J)=N3(I,J)*N2(I,J)*(BETA+1./BETA)/2.
```

```
      26 F3(I,J)=N3(I,J)*N3(I,J)*(BETA+1./BETA)/2.
C
C     EVALUATE THE INTEGRAL
C
      27 XL=SQRT((Y(JP)-Y(IP))**2+(X(JP)-X(IP))**2)
         YL=DET/XL
         SN(II)=0.0
         SM(II,1)=0.0
         SM(II,2)=0.0
         SM(II,3)=0.0
         DO 200 I=1,4
         CON=XL*(1.0-AA(I))/4.0
         AREA(I)=0.0
         AREA1(I)=0.0
         AREA2(I)=0.0
         AREA3(I)=0.0
         DO 28 J=L,4
         AREA1(I)=AREA1(I)+CON*H(J)*F1(I,J)
         AREA2(I)=AREA2(I)+CON*H(J)*F2(I,J)
         AREA3(I)=AREA3(I)+CON*H(J)*F3(I,J)
      28 AREA(I)=AREA(I)+CON*H(J)*FM(I,J)
         SN(II)=SN(II)+YL*H(I)*AREA(I)/2.0
         SM(II,1)=SM(II,1)+YL*H(I)*AREA1(I)/2.
         SM(II,2)=SM(II,2)+YL*H(I)*AREA2(I)/2.
         SM(II,3)=SM(II,3)+YL*H(I)*AREA3(I)/2.
```

```
  200 CONTINUE
C
C     INSERT INTO OVERALL MATRIX
C
      DO 303 L=1,3
      I=NY(L,NN)
      FX(I)=FX(I)-SN(L)-S(L,1)*FN(IP)-S(L,2)*FN(JP)-S(L,3)*FN(KP)
      DO 303 M=1,3
      J=NY(M,NN)-I+1
      IF (27-J) 304,305,305
  305 IF (MBAND-J) 306,307,307
  306 MBAND=J
  307 IF (J) 303,303,308
  308 D(I,J)=D(I,J)+S(L,M)+SM(L,M)
  303 CONTINUE
C
C     CALCULATE SPACE CHARGE
C
      C11=(EXP(FN(IP))-1./EXP(FN(IP)))/2.
      C12=(EXP(FN(JP))-1./EXP(FN(JP)))/2.
      C13=(EXP(FN(KP))-1./EXP(FN(KP)))/2.
      CHARGE=CHARGE+574308000000.*CONC*(C11+C12+C13)*DET/(6.*COEF2**2
  300 CONTINUE
C
C     MODIFY FOR BOUNDARY POINTS ON WHICH SLOPE IS FIXED
```

```
C
      IF(NUMSBC)425,425,63
   63 IF(NB-1)700,700,701
  700 WRITE(6,2003)
 2003 FORMAT(1H1,16X,27HSLOPE ON BOUNDARY CONDITION//10X,6HNODE I,
     110X,6HNODE J10X,5HSLOPE/)
      DO 62 N=1,NUMSBC
      READ(5,1002)I,J,QIJ
 1002 FORMAT()
      WRITE(6,2004)I,J,QIJ
 2004 FORMAT(1H ,10X,I5,10X,I5,10X,F10.0/)
      SIJ=SQRT((X(J)-X(I))**2+(Y(J)-Y(I))**2)
      FX(I)=FX(I)+0.5*QIJ*SIJ
      FX(J)=FX(J)+0.5*QIJ*SIJ
      N4(N,1)=I
      N4(N,2)=J
   62 N4(N,3)=QIJ
      GO TO 425
  701 DO 704 N=1,NUMSBC
      IK=N4(N,1)
      JK=N4(N,2)
      QK=N4(N,3)
      SIJ=SQRT((X(JK)-X(IK))**2+(Y(JK)-Y(IK))**2
      FX(IK)=FX(IK)+0.5*QK*SIJ
  704 FX(JK)=FX(JK)+0.5*QK*SIJ
```

```
C
C     MODIFY FOR BOUNDARY POINTS ON WHICH POTENTIAL IS FIXED
C
  425 CONT=CONT*(-1.0)
      IF(CONT-1.0)  791,790,790
  790 DO 650 K=1,NUMNP
  650 KODE(K)=KOD1(K)
      GO TO 691
  791 DO 651 K=1,NUMNP
  651 KODE(K)=KOD2(K)
  691 DO 400 K=1,NUMNP
      IF(KODE(K)-1) 400,400,401
  401 I=K+1
      DO 402 J=2,MBAND
      L=I-J
      IF (L) 403,403,404
  404 D(L,J)=0.0
  403 M=K+J-1
      IF (M-NUMNP) 405,405,402
  405 D(K,J)=0.0
  402 CONTINUE
      D(K,1)=1.0
      FX(K)=0.0
  400 CONTINUE
C
```

```
C     CALCULATE SURFACE CHARGE
C
      SURFCH=(20./3.1416)*(QIJ/COEF1)*SURFLT*COEF2
C
C     REDUCE TO TRIANGULAR FORM
C
      DO 406 J=1,NUMNP
      DO 408 K=2,MBAND
      CS=D(J,K)/D(J,1)
      I=J+K-1
      IF (NUMNP-I) 408,407,407
  407 L=0
      FX(I)=FX(I)-CS*FX(J)
      DO 409 NQ=K,MBAND
      L=L+1
  409 D(I,L)=D(I,L)-CS*D(J,NQ)
  408 D(J,K)=CS
      FX(J)=FX(J)/D(J,1)
  406 CONTINUE
C
      WRITE(6,2111) NB
 2111 FORMAT(1H1,5X,12HITERATION...,I5///)
      WRITE(6,2100) CHARGE
 2100 FORMAT(1H ,5X,12HSPACE CHARGE,5X,E12.6,2X,6HE.S.U.//)
      WRITE(6,2110) SURFCH
```

```
 2110 FORMAT(1H ,5X,14HSURFACE CHARGE,3X,E12.6,2X,6HE.S.U.///)
C
C     BACK SUBSTITUTION
      WRITE(6,2030)
 2030 FORMAT(1H ,5X,4HNODE,10X,9HPOTENTIAL//)
      I=NUMNP
      FN(I)=FN(I)+FX(I)
      WRITE(6,2031) I,FN(I)
  411 I=I-1
      IF (I) 410,64,410
  410 DO 412 K=2,MBAND
      L=I+K-1
      IF (NUMNP-L) 412,413,413
  413 FX(I)=FX(I)-D(I,K)*FX(L)
  412 CONTINUE
      FN(I)=FN(I)+FX(I)
      WRITE(6,2031) I,FN(I)
 2031 FORMAT(1H ,3X,I5,8X,E11.6)
      GO TO 411
  304 WRITE(6,2010)
 2010 FORMAT(1H1,19HBAND WIDTH EXCEEDED)
   64 CONTINUE
  500 CONTINUE
      END
```

APPENDIX B

Numerical Integration over a Triangular Domain

APPENDIX B

Numerical Integration over a Triangular Domain

The Gaussian quadrature formulae were used to evaluate the integral $\int \int_A \text{Sinh } \psi \, dxdy$ over a triangular domain. A more detailed discussion of the method is given in Zienkiewicz (1967).

The definite integral $\int_{-1}^{1} f(x)\, dx$ is replaced by the summation

$$\sum_{j=1}^{n} H_j \, f(a_j)$$

where H_j are the weighing coefficients, $f(a_j)$ the value of the function at specified points a_j and n the number of Gauss points used.

To integrate a function over a triangular domain the Gaussian quadrature formula is first applied in the x direction (parallel to the base of the triangle) and then in the y direction.

A mesh is first drawn over a triangle as shown in Fig. B-1. In the present case four points are used in each direction.

The area of the ith 'slice' parallel to the base is first computed by applying the formula in the x direction

$$A = \frac{(XL)}{2} \frac{(1-a_i)}{2} (0.348\, f_{i1} + 0.652\, f_{i2} + 0.652\, f_{i3} + 0.348\, f_{i4})$$

where f_{in} are the values of the function at the Gauss points along line i, and the position of the line i being determined by the coefficient a_i.

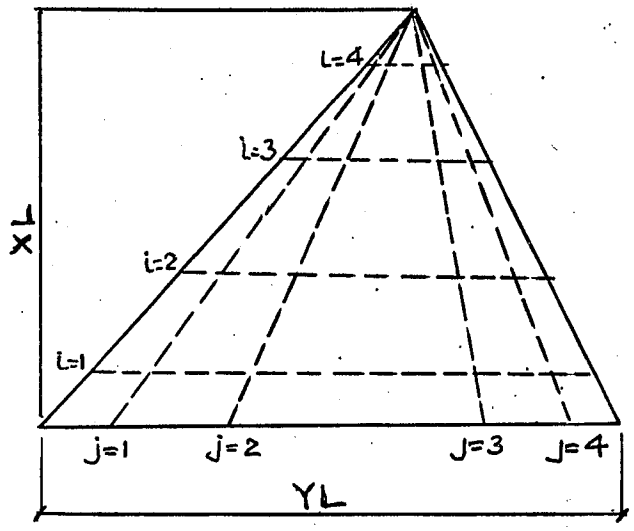

Fig. B-1 Gaussian Integration Mesh Over a Trangle

The formula is then applied to the area of the 'slice' in the y-direction to give the double integral.

$$\int\int f(x,y)\,dxdy = \frac{(YL)}{2}\{0.348\,A_1 + 0.652\,A_2 + 0.652\,A_3 + 0.348\,A_4\}$$

It should be noted that for triangles with bases which are not parallel to the global x axis, integration will have to be carried out in local coordinates first, and then transformed to the global coordinates.

APPENDIX C

Potential Distributions

APPENDIX C

Potential Distributions

In the following figures (C-1 to C-20) modal non-dimensional potentials and boundary pressures are tabulated for various plate separation distances, as indicated by dimensions a and b. (See Fig. 7-5a)

The potentials and boundary pressures are calculated as follows: The model element is subdivided into triangular elements (a typical subdivision is illustrated in Fig. 7-3). Through the use of computer program the non-dimensional potentials are calculated at the verticies of the triangular elements. The boundary pressures are calculated using Eq. (5-17) ($p=2nkT(\text{Cosh}\psi_o-1)$).

The following potential distributions may be used to determine the variations of hydrostatic pressures within the element.

(0.50)	(0.50)	(0.50)	(0.50)	(0.50)	(0.48)	(0.47)	(0.46)		
5.37	5.37	5.37	5.36	5.35	5.33	5.31	5.29	5.26	(0.46)
5.57	5.57	5.57	5.57	5.56	5.53	5.50	5.46	5.43	(0.55)
5.97	5.97	5.97	5.97	5.96	5.94	5.88	5.79	5.74	(0.76)
6.70	6.70	6.70	6.70	6.70	6.68	6.59	6.38	6.20	(1.18)
8.22	8.22	8.22	8.22	8.22	8.20	8.13	7.51	6.54	(1.76)
10.11	10.11	10.11	10.11	10.11	10.10	10.09	8.70	6.55	(1.76)

Note: (Pressure in kg/cm^2)

Figure C-1 Potential Distribution and Pressures on Boundaries
(a = 120Å, b = 15 Å)

(0.87)	(0.87)	(0.87)	(0.87)	(0.87)	(0.86)	(0.83)	(0.79)	(0.75)	
5.91	5.91	5.91	5.91	5.90	5.87	5.83	5.78	5.74	(0.75)
6.10	6.10	6.10	6.10	6.09	6.07	6.01	5.94	5.89	(0.86)
6.49	6.49	6.49	6.49	6.48	6.46	6.38	6.24	6.13	(1.08)
7.18	7.18	7.18	7.18	7.18	7.17	7.06	6.77	6.48	(1.59)
8.57	8.57	8.57	8.57	8.57	8.56	8.48	7.78	6.77	(1.77)
10.13	10.13	10.13	10.13	10.13	10.12	10.11	8.73	6.78	(1.77)

Note: (Pressure in kg/cm^2)

Figure C-2 Potential Distribution and Pressures on Boundaries
(a = 90 Å, b = 15 Å

(1.87)	(1.87)	(1.87)	(1.87)	(1.87)	(1.82)	(1.63)	(1.52)	(1.38)	
6.65	6.65	6.65	6.65	6.65	6.62	6.54	6.44	6.35	(1.38)
6.83	6.83	6.83	6.83	6.83	6.81	6.72	6.57	6.45	(1.52)
7.19	7.19	7.19	7.19	7.19	7.17	7.06	6.84	6.61	(1.76)
7.82	7.82	7.82	7.82	7.82	7.82	7.69	7.29	6.80	(2.14)
9.01	9.01	9.01	9.01	9.01	9.00	8.90	8.11	6.81	(2.15)
10.17	10.17	10.17	10.17	10.17	10.16	10.13	8.79	6.82	(2.15)

Note: (Pressure in kg/cm^2)

Figure C-3 Potential Distribution and Pressures on Boundaries ($a = 60$ Å, $b = 15$ Å)

(2.28)	(2.28)	(2.28)	(2.28)	(2.28)	(2.26)	(2.06)	(1.78)	(1.06)	
6.84	6.84	6.84	6.84	6.84	6.81	6.72	6.60	6.50	(1.60)
7.02	7.02	7.02	7.02	7.02	7.00	6.90	6.73	6.58	(1.75)
7.36	7.36	7.36	7.36	7.36	7.35	7.23	6.98	6.72	(2.06)
7.99	7.99	7.99	7.99	7.99	7.98	7.84	7.42	6.88	(2.35)
9.11	9.11	9.11	9.11	9.11	9.10	9.00	8.19	6.89	(2.36)
10.18	10.18	10.18	10.18	10.18	10.15	10.13	8.81	6.89	(2.36)

Note: (Pressure in kg/cm^2)

Figure C-4 Potential Distribution and Pressures on Boundaries
(a = 54 Å, b = 15 Å)

(2.76)	(2.76)	(2.76)	(2.76)	(2.76)	(2.65)	(2.52)	(2.15)	(1.86)	
7.05	7.05	7.05	7.05	7.05	7.02	6.93	6.78	6.65	(1.86)
7.23	7.23	7.23	7.23	7.22	7.20	7.10	6.90	6.72	(2.02)
7.56	7.56	7.56	7.55	7.55	7.55	7.42	7.15	6.84	(2.26)
8.15	8.15	8.15	8.15	8.15	8.14	8.01	7.56	6.98	(2.64)
9.22	9.22	9.22	9.22	9.22	9.21	9.09	8.28	6.98	(2.64)
10.19	10.19	10.19	10.19	10.19	10.17	10.12	8.84	6.99	(2.64)

Note: (Pressure in kg/cm^2)

Figure C-5 Potential Distribution and Pressures on Boundaries
(a = 48 Å, b = 15 Å)

(0.50)	(0.50)	(0.50)	(0.50)	(0.50)	(0.48)	(0.45)	(0.42)	(0.39)	(0.38)	
5.37	5.37	5.36	5.35	5.33	5.29	5.24	5.17	5.11	5.07	(0.38)
5.57	5.57	5.56	5.56	5.54	5.50	5.43	5.33	5.23	5.18	(0.42)
5.97	5.97	5.97	5.96	5.95	5.91	5.81	5.64	5.45	5.35	(0.50)
6.70	6.70	6.70	6.70	6.69	6.68	6.54	6.21	5.79	5.55	(0.62)
8.22	8.22	8.22	8.22	8.22	8.21	8.11	7.34	6.22	5.56	(0.62)
10.11	10.11	10.10	10.11	10.11	10.13	10.15	8.51	6.22	5.57	(0.62)

Note: (Pressure in kg/cm^2)

Figure C-6 Potential Distribution and Pressures on Boundaries
(a = 120 Å, b = 30 Å)

(0.87)	(0.87)	(0.87)	(0.87)	(0.86)	(0.83)	(0.75)	(0.67)	(0.59)	(0.55)	
5.91	5.91	5.91	5.90	5.88	5.84	5.76	5.64	5.52	5.45	(0.55)
6.10	6.10	6.10	6.10	6.08	6.04	5.95	5.79	5.62	5.52	(0.59)
6.48	6.48	6.48	6.48	6.48	6.44	6.32	6.08	5.79	5.62	(0.67)
7.18	7.18	7.18	7.18	7.18	7.17	7.02	6.61	6.06	5.62	(0.67)
8.57	8.57	8.57	8.57	8.57	8.56	8.46	7.61	6.38	5.62	(0.67)
10.13	10.13	10.13	10.13	10.13	10.13	10.11	8.54	6.37	5.63	(0.67)

Note: (Pressure in kg/cm^2)

Figure C-7 Potential Distribution and Pressures on Boundaries
(a = 90 Å, b = 30 Å)

(1.87)	(1.87)	(1.87)	(1.87)	(1.87)	(1.78)	(1.60)	(1.30)	(0.96)	(0.85)	
6.65	6.65	6.65	6.65	6.65	6.61	6.50	6.28	6.03	5.87	(0.87)
6.83	6.83	6.83	6.83	6.83	6.80	6.67	6.41	6.11	5.87	(0.87)
7.19	7.19	7.19	7.19	7.19	7.17		6.68	6.23	5.86	(0.87)
7.82	7.82	7.82	7.82	7.82	7.82	7.66	7.14	6.42	5.85	(0.84)
9.01	9.02	8.99	9.00	9.01	9.06	8.87	7.95	6.64	5.70	(0.72)
10.17	10.17	10.17	10.17	10.17	10.15	10.11	8.60	6.63	5.66	(0.67)

Note: (Pressure in kg/cm^2)

Figure C-8 Potential Distribution and Pressures on Boundaries
(a = 60 Å, b = 30 Å)

(2.28)	(2.28)	(2.28)	(2.28)	(2.28)	(2.16)	(1.96)	(1.52)	(1.14	(0.92)	
6.84	6.84	6.84	6.84	6.84	6.80	6.68	6.44	6.16	5.96	(0.92)
7.02	7.02	7.02	7.02	6.99	6.85	6.57	6.22	5.96	5.96	(0.92)
7.36	7.36	7.36	7.36	7.36	7.35	7.20	6.83	6.34	5.95	(0.92)
7.99	7.99	7.99	7.99	7.99	7.98	7.81	7.27	6.51	5.89	(0.88)
9.11	9.11	9.11	9.11	9.11	9.10	8.96	8.03	6.71	5.73	(0.75)
10.18	10.18	10.18	10.18	10.18	10.16	10.10	8.63	6.71	5.70	(0.65)

Note: (Pressure in kg/cm^2)

Figure C-9 Potential Distribution and Pressures on Boundaries
(a = 54 Å, b = 30 Å)

(2.76)	(2.76)	(2.76)	(2.76)	(2.76)	(2.64)	(2.40)	(1.86)	(1.30)	(1.02)	
7.05	7.05	7.05	7.05	7.05	7.02	6.89	6.62	6.29	6.04	(1.02)
7.23	7.23	7.23	7.23	7.23	7.20	7.06	6.75	6.35	6.03	(1.02)
7.56	7.56	7.54	7.55	7.56	7.55	7.39	7.00	6.46	6.00	(0.97)
8.15	8.15	8.15	8.15	8.15	8.14	7.98	7.42	6.62	5.93	(0.92)
9.22	9.22	9.22	9.22	9.22	9.21	9.06	8.12	6.80	5.78	(0.75)
10.19	10.19	10.19	10.19	10.19	10.17	10.09	8.66	6.79	5.74	(0.74)

Note: (Pressure in kg/cm^2)

Figure C-10 Potential Distribution and Pressures on Boundaries
(a = 48 Å, b = 30 Å)

(0.50)	(0.50)	(0.50)	(0.50)	(0.48)	(0.46)	(0.43)	(0.38)	(0.34)	(0.31)	(0.30)	
5.37	5.37	5.37	5.35	5.32	5.27	5.19	5.08	4.96	4.86	4.82	(0.30)
5.57	5.57	5.56	5.55	5.53	5.47	5.38	5.23	5.07	4.93	4.87	(0.31)
5.97	5.97	5.96	5.95	5.94	5.89	5.77	5.55	5.27	5.05	4.95	(0.35)
6.70	6.70	6.70	6.69	6.69	6.66	6.51	6.13	5.61	5.18	5.02	(0.35)
8.22	8.22	8.22	8.22	8.21	8.24	8.09	7.28	6.03	5.26	5.03	(0.35)
10.11	10.11	10.11	10.11	10.11	10.10	10.09	8.46	6.03	5.27	5.03	(0.35)

Note: (Pressure in kg/cm^2)

Figure C-11 Potential Distribution and Pressures on Boundaries
(a = 120 Å, b = 45 Å)

(0.87)	(0.87)	(0.87)	(0.87)	(0.87)	(0.83)	(0.73)	(0.62)	(0.55)	(0.43)	(0.40)	
5.91	5.91	5.91	5.90	5.88	5.83	5.72	5.55	5.35	5.18	5.10	(0.40)
6.10	6.10	6.10	6.09	6.08	6.03	5.91	5.70	5.44	5.22	5.12	(0.41)
6.49	6.49	6.49	6.48	6.47	6.43	6.29	6.00	5.62	5.29	5.12	(0.41)
7.18	7.18	7.18	7.18	7.18	7.16	7.00	6.54	5.88	5.36	5.13	(0.41)
8.58	8.58	8.58	8.57	8.57	8.56	8.45	7.55	6.21	5.38	5.13	(0.41)
10.13	10.13	10.13	10.13	10.13	10.13	10.12	8.48	6.19	5.38	5.13	(0.41)

Note: (Pressure in kg/cm^2)

Figure C-12 Potential Distribution and Pressures on Boundaries
(a = 90 Å, b = 45 Å)

(1.87)	(1.87)	(1.87)	(1.87)	(1.87)	(1.78)	(1.60)	(1.18)	(0.84)	(0.62)	(0.52)	
6.65	6.65	6.65	6.65	6.65	6.60	6.47	6.21	5.86	5.54	5.36	(0.52)
6.83	6.83	6.83	6.83	6.83	6.79	6.65	6.35	7.93	5.56	5.34	(0.50)
7.19	7.19	7.19	7.19	7.19	7.16	7.00	6.62	6.07	5.59	5.31	(0.48)
7.82	7.82	7.82	7.82	7.82	7.82	7.64	7.08	6.27	5.61	5.26	(0.46)
9.01	9.01	9.01	9.01	9.01	9.00	8.86	7.89	6.49	5.59	5.19	(0.42)
10.17	10.17	10.17	10.17	10.17	10.16	10.10	8.54	6.48	5.59	5.17	(0.42)

Note: (Pressure in kg/cm^2)

Figure C-13 Potential Distribution and Pressure on Boundaries
(a = 60 Å, b = 45 Å)

(2.28)	(2.28)	(2.28)	(2.28)	(2.28)	(2.16)	(1.86)	(1.45)	(0.97)	(0.67)	(0.55)	
6.84	6.84	6.84	6.84	6.84	6.80	6.66	6.38	5.99	5.63	5.40	(0.53)
7.02	7.02	7.02	7.02	7.02	6.99	6.84	6.51	6.06	5.64	5.38	(0.51)
7.36	7.36	7.36	7.36	7.35	7.34	7.18	6.77	6.19	5.66	5.34	(0.50)
7.99	7.99	7.99	7.98	7.98	7.98	7.80	7.22	6.37	5.67	5.29	(0.48)
9.11	9.11	9.11	9.11	9.11	9.10	8.95	7.97	6.57	5.65	5.22	(0.43)
10.18	10.18	10.18	10.18	10.18	10.15	10.09	8.56	6.56	5.65	5.19	(0.42)

Note: (Pressure in kg/cm^2)

Figure C-14 Potential Distribution and Pressures on Boundaries
(a = 54 Å, b = 45 Å)

(2.76)	(2.76)	(2.76)	(2.76)	(2.76)	(2.64)	(2.40)	(1.86)	(1.13)	(0.72)	(0.55)	
7.05	7.05	7.05	7.05	7.05	7.02	6.87	6.57	6.13	5.72	5.44	(0.55)
7.23	7.23	7.22	7.22	7.22	7.20	7.04	6.70	6.20	5.73	5.42	(0.54)
7.56	7.56	7.56	7.55	7.56	7.54	7.38	6.94	6.31	5.74	5.37	(0.52)
8.15	8.15	8.15	8.15	8.15	8.14	7.97	7.36	6.48	5.75	5.31	(0.46)
9.22	9.22	9.22	9.12	9.22	9.21	9.05	8.05	6.66	5.73	5.24	(0.44)
10.19	10.19	10.19	10.19	10.19	10.17	10.08	8.59	6.65	5.73	5.22	(0.42)

Note: (Pressure in kg/cm^2)

Figure C-15 Potential Distribution and Pressures on Boundaries
(a = 48 Å, b = 45 Å)

(0.50)	(0.50)	(0.50)	(0.48)	(0.48)	(0.45)	(0.42)	(0.36)	(0.31)	(0.26)	(0.24)	(0.23)	
5.37	5.37	5.35	5.33	5.30	5.25	5.15	5.01	4.85	4.70	4.59	4.54	(0.23)
5.57	5.57	5.55	5.53	5.51	5.46	5.34	5.18	4.97	4.77	4.63	4.57	(0.24)
5.97	5.97	5.95	5.93	5.92	5.86	5.74	5.15	5.18	4.88	4.68	4.60	(0.24)
5.70	5.70	6.69	6.67	6.68	6.65	6.49	6.09	5.51	5.01	4.72	4.63	(0.25)
8.22	8.22	8.22	8.21	8.21	8.24	8.09	7.25	5.94	5.06	4.74	4.63	(0.25)
10.11	10.11	10.11	10.11	10.11	10.11	10.10	8.43	5.93	5.08	4.75	4.63	(0.25)

Note: (Pressure in kg/cm^2)

Figure C-16 Potential Distribution and Pressures on Boundaries
(a = 120 Å, b = 60 Å)

(0.87)	(0.87)	(0.87)	(0.87)	(0.86)	(0.83)	(0.71)	(0.59)	(0.46)	(0.36)	(0.30)	(0.28)	
5.91	5.91	5.90	5.89	5.87	5.82	5.69	5.50	5.25	5.00	4.82	4.75	(0.28)
6.10	6.10	6.09	6.08	6.07	6.02	5.89	5.66	5.35	5.05	4.84	4.75	(0.28)
6.49	6.49	6.49	6.48	6.47	6.42	6.28	5.96	5.53	5.12	4.85	4.75	(0.28)
7.18	7.18	7.18	7.18	7.18	7.16	7.00	6.51	5.80	5.19	4.86	4.74	(0.28)
8.57	8.57	8.57	8.57	8.56	8.61	8.45	7.53	6.12	5.21	4.86	4.72	(0.27)
10.13	10.13	10.13	10.13	10.13	10.12	10.10	8.46	6.11	5.21	4.86	4.72	(0.27)

Note: (Pressure in kg/cm^2)

Figure C-17 Potential Distribution and Pressures on Boundaries
(a = 90 Å, b = 60 Å)

(1.87)	(1.87)	(1.87)	(1.87)	(1.87)	(1.78)	(1.60)	(1.18)	(0.75)	(0.53)	(0.39)	(0.32)	
6.65	6.65	6.65	6.65	6.65	6.60	6.46	6.18	5.78	5.37	5.07	4.92	(0.33)
6.83	6.83	6.83	6.83	6.83	6.79	6.64	6.32	5.86	5.39	5.07	4.91	(0.33)
7.19	7.19	7.19	7.19	7.19	7.16	7.00	6.59	5.99	5.43	5.06	4.89	(0.32)
7.82	7.82	7.82	7.82	7.82	7.82	7.64	7.09	6.19	5.45	5.04	4.86	(0.30)
9.01	9.01	9.01	9.01	9.01	9.01	8.86	7.86	6.41	5.44	5.03	4.83	(0.30)
10.17	10.17	10.17	10.17	10.17	10.13	10.10	8.52	6.39	5.44	5.03	4.83	(0.30)

Note: (Pressure in kg/cm^2)

Figure C-18 Potential Distribution and Pressures on Boundaries
($a = 60$ Å, $b = 60$ Å)

(2.28)	(2.28)	(2.28)	(2.28)	(2.28)	(2.16)	(1.86)	(1.38)	(0.88)	(0.57)	(0.40)	(0.35)	
6.84	6.84	6.84	6.84	6.84	6.80	6.65	6.35	5.91	5.46	5.12	4.94	(0.34)
7.02	7.02	7.02	7.02	6.98	6.83	6.49	5.98	5.48	5.12	4.93	4.93	(0.34)
7.36	7.36	7.36	7.36	7.35	7.34	7.18	6.74	6.11	5.50	5.11	4.91	(0.32)
7.99	7.99	7.99	7.98	7.98	7.98	7.78	7.19	6.29	5.52	5.09	4.89	(0.32)
9.11	9.11	9.11	9.11	9.11	9.10	8.95	7.94	6.49	5.51	5.07	4.86	(0.30)
10.18	10.18	10.18	10.18	10.18	10.15	10.09	8.54	6.48	5.50	5.07	4.85	(0.30)

Note: (Pressure in kg/cm^2)

Figure C-19 Potential Distribution and Pressures on Boundaries
(a = 54 Å, b = 60 Å)

(2.76)	(2.76)	(2.76)	(2.76)	(2.76)	(2.64)	(2.40)	(1.86)	(1.02)	(0.62)	(0.43)	(0.35)	
7.05	7.05	7.05	7.05	7.05	7.02	6.87	6.54	6.06	5.56	5.18	4.96	(0.35)
7.23	7.23	7.23	7.23	7.23	7.20	7.04	6.67	6.13	5.57	5.17	4.95	(0.35)
7.56	7.56	7.56	7.56	7.56	7.54	7.37	6.92	6.24	5.59	5.16	4.93	(0.34)
8.15	8.15	8.15	8.15	8.15	8.16	7.96	7.34	6.40	5.60	5.14	4.90	(0.32)
9.22	9.22	9.22	9.22	9.22	9.28	9.05	8.03	6.58	5.59	5.13	4.87	(0.30)
10.19	10.19	10.19	10.19	10.19	10.16	10.08	8.57	6.57	5.59	5.12	4.86	(0.30)

Note: (Pressure in kg/cm^2)

Figure C-20 Potential Distribution and Pressures on Boundaries
(a = 48 Å, b = 60 Å)

APPENDIX D

Surface Charge Calculation for Clay Particles

APPENDIX D

Surface Charge Calculation for Clay Particles

The montmorillonite used for the consolidation testing was supplied by the Baroid Division, National Lead Company of Houston, Texas.

The cation exchange capacity (C.E.C.) was reported as 96 meq/100 grams or 0.96 meq/gram. The specific surface of the clay was estimated at 800 m^2/gr, or 800 x 10^{20} sq $\mathring{A}$/gr.

The total number of monovalent cations in a gram* is equal to the C.E.C. x Avagadro's number = 0.96 x 10^{-3} x 6.02 x 10^{23}. This number of cations corresponds to a surface area of 800 x 10^{20} sq. $\mathring{A}$. Thus, the number of monovalent cations per square Angstrom is

$$0.96 \times 6.02 \times 10^{20}/800 \times 10^{20} = 7.25 \times 10^{-3} \text{ ions/sq. } \mathring{A}.$$

or

$$7.25 \times 10^{13} \text{ ions/sq. cm.}$$

The surface charge density can be computed as follows: on each sq. cm. there are 7.25 x 10^{13} elementary charges. This is equivalent to a charge density of 4 x 10^4 esu/sq. cm.

---

*C.E.C. = $\frac{0.67}{\text{unit cell wt.}}$ x 1000 x 100 meq/100 gr.